Evaluation of Labrador Sea Water formation in a global Finite-Element Sea-Ice Ocean Model setup, based on a comparison with observational data

P. Scholz,[1,2] D. Kieke,[2,3] G. Lohmann,[1,2,3] M. Ionita,[1,2], and M. Rhein,[2,3]

Corresponding author: P. Scholz, Alfred Wegener Institute, Helmholtz Centre for Polar and Marine Research, Bussestraße 24, 27570 Bremerhaven, Germany. (Patrick.Scholz@awi.de)

[1]Alfred Wegener Institute, Helmholtz Centre for Polar and Marine Research, Paleoclimate Dynamics Division, Bremerhaven, German

[2]MARUM, University of Bremen, Germany

[3]IUP, University of Bremen, Germany

Abstract. The deep water formation in the Labrador Sea is simulated with the Finite-Element Sea-Ice Ocean Model (FESOM) in a regionally focused, but globally covered model setup. The model has a regional resolution of up to 7 km and the simulations cover the time period 1958-2009. We evaluate the capability of the model setup to reproduce a realistic deep water formation in the Labrador Sea. Two classes of modeled Labrador Sea Water (LSW), the lighter upper LSW (uLSW) and the denser deep LSW (dLSW), are analysed. Their layer thicknesses are compared to uLSW and dLSW layer thicknesses derived from observations in the formation region for the time interval 1988-2009. The results indicate a suitable agreement between the modeled and from observations derived uLSW and dLSW layer thicknesses except for the period 2003-2007 where deviations in the modeled and observational derived layer thickness could be linked to discrepancies in the atmospheric forcing of the model. It is shown that the model is able to reproduce four phases in the temporal evolution of the potential density, temperature and salinity, since the late 1980s, which are known in observational data. These four phases are characterized by a significantly different LSW formation. The first phase from 1988 to 1990 is characterized in the model by a fast increase in the convection depth of up to 2000 m, accompanied by an increased Spring production of deep Labrador Sea Water (dLSW). In the second phase (1991-1994), the dLSW layer thickness remains on a high level for several years, while the third phase (1995-1998) features a gradual decrease in the deep ventilation and the renewal of the deep ocean layers. The fourth phase from 1999 to 2009 is characterized by a slowly continuing decrease of the dLSW layer thickness on a deeper depth level. By applying a Composite Map Analysis between an index of dLSW and sea level pressure over the entire simulation period from 1958 to 2009, it is shown that a pattern which resembles the structure of the North Atlantic Oscillation (NAO) is one of the main triggers for the variability of LSW formation. Our model results indicate that the process of dLSW formation can act as a low-pass filter to the atmospheric forcing, so that only persistent NAO events have an effect, whether uLSW or dLSW is formed. Based on composite maps of the thermal and haline contributions to the surface density flux we can demonstrate that the central Labrador Sea in the model is dominated by the thermal contributions of the surface density flux, while the haline contributions are stronger over the branch of the Labrador Sea boundary current system (LSBCS), where they are dominated by the haline contributions of sea ice melting and formation. Our model results feature a shielding of the central Labrador Sea from the haline contributions by the LSBCS, which only allows a minor haline interaction with the central Labrador Sea by lateral mixing. Based on the comparison of the simulated and measured LSW layer thicknesses as well as vertical profiles of potential density, temperature and salinity it is shown that the FESOM model is a suitable tool to study the regional dynamics of LSW formation and its impact on a global, not regional restricted, scale.

1. Introduction

In the Labrador Sea a major component of the cold limb of the Atlantic meridional overturning circulation (AMOC) is formed by deep convection: the Labrador Sea Water (LSW) [e.g., *Rhein et al.*, 2011]. LSW can be separated into two different density modes, the deep LSW (dLSW), in some publications referred as "classical LSW", and the less dense upper LSW (uLSW) [e.g., *Rhein et al.*, 2002; *Stramma et al.*, 2004; *Kieke et al.*, 2006]. Both LSW modes are formed by different depths of convection, caused by strong surface cooling during winter and spring in areas which are roughly limited by the 3000 m isobath [*Pickart et al.*, 2002]. The buoyancy loss during winter and spring leads to an increase in the near surface densities and to an unstable stratification and a homogenization of the water column. This homogenization of the water column can reach down to 2400 m depth [*Lazier et al.*, 2002] and can result in events of extreme dLSW formation. The formation of LSW is crucial for the heat and freshwater exchange between the atmosphere and deep ocean layers as well as for the oceanic input of oxygen, carbondioxide and anthropogenic tracers like chlorofluorocarbons (CFC) due to vertical ventilation in the ocean [*Kieke et al.*, 2006; *Steinfeldt et al.*, 2009]. The formation of either uLSW or dLSW, meaning the extent of the deep ventilation, depends on various factors. One major factor is the intensity of deep ventilation in the preceding winter and the amount of horizontal advection of heat and salt which mainly influence the density stratification in the Labrador Sea [*Lazier et al.*, 2002; *Yashayaev*, 2007]. This determines how much buoyancy flux is needed to transform water of a certain density. Another major factor is the strength of the atmospheric forcing in winter which provides the necessary buoyancy forcing to form either uLSW or dLSW. Many authors [*Dickson et al.*, 1996; *Pickart et al.*, 2003; *Yashayaev et al.*, 2007] suggest that the buoyancy flux is mostly controlled by the strength of the North Atlantic Oscillation (NAO). The NAO index is defined as the normalized atmospheric pressure gradient between the Azores High and the Icelandic Low [e.g. *Barnston and Livezey*, 1978; *Hurrell*, 1995]. Other factors that can affect the formation of dLSW or uLSW are the density stratification that remains from preceding winters or large fresh water pools that propagate within the subpolar gyre like the Great Salinity Anomaly (GSA) of the 1970s described by *Dickson et al.* [1988], or the later salinity anomalies described by *Belkin et al.* [1998] and *Belkin* [2004].

Due to the harsh weather conditions, the temporal and spatial availability of ship data for the Labrador Sea, especially regarding the properties of the LSW, is limited especially to the summer season. Nowadays, profiling data from Argo drifters allow also a partial experimental insight into the winter deep convection of the Labrador Sea [*Vage et al.*, 2009], although these data are still limited in their spatial and temporal availability. At this point, numerical ocean model approaches with high resolutions provide the possibility to analyze the spatial and temporal variability patterns. Such model simulations allow to investigate the processes and mechanisms responsible for setting the strength of the deep water formation, especially in regions that are usually difficult to access.

Over the last decades different regional model studies regarding the ventilation and transformation of LSW have been carried out [e.g., *Böning et al.*, 1996; *Marshall and Schott*, 1999; *Brandt et al.*, 2007; *Chanut et al.*, 2008]. However, regional modeling requires the boundary conditions to be defined at the open domain borders. The complexity of these boundary conditions is of course limited, which in turn restricts the degrees of freedom

(DOF) and the variability of the model. In contrast, global model studies do not have this restriction and allow the analysis of the full variability of a model in a global context without artificial lateral boundary conditions. Due to the high numerical costs, global setups are usually limited in their resolution and have deficiencies in reproducing regional effects. The Finite-Element Sea-Ice Ocean Model (FESOM) [*Danilov et al.*, 2004, 2005; *Wang et al.*, 2008] developed at the Alfred Wegener Institute, Helmholtz Centre for Polar and Marine Research, Bremerhaven, Germany, provides a compromise between a regional focus and a global coverage by using an unstructured triangular surface mesh. These kind of meshes offer the opportunity to locally increase the resolution to a high degree in an otherwise coarser global setup.

Scholz et al. [2013] evaluated such a model setup in reproducing a reliable sea ice distribution by comparing it to observational satellite data. They further compared modeled and observed vertical profiles at the position of ocean weather station Bravo and Charlie and pointed out that the model performs well in areas with high resolutions, while in coarser resolved areas the model shows some deviations from the observed profiles. In addition, *Scholz et al.* [2013] determined the time-evolution of the Denmark Strait overflow water (DSOW) and Iceland Scotland overflow water (ISOW) into the North Atlantic and pointed out that the model tends to underestimate these water masses. Recent improvements in the FESOM model code, with respect to the vertical mixing, have partially overcome this problem. *Scholz et al.* [2013] also evaluated the model setup regarding its ability in reproducing the GSA events in the Labrador Sea around 1970, 1981 and 1988, based on a comparison of modeled and observed temperature and salinity in the Labrador Sea at a pressure level of 1500 dbar.

The present paper focuses on the regional ability of the global FESOM setup introduced and evaluated by *Scholz et al.* [2013] to reproduce a realistic deep water formation in the Labrador Sea for the period 1988-2009, which is characterized by an extreme change in the formation of LSW. For this purpose, the modeled hydrography in the central Labrador Sea as well as the variability in the layer thickness of different LSW modes is analyzed. The latter model results are compared to LSW layer thickness time-series derived from hydrographic observations from the central Labrador Sea [*Kieke et al.*, 2006; *Rhein et al.*, 2011]. To further assess the performance of the model in reproducing a reliable deep water formation, we compare modeled and measured vertical profiles of potential density, temperature and salinity for various years in the interval 1988-2009.

Section 2 and 3 describe the FESOM model setup and the observational data considered for the comparison, respectively. Section 4 deals with the location of the deep convection area in the model, which is required for defining an index for the model LSW. The evolution of the potential density, temperature and salinity is analyzed over depth and time in the central Labrador Sea (section 5.1). In the following sections we present the time evolution of the model uLSW and dLSW layer thickness indices, the modeled vertical profiles of potential density, temperature and salinity and the vertical cross-sections of the AR7W cruise section and compare them to the corresponding data derived from hydrographic observations. To further highlight the atmospheric processes in the FESOM model which are responsible for the fluctuation in the formation of dLSW, the atmospheric surface temperature, net heat flux to the ocean and sea level pressure (SLP) are analyzed in section 5.5 by applying a composite map analysis (CMA) over the entire simulation period from 1958 to 2009 [*von Storch and Zwiers*, 2003]. In addition, the thermal and haline surface density flux to the ocean are analyzed by using a CMA and their contributions to the deep water formation in the central Labrador Sea are determined. The main discussion and conclusions are presented in sections 6 and 7 respectively.

2. FESOM Model Setup

In this study we use the Finite-Element Sea-Ice Ocean Model (FESOM) developed at the Alfred Wegener Institute, Helmholtz Centre for Polar and Marine Research, Bremerhaven [*Danilov et al.*, 2004, 2005, 2008; *Wang et al.*, 2008]. This model approach uses an unstructured triangular surface mesh, which gives the opportunity to model complex coastlines and locally higher resolutions without complicated grid nesting. FESOM consists of the Finite Element Ocean Model (FEOM) [*Danilov et al.*, 2004], which is coupled to a finite-element dynamic-thermodynamic sea ice model [*Timmermann et al.*, 2009]. FEOM is an ocean general circulation model based on solving the primitive equations under Boussinesq approximation. The model setup was designed to have a local increased resolution in important deep water formation areas in the Labrador Sea, Irminger Sea, Greenland-Iceland-Norwegian Sea, Weddell Sea and Ross Sea [*Scholz et al.*, 2013]. We also increased the resolution in the upwelling regions like coastal and equatorial areas. The maximum resolution of the model is a trade off between global coverage, extent of the region of maximum resolution and amount of available computer memory. The approximated mesh resolution of the global setup in the Northwest Atlantic is shown in Fig. 1. There, a minimum resolution of $\sim$ 7 km is reached around the coast of Greenland. In the Labrador Sea the resolution varies between $\sim$ 30 km in the southern part and $\sim$ 10 km in the northern part. The through-flow from the Canadian Archipelago (CAA) into the Labrador Sea is enabled by an open Lancaster Sound and Nares Strait with resolutions of 20-25 km and 15-20 km, respectively. The rather insufficient resolution in the Lancaster Sound and Nares Strait, which is below the Rossby radius in this area, allows in the model a netto volume transport of $\sim 1/5$ and $\sim 1/10$ of the observational values described by *Münchow and Melling* [2008] and *Peterson et al.* [2012], respectively. The resolution in the Davis Strait is in the order of around 15 km with an southward directed volume transport that is $\sim 1/3$ of the observational values provided by *Cuny et al.* [2005]. This has the consequence that the fresh-water supply of the Labrador Sea through the CAA is underestimated in our model setup.

The bottom topography of the model is derived from the ETOPO5 gridded elevation data [*Edwards*, 1989] that have a resolution of $1/12°$. The model setup has 41 vertical levels in a full cell z-level approach, with a vertical resolution of 10 m at the surface and stepwise increasing to 300 m at a depth of 2700 m and deeper. The increased model resolution in the Denmark Strait and over the Iceland-Scotland Ridge, allows us to avoid prescribing the overflows or artificially tuning the bottom topography, which is an adopted practice in many other OGCMs [e.g., *Campin and Goose*, 1999]. The model resolution in these regions is close to the resolution of the ETOPO5 data set. Nevertheless, the strength of DSOW and ISOW is still underrepresented in this model setup, as discussed by *Scholz et al.* [2013]. This issue has been partly resolved in the latest FESOM version by improvements in the vertical mixing scheme of the model.

In order to reach an equilibrium state we have applied 188 years of spinup consisting of 4 spinup cycles, each with a simulation period from 1958 to 2004. All the spinup rounds are forced by the Common Ocean-Ice Reference Experiment version 2 (COREv2) [*Large and Yeager*, 2009]. Sea surface temperature (SST), specific humidity and surface wind speed are forced at time steps of 6 hours, the radiation flux is calculated at daily time steps, whereas precipitation is calculated at monthly time steps. For the forcing of sea surface salinity (SSS) the salinity data of the transient Simple Ocean Data Assimilation (SODA) version 2.0.3 from 1958 to 2004 [*Carton and Giese*, 2008] is used in the spinup cycle. The model is first initialised with the temperature and salinity data from the World Ocean Atlas (WOA) 2001 [*Stephens et al.*, 2002]. For this study we initialized the model with the last output year of the last spinup cycle and applied the same forcing, except for the SSS. Model tests with different SSS forcings (SODA v. 2.0.3, SODA v. 2.1.6 and COREv2 climatology) (not shown) revealed that, if the model is forced with the transient SODA SSS data, the model tends to reproduce unrealistic deep ventilation events after 2000. The model results forced with the SSS climatology provided by COREv2 are more realistic compared with observational data, especially towards the end of the simulation period. For this reason we used here the COREv2 salinity climatology as SSS forcing which also allows us to take advantage of the full temporal coverage of the COREv2 data set and to extend the simulation period to 2009.

Although the temporal coverage of the model simulation used in this study is from 1958 to 2009 we will focus on the time interval 1988-2009, which is characterized by an extraordinary change in the intensity of the LSW formation [*Kieke et al.*, 2006; *Yashayaev et al.*, 2007]. Only for the CMA the entire simulation period 1958-2009 is considered to ensure a more meaningful result regarding the high and low composite maps. The model data used in this study have a monthly resolution.

3. LSW index derived from hydrographic observations

For the comparison between model and experimental data we analyze the layer thicknesses of uLSW and dLSW as calculated by *Kieke et al.* [2006] and *Rhein et al.* [2011] for the central Labrador Sea. They reconstructed time series of layer thicknesses for uLSW and dLSW from different hydrographic databases (Bedford Institute of Oceanography, Hydrobase, National Oceanographic Data Center, WHPO, SFB 460 and BMBF Nordatlantik) for the period from 1948 to 2009 by choosing profiles from the central Labrador Sea close to the position of the former Ocean Weather Station Bravo (OWS-B, $56^{\circ}30'$N, 51° W). The applied methods for the data acquisition and selection are described by *Kieke et al.* [2006]. The different time-series of the dLSW and uLSW layer thicknesses are directly connected to the formation of the corresponding water mass and can therefore be considered as an index for the produced volume of the respective LSW mode. The period from 1988 to 1996 is of potential importance because the atmospheric forcing had the strongest impact on the convective activity in the Labrador Sea [*Yashayaev et al.*, 2007; *Rhein et al.*, 2011]. To quantify the strength of the westerly winds, we use the NAO index derived from the COREv2 SLP via the normalized pressure gradient between the Azores High and the Icelandic Low [*Barnston and Livezey*, 1978; *Hurrell*, 1995] averaged over January, February and March (JFM).

Different definitions for LSW limits can be found in the literature [e.g., *Pickart et al.*, 2002; *Stramma et al.*, 2004; *Yashayaev*, 2007; *Yashayaev and Loder*, 2009]. To ensure a better comparability of modeled and measured LSW properties, we followed the definitions of *Stramma et al.* [2004] and *Kieke et al.* [2006, 2007] and defined the density range $\sigma_\theta = 27.68 - 27.74\ \mathrm{kg\,m^{-3}}$ as uLSW, and $\sigma_\theta = 27.74 - 27.80\ \mathrm{kg\,m^{-3}}$ as the dLSW layer.

4. Modeled Mixed Layer Depth in the Northwest Atlantic Ocean

Fig. 2a shows the maximum mixed layer depth of the FESOM model in March, averaged over the years 1988-2009. The mixed layer depth in the model is calculated as the depth at which the buoyancy force does not deviate more than 0.03% from its surface value. The North Atlantic Ocean of the FESOM setup reveals three major oceanic convection areas which are located in the Labrador Sea, Irminger Sea and at the continental slope southwest of Iceland. The most important convective area in the northwestern Atlantic Ocean is located in the Labrador Sea with a mean March mixed layer depth of 1844 m. The modeled center of the maximum convective cell in the Labrador Sea is not exactly located in the central Labrador Sea, but is shifted northwestward to 59.5°N, 55.5°W at a bottom depth of $\sim$ 2750 m. In the Irminger Sea and southwest of Iceland, the mixed layer depth is shallower and reaches only a maximum value of 840 m and 600 m, respectively. During 1988 to 2009 the mixed layer depth in the northwestern Atlantic shows a strong change (Fig. 2b, 2c). The period 1988-1955 (Fig. 2b) is characterized in the model by an intensified convection in the northwestern Labrador Sea, Irminger Sea and south of Greenland. The mean March mixed layer depth in the Labrador Sea and Irminger Sea, reaches a maximum depth of 2435 m and 1531 m, respectively. The following period from 1996 to 2009 (Fig. 2c) is characterized by a drastic decrease in the deep convection in the northwestern part of the Atlantic Ocean. The mixed layer depth in the Labrador Sea declines by a factor of $\sim$ 1.6, from 2435 m to 1482 m. The decline in the Irminger Sea is even stronger, the mixed layer depth drops there from 1531 m to 466 m.

To select the areas for the calculation of dLSW and uLSW layer thickness indices we apply the same methodology as *Kieke et al.* [2006]. They have used only those hydrographic profiles located in the vicinity of the AR7W cruise line, a hydrographic section crossing the central Labrador Sea in the vicinity of the Ocean Weather Station Bravo where the bottom topography exceeded 3300 m. Due to the fact that the modeled location of the convective area in the Labrador Sea is shifted to the northwest, a larger area for the calculation of the indices was considered. As a result, a box from the northwestern boundary until the position of the AR7W cruise line was selected and all surface nodes located within this box were identified. To further eliminate the influences of the boundary currents, like in *Kieke et al.* [2006], we excluded from the remaining surface nodes all surface nodes with a bottom depth shallower than 2500 m. The area of the resulting surface nodes includes now the central Labrador Sea and the area with the highest mixed layer depths (Fig. 2a, dashed contour line). Tests with different index definition areas revealed that our results are robust against changes in the size of this area as long as the area with highest mixed layer depths was included.

5. Results

5.1. Modeled Labrador Sea Hydrography

Fig. 3 presents the potential density $\sigma_\theta(z,t)$, temperature $T(z,t)$ and salinity $S(z,t)$ as represented in the FESOM setup for the index definition area (Fig. 2a, dashed contour) over time and depth for the period from 1988 to 2009. The isopycnals $\sigma_\theta = 27.68\ \mathrm{kg\,m^{-3}}$, $27.74\ \mathrm{kg\,m^{-3}}$ and $27.80\ \mathrm{kg\,m^{-3}}$, which are used for the definition of the dLSW and uLSW, are indicated as thick white lines.

The temporal evolution of the potential density over depth (Fig. 3a) changes considerably during this time range, as it is described by various authors based on observational data [e.g., *Kieke et al.*, 2006; *Yashayaev*, 2007; *Yashayaev and Loder*, 2009]. The simulation period is divided here into four phases, which are characterized by major changes in the properties of the Labrador Sea hydrography. The first phase, from 1988-1990, is characterized by a gradual increase in the potential density of around $\Delta\sigma_\theta = 0.03\,\mathrm{kg\,m^{-3}}$ at intermediate depths. Due to increasing vertical ventilation from the surface during winter times the dLSW class (between the $\sigma_\theta = 27.74 - 27.8\,\mathrm{kg\,m^{-3}}$ isopycnals) gets gradually connected to the cold and fresh surface layers.

The subsequent period from 1991 until 1994 is described by a strong deep ventilation, which leads to high densities ($> 27.74\,\mathrm{kg\,m^{-3}}$) in the entire water column below a depth of 100 m. In each winter of this period the ventilation is strong enough, so that the cold and fresh surface layers are directly connected to the density range of dLSW. This leads to a fast build up of a homogeneous cold, fresh and dense body of water, extending from the surface to a depth of about 2000 m. The winters of 1993 and 1994 reveal an exceptionally strong vertical ventilation, where the coldest and freshest water is ventilated down to a depth greater than 2000 m. The highest density in the intermediate depth layers is reached in the winter of 1993 with a maximum of around $\sigma_\theta = 27.785\,\mathrm{kg\,m^{-3}}$. It should be mentioned that at the transition from phase one to phase two, in comparison to the abrupt decrease in temperature (Fig. 3b), the salinity (Fig. 3c) features a more gradual decrease. This suggests that the underlying mechanism that dominates the decrease in salinity in the FESOM model is different from a fast vertical deep convection process and will be discussed in section 6.

In the third phase, from 1995 to 1998, the dLSW mode water starts to get isolated from the surface and the supply of cold and fresh waters (Fig. 3a). This is associated with a reduction of the deep ventilation. The horizontal mixing with a warmer and more saline

Labrador Sea Boundary Current system (LSBCS) that consists of the West Greenland Current in the northeast and the Labrador Current in southwest, leads to a gradual decrease of the density in intermediate depths and a lowering of the $\sigma_\theta = 27.74\,\mathrm{kg\,m^{-3}}$ isopycnal of ~ 900 m until 1998. The mean depth of the $\sigma_\theta = 27.68\,\mathrm{kg\,m^{-3}}$ isopycnal remains at a level of ~ 100 m. The strong increase in the depth of the $\sigma_\theta = 27.74\,\mathrm{kg\,m^{-3}}$ isopycnal and the constant remaining depth of the $\sigma_\theta = 27.68\,\mathrm{kg\,m^{-3}}$ isopycnal indicates a thickening of the lighter uLSW layer in this phase. The fourth phase from 1999 to 2009 features a slowly decreasing depth of the $\sigma_\theta = 27.74\,\mathrm{kg\,m^{-3}}$ isopycnal from ~ 1000 m to ~ 1200 m. The $\sigma_\theta = 27.68\,\mathrm{kg\,m^{-3}}$ isopycnal shows a continuous sinking trend until 2008 to a depth of ~ 500 m, which is associated with an accumulation of less dense water in the surface layer. The sinking of the $\sigma_\theta = 27.68\,\mathrm{kg\,m^{-3}}$ isopycnal, after 2004, is connected to an increase in temperature and salinity (Fig. 3 (b), (c)) in the intermediate layers between 500 m and 1500 m by ~ 0.4 °C and ~ 0.03 psu, respectively. After 2008, the depth of the $\sigma_\theta = 27.68\,\mathrm{kg\,m^{-3}}$ isopycnal indicates a rapid jump back to a depth of around 100 m.

5.2. Comparison of simulated and observed LSW layer thickness

Fig. 4 shows the time evolution of the monthly uLSW and dLSW layer thickness of the model (thin line), the 3-year-running-mean filtered time series (thick line) and the summer layer thicknesses estimated from observational data (filled circles) [*Kieke et al.*, 2006; *Rhein et al.*, 2011]. Additionally, the positive and negative phase of the January, February and March averaged normalized NAO index is shown by dark and light grey shaded areas, respectively.

Both time series of simulated and observed dLSW (uLSW) show an increase (decrease) in the layer thickness within the first phase from 1988 to 1990. The observed dLSW thickness is less than what is simulated by the FESOM model. Between 1991 and 1994 a large homogeneous dLSW body develops and the system is "charged with dense water" from the surface, undergoing a transition to deep convection depths. The build-up of the dLSW layer thickness occurs on the cost of the uLSW layer thickness which erodes into the dLSW class. For the second phase the simulated and measured layer thicknesses reveal that the Labrador Sea remained for several years in a deep convection state, when the dLSW and uLSW layer thickness reached its maximum and minimum value, respectively. The maximum value of the simulated and observed dLSW layer thickness with ~ 2100 m and ~ 2150 m as well as the minimum value of the simulated and observed uLSW layer thickness with ~ 50 m and ~ 90 m are in close agreement.

In the period from 1995 to 1998 (phase three), the simulated and observed layer thicknesses show a gradual transition towards thinner dLSW and thicker uLSW layer thicknesses, which coincides with a strong variability in the magnitude of the NAO index. The dLSW index in Fig. 4 and the temporal evolution of the potential density and temperature in Fig. 3 reveal that the system does not react instantaneous to a change in the wind and temperature forcing as indicated by the NAO index. The modeled uLSW layer thickness shows in the third phase a faster increase with a slope of 219 m/yr, compared to the slope of the observational derived uLSW layer thickness with a value of 154 m/yr. The difference in the decrease of the modeled and observational derived dLSW layer thicknesses is smaller with slopes of -200 m/yr and -172 m/yr, respectively.

At the beginning of the fourth phase (1999-2009), the layer thickness of the modeled uLSW layer increases to a maximum between 2000 and 2002, with a thickness of ~ 1000 m. From 2002 until 2006, the uLSW layer thickness of the model decreases again. This is associated with the sinking of the isopycnal $\sigma_\theta = 27.68\,\mathrm{kg\,m^{-3}}$ and the accumulation of a kind of "new LSW" class in the surface and upper ocean layers of the model which is lighter than uLSW. At this point, a detailed description of this new LSW class is omitted because this would require further comprehensive sensitivity experiments. The modeled uLSW layer thickness starts to increase again after 2006 until the end of the simulation period. In contrast, the observational derived uLSW layer thickness increases continuously from 1999 until 2009, but more slowly when compared to the third phase.

The modeled and observational derived dLSW layer thickness reveals a continuous decrease from 1999 until 2009, except for the years 2000 and 2008 where only the observational derived dLSW layer thickness features, besides the underlying trend, a slightly decreasing and increasing dLSW layer thickness, respectively. Both dLSW time-series run quite synchronous from 1999 until 2002. After 2002 the dLSW layer thickness derived from observations shows a stronger decreasing trend compared to the modeled dLSW layer thickness.

5.3. Comparison of modeled and measured vertical Labrador Sea profiles

Fig. 5 presents observed (dashed) vertical density profiles for the upper 2500 m of the water column averaged over the AR7W cruise section [*WOCE Data Product Committee*, 2002] and modeled (solid lines) summer (JJA) potential density profiles averaged over the Labrador Sea index area for various years during phases of increasing (I, 1988-1990), maximal (II, 1991-1994), decreasing (III, 1995-1998) and minimal (IV, 1999-2009) dLSW layer thickness.

The density profiles during phase I and II reveal a depth evolution that is overall comparable between the modeled and observed density profiles. The latter shows a faster decrease in the surface and intermediate layer density compared to the modeled density profiles. In the deep layers ($>$ 2000 m), the comparison between modeled and observed density profiles is vice versa. The dLSW (uLSW) layer thickness of 1990, calculated from the measured vertical profiles (hashed bars) indicate a slightly reduced (increased) value compared to the modeled (solid bars) dLSW layer thicknesses. In phase II, for the years 1992, 1993 and 1994, modeled and observed uLSW and dLSW layer thicknesses indicate a very good agreement, the differences being less than 90 m.

Phase III, reveals a different evolution of the measured and observed vertical density profiles. During 1995-1998, the slope in the modeled density profiles below 150 m decreases much stronger than it is the case of the observed profiles. The observed profiles feature a generally higher potential density in the depth ranges between 250 m and 2000 m compared to the modeled profiles. The difference in the slope between modeled and observed profiles leads to strong differences in the depth of the isopycnal $\sigma_\theta = 27.74\,\mathrm{kg\,m^{-3}}$. This in turn leads to increasing differences in the modeled and observed layer thicknesses of uLSW and dLSW within the third phase. The difference in the slope between modeled and measured profiles is diminishing below a depth of 2200 m, which leads to a reduced spread in the depth of the isopycnal $\sigma_\theta = 27.80\,\mathrm{kg\,m^{-3}}$, between modeled and measured profiles.

At the beginning of phase IV (1999 and 2001), modeled and observed density profiles reveal a comparable slope between 200 m and 2200 m. In 2003 and 2005, the depth of the isopycnals increased in the range between 250 m and 1000 m. In this depth range the modeled density profile of phase four indicate a more linear behaviour when compared to the observed profiles. Both, modeled and observed density profiles indicate In the depth range from 1000 m to 2000 m a more linear density behaviour, where the observed density profiles have a stronger slope and more underlying variability

Fig. 6 presents modeled (solid lines) and measured (dashed lines) vertical temperature profiles in the central Labrador Sea for the four different phases. In 1990, during the phase of increasing dLSW thickness, modeled and measured temperature profile agree well, although the measured profile shows a more gradual temperature decrease in the upper 500 m. The FESOM model is not able to reproduce the temperature increase between 2100 m and 2400 m. For the years 1992, 1993 and 1994, modeled and measured temperature profiles indicate a general offset of ~ 0.15 °C with the model profiles being warmer. Also here the measured profiles show a more gradual temperature decrease in the upper layers.

The years 1996, 1997, 1998 in phase III feature a similar depth evolution between the modeled and measured temperature profiles for the upper 100 m of the water column as well as in the depth range between 500 m and 2000 m. The model is not able to reproduce the entire depth variability between 500 m and 2000 m. The model is also not able to simulate the gradual temperature decrease between 100 m and 500 m or the temperature increase below 2000 m. At the beginning of phase IV (1999 and 2001), modeled and measured temperature profile reveal a comparable evolution in the range between 500 m and 2000 m. Although the entire depth variability of the observed profiles could not be reproduced in the model. The measured temperature profile of 1999 features in the depth range between 100 m to 500 m a more gradual temperature decrease, while the modeled profile features for this depth range reveals even a slight increase in temperature. The modeled temperature profiles for 2003 and 2005 have the tendency to underestimate the measured temperature profiles in the depth range of $100-400$ m as well as below 1400 m and to overestimate the temperature in the depth range between 400 m and 1400 m. Fig. 7 shows modeled (solid lines) and measured (dashed lines) vertical salinity profiles in the central Labrador Sea, during phase I-IV. Throughout phase I-III and also at the beginning of phase IV (1999 and 2001) the FESOM model is able to reproduce the slope and evolution of the measured salinity profiles in the upper 2000 m of the water column. But the modeled salinity profiles reveals a general offset towards lower salinities when compared to the measured profiles. At the end of phase IV (2003 and 2005) modeled and measured profiles diverge.

5.4. Comparison of modeled and measured Labrador Sea AR7W cruise sections

Due to rough winter conditions in the Labrador Sea, most available cruise sections were measured in late spring to late summer. In the following, we compare two simulated and measured hydrographic AR7W sections of the World Ocean Circulation Experiment (WOCE, http://cchdo.ucsd.edu) and follow-up programs. The section crosses the central Labrador Sea from the Canadian towards the Greenland continental shelf. Observational data were retrieved from http://cchdo.ucsd.edu. Concerning years with highest dLSW and uLSW layer thicknesses, data of the R/V Hudson cruises 93019/1 carried out in June 1993 and 2002/32 conducted in July 2002, respectively, were considered as appropriate representatives (Figs. 8 (a), (b)). The corresponding AR7W cross sections of the FESOM model are presented in Figs. 8 (c) and (d). We are aware that the area of maximum deep water formation in the model is slightly shifted to the northwest when compared to observed MLD (see Fig. 2), which provokes us to expect a certain difference in the modeled and measured cross sections. However, to assure a better comparability for the reader, also in terms of bottom topography, we show here the same AR7W cruise line for the modeled and measured sections.

The measured data from the AR7W line in June 1993 (Fig. 8a) feature a thick layer of dLSW. This massive dLSW body was gradually built up by a strong vertical mixing in the spring of 1993 and an intense winter time convection in the preceding three years [*Lazier et al.*, 2002; *Kieke et al.*, 2006; *Yashayaev and Loder*, 2009]. The observational data feature a maximum dLSW layer thickness of 2150 m in the central Labrador Sea and a minimum dLSW layer thickness of $\sim$ 1000 m on the continental slope. The uLSW mode water has a very limited thickness of around 200 m.

The corresponding modeled cross section in Fig. 8c reveals on the first view a perceptible deviation from the observed section, which can be mostly attributed to the shift between modeled and observed maximum MLD. The western part of the model Labrador Sea cross section is occupied by a lighter water body that reaches from $\sim$ 300 m down to a depth of 2200 m, as a consequence of the northwestward shift of the deep convection area in the model (see Fig 2b). Fig. 9a shows a horizontal mean density distribution in the northwest Atlantic, which indicates that the location of the dense water is more concentrated on the northeastern part of the modeled Labrador Sea. In the model this leads to the formation of a tongue of lighter water in the southern part of the Labrador Sea, which is obvious in the model data at the AR7W line. Nevertheless, the potential density of this tongue is still in the defined range of the dLSW. Due to this fact, the vertical location of the $\sigma_\theta = 27.68$, 27.74 and 27.80 $\mathrm{kg\,m^{-3}}$ isopycnals and the layer thickness of the dLSW and uLSW in the central Labrador Sea are hardly affected. However, this is not the case for the area of the Canadian shelf, where big differences in the location of the isopycnals can be found in the modeled cross section. The depth of the $\sigma_\theta = 27.8\,\mathrm{kg\,m^{-3}}$ isopycnal within the model in June 1993 is around 350 m lower than in the observed cruise section. Also the characteristic bowl structure of the observed $\sigma_\theta = 27.8\,\mathrm{kg\,m^{-3}}$ isopycnal close to the continental slope is missing in the modeled AR7W section. The depth levels of the measured and simulated isopycnals $\sigma_\theta = 27.68,\ 27.74\,\mathrm{kg\,m^{-3}}$ are quite similar in the central Labrador Sea. On the eastern and western boundary of the Labrador Sea the $\sigma_\theta = 27.68,\ 27.74\,\mathrm{kg\,m^{-3}}$ isopycnals differ from the measured cruise section, but this is also a consequence of the northwestward shift of the deep convection region in the model. The AR7W cruise section in July 2002 (Fig. 8b), shows, in comparison to 1993, a quite thick uLSW layer, with an average layer thickness of ~ 850 m. The thickness of the dLSW layer has decreased clearly. In 2002, the depth of the vertical ventilation has decreased so much, that the dLSW was not renewed anymore from the surface during winter time (see Fig. 3a). The decrease in the dLSW layer is due to the deepening of the $\sigma_\theta = 27.74\,\mathrm{kg\,m^{-3}}$ isopycnal. Also the depth of the $\sigma_\theta = 27.68\,\mathrm{kg\,m^{-3}}$ isopycnal deepens by ~ 200 m in the central Labrador Sea. The depth of the $\sigma_\theta = 27.80\,\mathrm{kg\,m^{-3}}$ isopycnal remains almost the same between summer 1993 and 2002.

The corresponding AR7W model section in July 2002 (Fig. 8d) reveals a similar behaviour, with a thickened uLSW layer. The western Labrador Sea features slightly lighter water masses within the uLSW layer, which are again a consequence of the northwestward shift of the deep convection area (see Fig. 9b). From 1993 until 2002, the $\sigma_\theta = 27.74\,\mathrm{kg\,m^{-3}}$ isopycnal sinks to a depth of ~ 1400 m, while the $\sigma_\theta = 27.80\,\mathrm{kg\,m^{-3}}$ isopycnal remains at the same depth, which decreases the dLSW layer in the model. Also here the model indicates deficiencies in reproducing the observed bowl structure of the $\sigma_\theta = 27.80\ \mathrm{kg\,m^{-3}}$ isopycnal close to the continental slope.

5.5. Relationship between changing dLSW formation and changing surface forcings

It is known from observations that LSW formation is initiated/modulated by atmospheric surface buoyancy forcing during winter conditions [*Lab Sea Group*, 1998; *Marshall and Schott*, 1999; *Lazier et al.*, 2002]. The switch between the formation of different LSW classes depends on the strength and lateral structure of the surface buoyancy forcing fields. In the following we want to analyze the relationship between the formation of a certain class of Labrador Sea mode water and different atmospheric fields of net heat flux to the ocean, atmospheric surface temperature, sea level pressure and thermal and haline surface density flux.

To analyze the responsible forcing mechanism in the model that causes fluctuation in the thickness of the dLSW class we apply a Composite Map Analysis (CMA) [*von Storch and Zwiers*, 2003] between a layer thickness time series of a certain LSW class and the aforementioned atmospheric forcing fields. For the CMA we use the detrended layer thickness time series of the January, February March (JFM) averaged dLSW class, because it is the most prominent LSW product observed in the last five decades, and it features the most pronounced layer thicknesses in JFM (see Fig. 4). For the forcing fields in the CMA we use the boreal winter season averaged over December, January and February (DJF), when we expect the highest magnitude in the surface buoyancy forcing and to account for a response time of one month for the onset of the winter time convection. The results of the CMA are affected to a minor extent when the dLSW index is changed to DJF or the forcing fields are changed to JFM. To get a more meaningful result regarding the CMA, the analysis was extended to the entire simulation period from 1958 to 2009, although the results were very similar when they were limited to the period 1988-2009. For the CMA only those years were considered when the dLSW time series was higher than $+0.75$ standard deviation (high composite map) and lower than -0.75 standard deviation (low composite map), respectively. This threshold was chosen as a compromise between the strength of the oceanic signal and the number of maps that are necessary to have an appropriate representation of the mean field. The analysis revealed that the results are less influenced by the exact threshold values in the CMA (not shown).

First, we determine the response time of the ocean in the Labrador Sea to changes in the atmospheric forcing. A lag-correlation analysis between the detrended dLSW index for JFM and the detrended NAO index for JFM (Fig. 10) covering the period 1958-2009 reveals a significant correlation at a lag of 1-3 years with a maximum correlation of 0.52 (99.9% significance level, using the method of *Dawdy and Matalas* [1964] to calculate the significance of auto-correlated time series), when the NAO leads dLSW variability by one year. Fig. 11 presents the resulting composite maps when the modeled JFM dLSW index is put into relation to the winter atmospheric surface temperature of the forcing and the modeled net heat flux to the ocean. Only those years are taken into account when the detrended JFM dLSW index is 0.75 above/below standard deviation (red and blue bars in Fig. 10). For the calculation of the composite maps, a lag of -1 year between the oceanic index and the atmospheric field is considered (atmosphere leads). The left column of Fig. 11 presents the high (Fig. 11a), low (Fig. 11c) and difference (Fig. 11e, high minus low) composite maps of atmospheric surface temperature with respect to the dLSW index. In years with a high dLSW index the mean surface temperature shows a strong negative anomaly of -3 °C to -6 °C in the northwestern Labrador Sea and a weak positive anomaly of 2 °C northeast of Iceland. During low dLSW years, the pattern is reversed: positive temperature anomalies are found in the Labrador Sea and negative anomalies northeast of Iceland. The difference composite map displays, in summary, that the atmospheric surface temperature in the northwest Labrador Sea cools down by up to 10 °C between a low and a high dLSW formation event. Additionally, a warming of 4 °C occurs northeast of Iceland. The right column of Fig. 11 displays the composite maps of the net heat flux to the ocean (downward heat flux positive) in relation to the JFM dLSW index. The heat flux indicates a strong negative anomaly of $-100\ \mathrm{W\,m^{-2}}$ over the central Labrador Sea during events with a high dLSW thickness. The positive anomaly that extends southwards from the northwest coast of Greenland (Fig. 11b) is caused by an increased sea ice transport through Davis Strait (57.7°W, 66.9°N, Fig. 13a) and subsequent melting. During low dLSW, the Labrador Sea has a positive net heat flux of 60 $\mathrm{W\,m^{-2}}$. Between high and low dLSW formation events (Fig. 11f) the net heat flux over the Labrador Sea reveals a strong negative anomaly of $-175\ \mathrm{W\,m^{-2}}$. This strong negative anomaly triggers a further cooling of the sea surface temperature and the formation of denser water masses. Additionally, we find that the modeled net heat flux mainly reflects the changes in the sensible heat flux, while the latent heat flux is only in the order of 20% of the sensible heat flux (not shown).

The contour lines in Fig. 11 show furthermore the high, low and difference composite maps between the dLSW index and the sea level pressure (SLP). In the high and low composite maps (Fig. 11 (a)-(d)), the Azores High and Icelandic Low pressure systems are indicated by red and black contour lines, respectively. The difference composite maps of the SLP features a clear dipole structure with a negative center of -5 hPa close to Iceland and a less expressed positive center of 3 hPa over the central North Atlantic. This dipole-like structure resembles to a large degree the spatial fingerprint of the NAO [*Barnston and Livezey*, 1978; *Hurrell*, 1995]. During increased dLSW formation (Fig. 11a, high composite map) the Icelandic Low is deepened. Due to the increased pressure gradient between the Azores High and the Icelandic Low, the northwesterly winds are intensified and bring very strong and cold winds from North Canada and the Canadian Archipelago to the Labrador Sea. These winds lead to a strong cooling of the surface and increase the net heat loss of the ocean, which can be seen in the high composite maps of the surface temperature and the net heat flux (Fig. 11a, 11b).

To directly analyze the influence of the buoyancy forcing, we applied a CMA to the surface density flux to the ocean (calculation follows *Josey* [2003]). We distinguish here between the thermal and haline related contributions to the surface buoyancy forcing in the Labrador Sea. Fig. 12 presents the composite map between the JFM dLSW index and the DJF thermal (left column) and haline (right column) surface density flux. The thermal surface density flux takes into account the contributions of sensible, latent and radiative heat fluxes, respectively. The haline surface density flux includes the contributions of precipitation, snow, evaporation, sea ice formation and sea surface salinity restoring. The left column of Fig. 12 shows the high (Fig. 12a), low (Fig. 12c) and difference (Fig. 12e) composite maps of the dLSW index and the thermal surface density flux. Positive values indicate an increase in the surface density of the ocean. During years with a high dLSW thickness, the thermal contribution of the surface density flux is positive in the central Labrador Sea and Irminger Sea as well as southwest of Iceland with a maximum value of $1.75 \cdot 10^{-6}\,\mathrm{kg/(m^2 s)}$ in the central Labrador Sea. The increase of surface density is mainly related to an increased heat loss by sensible heat during years with high dLSW formation. The coastal areas of the Labrador and Irminger Seas, however, indicate a negative thermal surface density flux. Here, the major influence is provided by the presence of sea ice which largely reduces the heat exchange between ocean and atmosphere. The negative thermal density flux in the northwestern Labrador Sea is related to a massive sea ice export through Davis Strait (57.7°W, 66.9°N, Fig. 13a). In years with a low dLSW thickness the central Labrador Sea reveals a negative thermal surface density flux which is again mainly related to an increased sensible heat flux during that phase. The northwestern Labrador Sea as well as the Davis Strait feature a slightly positive thermal density flux which indicates a reduced sea ice coverage.

The haline surface density flux (Fig. 12, right column) is dominated by the formation, melting and advection of sea ice. The contributions of precipitation, snow, evaporation and sea surface salinity restoring are smaller by a factor of 10 (not shown), but also the magnitude of the thermal density flux is almost an order of magnitude smaller than the density flux from sea ice melting, when comparing Fig. 12a and Fig. 12b . During years with high dLSW, the high composite map of the haline surface density flux (Fig. 12b) features a decrease in the surface density in the area of the LSBCS. This is similar in the Irminger Sea, which reveals an extreme value of $-16 \cdot 10^{-6}\,\mathrm{kg/(m^2 s)}$. The high decrease in the surface density of the Labrador Sea is related to an intensified transport and subsequent melting of sea ice through Davis Strait. The high formation rate of sea ice can be seen in positive surface density fluxes of $\sim 4 \cdot 10^{-6}\,\mathrm{kg/(m^2 s)}$ at the shelf areas and the associated extraction of freshwater. This is proven by the time evolution of the sea ice transport through a Davis Strait cross section at 61.7°W, 66.6°N - 53.7°W, 67.2°N (Fig. 13a). Due to intense westerly winds during the high dLSW phase, sea ice is transported towards the location of the LSBCS. The melting of sea ice releases large quantities of freshwater at the surface and causes a high negative haline surface density flux. One can ask why this high negative haline surface density flux from the sea ice melting has a minor influence on the central Labrador Sea. Fig. 13b shows the difference composite map of the winter salinity of a northwest to southeast vertical cross section through the Labrador Sea with the JFM dLSW index. This section has a positive salinity anomaly of ~ 0.25 psu on the shelf at around 63°W which is caused by intensified sea ice formation in Davis Strait and subsequent advection of a positive salinity anomaly in a depth of around ~ 100 m southwestward along the shelf during high dLSW phase. The negative salinity anomaly of ~ -0.25 psu at around 60.5°W is related to the melting of sea ice and the release of fresh water at this location. On this cross-section the negative anomaly is mostly confined to the location of the LSBCS. Only a minor interaction between the LSBCS and the central Labrador Sea was observed in the model. This interaction could be caused by a slow horizontal mixing process indicated by the salinity evolution in Fig. 3c. In years with a low dLSW thickness (Fig. 12d) the whole central Labrador Sea has a zero to slightly negative surface density flux which is mostly related to precipitation (not shown). Only the western part of the LSBCS and the eastern coast of Greenland feature positive values in the low composite map of the haline surface density flux. This is again related to an increased sea ice formation.

6. Discussion

In this study we have investigated the deep water formation in the Labrador Sea using a global FESOM model setup that has an increased, but non-eddy-resolving, regional resolution in the deep water formation areas of the North Atlantic Ocean. This setup allows us to simulate the effect of regional deep water formation and its global consequences beyond the usual limitation of regional restricted models at moderate computational costs. A drawback of this kind of model class is, that the time-step δt of the entire setup is limited by the size of the smallest mesh triangle. However, the commonly used nesting techniques have the problem that their interaction between different scales is usually just one directional.

The general climatology of this setup was evaluated in *Scholz et al.* [2013]. Here, we concentrate on the variability of the dLSW and uLSW layer thicknesses, which are formed during the winter and spring deep convection for the period 1988-2009. It is shown that the model is able to reproduce the temporal evolutions of the potential density, temperature and salinity since the late 1980s as shown by e.g. *Yashayaev* [2007] and *Yashayaev and Loder* [2009]. The temporal evolution reveals four different phases of LSW formation which differ significantly from each other. The first phase (1988-1990) is characterized in the FESOM model by a rapid increase in the production of spring dLSW. In a second phase (1991-1994) the Labrador Sea remained in a stable period of cold and fresh deep convection with a maximum convection depth of > 2000 m. The modeled time evolution of the surface to intermediate ocean temperature shows in that phase an abrupt drop of ~ 0.7 °C, which is associated with a sudden onset of deep convection and downward ventilation of cold surface waters. This trend in the ocean temperature of the Labrador Sea of the 1990s is also documented by observational studies [*Curry et al.*, 1998], which refer this strong trend to an exceptional high positive NAO. In contrast, the time evolution of the salinity shows a more gradual decrease of ~ 0.04 psu within the first two phases. Analysis of a Davis Strait cross section (Fig. 13a) revealed that the period from 1989 to 1995 is characterized in the model by an increased sea ice export from Baffin Bay that features its highest value in 1990. In the same time, this period is characterized also by a strong interannual variability with a drop in Davis Strait sea ice transport from 1991 to 1992. Sea ice is transported by surface winds from the area of the Davis Strait to the location of LSBCS and leads to a high fresh water input caused by sea ice melting (Fig. 13b). The slow decrease in salinity seems to originate from a horizontal mixing process with a fresher LSBCS. Furthermore, we see in the modeled data a freshening trend between 1988-1994 in a depth below 2000 m. This freshening trend has its origin already in the late 1960s (not shown), from 1969 until 1994, when the salinity decreased gradually by 0.04 psu. This value is comparable to other model results of *Wu et al.* [2004]. Observational studies of *Dickson et al.* [2002] confirm a similar decrease of 0.012 psu per decade, for the period 1965-2000, in the salinity evolution of the the deep Labrador Sea and the entire deep North Atlantic Ocean. Our model data indicate for the same period a salinity decrease of 0.010 psu per decade. *Dickson et al.* [2002] account this salinity decrease to a continuously freshening of the overflow water masses due to an intensified freshwater input from sea ice melting. Analysis of different cross sections within our model (e.g. Denmark Strait, Iceland Scotland Ridge) (not shown) support this theory [*Scholz et al.*, 2013]. Studies of *Yashayaev and Clark* [2005] suggest that the freshening trend has stopped, and reversed since the mid 1990s to an increasing salinity. Also the FESOM model results of [*Scholz* *et al.*, 2013] feature an increase in the salinity of the overflow water masses since 1995. The third phase (1995-1998) is dominated by an increased production of the uLSW and a reduction of dLSW, which becomes isolated from the supply of cold and fresh surface waters. The third phase goes along with a drop in the NAO-index from 1995-1996 (Fig. 4) in the model. The downward ventilation of the surface water and the renewal of dLSW mode water in the winter time convection weakens. The previously formed homogeneous dLSW body starts to slowly degenerate due to horizontal mixing with a warmer and saltier LSBCS [*Myers et al.*, 2007]. This leads to a gradual increase in temperature and salinity which then extends over the entire fourth phase from 1999 to 2009. Also the deep ocean levels below 2500 m, which mainly originate from the overflow water masses, show a moderate increase in the salinity between 1995 and 2009. This slight increase in the modeled salinity is connected to the observed reversal in the salinity trend after 1995 documented by *Yashayaev and Clark* [2005] and *Yashayaev and Loder* [2009].

Yashayaev and Loder [2009] have used observations to identify a period of "dense and voluminous" LSW mode water between 1987-1994. Their mode of LSW extends into a depth of 2400 m and is equivalent to the dLSW formation event captured by the FESOM model. A second event, from 2000 to 2003, was described by *Kieke et al.* [2006, 2007] and *Yashayaev and Loder* [2009] which reached depths of $\sim$ 1300 m. This event is analogous to the increased formation of the uLSW mode water in our model between 1999 to 2009 (Fig. 3).

The increase in the modeled temperature and salinity (see Fig. 3b and 3c) between 500 m and 1500 m in the period from 2003 to 2008 is mostly caused by a sustained high reduction of the oceanic heat loss to the atmosphere. The warming and salinity increase for this period in the model could not be related explicitly to a horizontal mixing process with the LSBCS. Fig 14 shows the time evolution of the observed (blue line) Hadley Center sea surface temperature (SST) from *Rayner et al.* [2003] and the modeled FESOM SST, both averaged over the Labrador Sea index area in winter (DJF) for the period 1988-2009. Between 2003 and 2007 both time series feature a strong warming period in winter. The observed SST time series indicates two exceptional high warming events around 2004 and 2005 that were above 125% of standard deviation (see dashed lines). The period from 2005 to 2006 is characterized in the model by a extreme negative phase of NAO (see Fig. 4). The modeled FESOM SST time series has five exceptional high warming events that were above 125% of standard deviation, which run synchronously with the surface air temperature of the COREv2 forcing field (black line). This resulted in the model in an anomalously small heat flux out of the ocean and to a pronounced reduction of the surface buoyancy forcing over the Labrador Sea between 2003 and 2007. The sustained loss in the buoyancy forcing was strong enough to form (in the model) a kind of new class of Labrador Sea Water that was lighter than uLSW, which is also the cause for the sinking of the isopycnal $\sigma_\theta = 27.68\,\mathrm{kg\,m^{-3}}$ and the decrease in the uLSW layer thickness within this period. The drop in the surface buoyancy forcing results in an accumulation of heat and salt in the intermediate layers, due to a reduction of the vertical ventilation and the associated reduced renewal of the uLSW during winter time convection. After 2007, when the SST in the model Labrador Sea decreases, enough surface buoyancy forcing is built up. The system goes back to a more “normal” uLSW formation, as its shown in Fig 3a and Fig. 4. Due to the missing preconditioning and weak surface heat loss before 2007 we are also not able to simulate the return of the deep convection to a depth of ~ 1800 m for the winter 2007-2008 as described by *Vage et al.* [2009]. A comparable increase in the temperature and salinity of the intermediate layers between 2003 and 2007 is documented in the observations of *Yashayaev and Loder* [2009], with the difference that here the loss in surface buoyancy forcing was in an order that still uLSW could be formed, as its proved by the observational derived uLSW time series shown in Fig. 4.

Major changes of the model mixed layer depth of the deep water formation areas were observed: i) the mixed layer depth in the Labrador Sea is reduced by $\sim 60\%$ between 1988-1995 and 1996-2009 and ii) the decrease in the mixed layer depth of the Irminger Sea is even more drastic ($\sim 70\%$). The main deep convection cell in the Labrador Sea in our model is shifted to the northwest. This bias could be explained by a lack of eddy-induced mixing with the West Greenland Current in the Labrador Sea caused by the limited horizontal resolution as described by *Chanut et al.* [2008]. They argued that the existence of eddies that mix with the warm Irminger Current, the so-called Irminger Rings, can limit the northward extent of the main deep convection area. Also a reduced liquid freshwater export from the Arctics through the CAA and Davis Strait as is observed in our model setup (not shown) could lead to a densification and increased mixed layer thickness of the modeled northwestern Labrador Sea [*Wekerle et al.*, 2013].

The results for the layer thickness of the LSW mode waters (Fig. 4) are also in good agreement with observations [*Curry et al.*, 1998; *Kieke et al.*, 2006, 2007; *Yashayaev*, 2007; *Yashayaev et al.*, 2007; *Rhein et al.*, 2011] except for the period 2003-2007 when the FESOM model switched to the formation of a “new” kind of lighter LSW, due to insufficiencies of the atmospheric COREv2 forcing, which resulted in a deviating modeled uLSW and dLSW layer thickness. The offset in the transition rate from the low uLSW layer thickness to the high uLSW layer thickness between model and observations might give a hint regarding a missing feedback mechanism from the ocean surface to the atmosphere within the model that could be related to the relatively sparse resolution but also to further temporal deficits of the atmospheric forcing reanalysis data. In the fourth phase, the observational derived dLSW layer thickness continues its decay at a rate (47.2 m/yr) that is higher than the simulated dLSW decay rate (34.7 m/yr). The dLSW was not renewed during the last two phases of its decay process. Thus, the decay is caused by the general ocean circulation in the Labrador Sea and over a wider extent of the North Atlantic Ocean. The deviating simulated dLSW decay rate within the fourth phase gives a hint to further model deficiencies in simulating the ocean circulation as well as the interaction of the central Labrador Sea with the surrounding currents and water masses due to a still insufficient resolution.

Our simulated dLSW data reveal further that the system that was "charged with dense water" in the period from 1991 to 1994, does not afterwards react instantaneous to a change in the NAO index, due to the memory effect of the Labrador Sea described by *Lazier et al.* [2002]. Based on observational data, *Curry et al.* [1998] suggest a general time lag of $2-4$ years between the NAO index and dLSW index. Our model results indicate a smaller time lag of not more than $1-3$ years. If the system is once "charged with dense water" and a massive dLSW body with a corresponding weak density stratification is built up, like in the period from 1991-1994, then also a lower surface buoyancy forcing can be sufficient enough to further produce dLSW as mentioned by *Lazier et al.* [2002]. In this case the system acts as a filter to short time fluctuations in the atmospheric forcing until the dLSW body further degenerates due to reduced surface buoyancy flux and mixing with the LSBCS.

The analysis of the vertical potential density profiles revealed, that during phase I and II the model is able to reproduce a comparable vertical density structure. During phase III with decreasing dLSW thickness and at the end of phase IV, the model revealed clear deficiencies in reproducing the measured vertical density structure. The observed deficiencies in the modeled vertical profiles can be attributed in part to the much coarser vertical resolution of the model compared to the observations but also due to the spatial bias in the location of the convection center. The modeled vertical salinity profiles indicate a general offset to lower values when compared to observations, as is also proven in *Scholz et al.* [2013]. The comparison of the observed and modeled AR7W section data indicates a deeper location of the isopycnal $\sigma_\theta = 27.80\ \mathrm{kg\,m^{-3}}$ in the model, which can be explained by an insufficient production rate of Denmark Strait Overflow water (DSOW), which is usually the main contributor to the densest and deepest water mass in the Labrador Sea. The deficit of the model setup in producing DSOW is discussed in more detail by *Scholz et al.* [2013].

Different authors [e.g., *Marshall and Schott*, 1999; *Pickart et al.*, 2002, 2003; *Lazier et al.*, 2002] assume that there is a set of required conditions in order to favor deep convection in the ocean: a weakly stratified water mass, a closed cyclonic circulation to trap the water masses and to prevent the surface waters from being advected, and the most important condition is a strong atmospheric winter time buoyancy forcing [*Pickart et al.*, 2003]. To investigate the atmospheric forcing conditions within our model we have applied a CMA between the dLSW index and the SLP field. We could clearly identify in the model that a pattern in the SLP field which has a low pressure center over Iceland is one of the main

triggers for the variability in the model LSW formation. *Dickson et al.* [1996] already assumed that the variability in the LSW formation, on longer time scales, is mainly influenced by the atmospheric forcing. Based on CMA it is shown that a high dLSW index (Fig. 7) in our model setup is associated with a SLP pattern which resembles the positive phase of NAO: a deepened Icelandic Low and a strong Azores High. Associated to this SLP dipole-like structure is the advection of dry and cold polar air from the Canadian landmass over the relatively warm Labrador Sea, which induces an enhanced heat loss, leading to the formation of dense surface water masses and increased deep convection as described by a variety of authors [e.g., *Dickson et al.*, 1996; *Pickart et al.*, 2003].
Furthermore, we show from the analysis of the surface density flux that our index definition area, which is marked by the dashed lines in Fig. 12, is mostly dominated by the thermal contribution of the surface density flux, where the sensible heat flux is the main contributor. In our simulation, the haline contributions, especially in the high dLSW phase, are determined largely by a regional contribution of sea ice melting that are confined to the LSBCS. This is in contradiction to the explanations of *Dickson et al.* [1988] and *Belkin* [2004], who suggested that the central Labrador Sea is strongly influenced by propagating negative salinity anomalies which are induced by melting of sea ice from different source regions, such as the Arctic Ocean or the Canadian Archipelago. We showed that within our model setup the central Labrador Sea is mostly shielded from the haline contributions of the surface density flux by the LSBCS. We detect only a minor interaction between the central Labrador Sea and the LSBCS by lateral mixing. The lack of lateral mixing with the LSBCS could be caused by an absence of eddy-induced mixing with the west Greenland Current [*Katsman et al.*, 2004], due to an insufficient eddy resolving resolution

in the model Labrador Sea. *Katsman et al.* [2004] described in an idealized regional model study that the existence of eddies, especially the so-called Irminger Rings are crucial for the lateral mixing and restratification process in the central Labrador Sea.

7. Conclusions

In this paper a FESOM model setup is used, which provides a compromise solution between a global coverage and a regional focus on the Labrador Sea. The FESOM approach has the advantage that it is not limited by artificial lateral boundary conditions and allows at relatively moderate computational costs to simulate an adequate regional deep water formation and its potential global impact. We demonstrate that this model is suitable to simulate the spatio-temporal evolution of the layer thicknesses of the different LSW modes. The model succeeds in simulating the evolution of LSW indices that is in agreement with observed time series of *Curry et al.* [1998]; *Kieke et al.* [2006, 2007] and *Rhein et al.* [2011]. Based on these indices we show that the Labrador Sea in our global model setup can act as a low-pass filter to fluctuations in the NAO index, so that only persistent NAO events correlate with the dLSW index.

The period 2003-2007 indicates some discrepancies between the modeled and observational derived uLSW layer thickness. We could related these deviations to regional shortcomings in the COREv2 surface air temperature forcing field and discovered an extended warming period between 2003 and 2007 in the COREv2 data set [*Large and Yeager*, 2009] when compared to observational Hadley Center SST [*Rayner et al.*, 2003]. This slightly extended warm period has a large effect on the modeled hydrography in the Labrador Sea and led to the production of an unrealistic light LSW. This demonstrates how ocean model evaluation relies not only on spatial but also temporal correct forcing data.

Our global model setup also confirms a dominance of the atmospheric circulation as one of the main triggers for the variability in the dLSW and uLSW layer thickness, which affects the deep water formation by increased heat loss and by intensified mixing. Our analysis of the thermal and haline surface density flux indicate that the central Labrador Sea is dominated by the thermal contributions of the surface density flux, while the haline contributions, that are dominated by the effects of sea ice melting, are limited in our model setup to the area of the LSBCS.

A next logical step will be the use of our model approach for further studies regarding the variability of deep water mass formation areas, like the Irminger Sea or Greenland Sea and their influence on the large-scale ocean circulation. In order to improve the lateral mixing processes in the Labrador Sea one needs to further increase the local resolution to be able to resolve eddy processes that could affect the deep water formation in the Labrador Sea.

Acknowledgments. The work was funded through MARUM DFG project, "Seasonal to decadal climate variability from oceanographic data, coral records and model simulations" which is part of the Excellence Cluster Initiative, through the MARUM project OC1, "Changes in large-scale overturning circulation: present and past" and through the BMBF "Verbundvorhaben Nordatlantik" and "Verbundvorhaben RACE". We thank the Met Office Hadley Center for providing their SST data available at http://www.metoffice.gov.uk/hadobs as well as the GFDL scientists for providing the COREv2 data set to the international modeling community. The forcing data was received from http://data1.gfdl.noaa.gov/nomads/forms/mom4/COREv2.html. We thank the two reviewers whose comments helped to improve the paper.

References

Barnston, A. G., and R. E. Livezey (1978), Classification, Seasonality and Persistence of Low-Frequency Atmospheric Circulation Patterns, *Mon. Wea. Rev.*, *115*(6), 1083–1126, doi:10.1175/1520-0493(1987)115<1083:CSAPOL>2.0.CO;2.

Belkin, I. (2004), Propagation of the "Great Salinity Anomalies" of the 1990s around the northern North Atlantic, *Geophys. Res. Lett.*, *31*(L08306), doi:10.1029/2003GL019334.

Belkin, I., S. Levitus, J. Antonov, and S. Malmberg (1998), "Great Salinity Anomalies" in the North Atlantic, *Prog. Oceanog.*, *41*(1), 1–68, doi:10.1016/S0079-6611(98)00015-9.

Böning, C. W., F. O. Bryan, W. R. Holland, and R. Döscher (1996), Deep-water formation and meridional overturning in a high-resolution model of the North Atlantic, *J. Phys. Oceanogr.*, *26*(7), 1142–1164, doi:10.1175/1520-0485(1996)026<1142:DWFAMO>2.0.CO;2.

Brandt, P., A. Funk, L. Czeschel, C. Eden, and C. W. Böning (2007), Ventilation and transformation of Labrador Sea Water and its rapid export in the Deep Labrador Current, *J. Phys. Oceanogr.*, *37*(4), 946–961, doi:10.1175/JPO3044.1.

Campin, J. M., and H. Goose (1999), Parameterization of density-driven downsloping flow for a coarse-resolution ocean model in z-coordinate, *Tellus A*, *51*(3), 412–430, doi:10.1034/j.1600-0870.1999.t01-3-00006.x.

Carton, J. A., and B. S. Giese (2008), A reanalysis of ocean climate using Simple Ocean Data Assimilation (SODA), *Mon. Wea. Rev.*, *136*(8), 2999–3017, doi:10.1175/2007MWR1978.1.

Chanut, J., B. Barnier, W. Large, L. Debreu, T. Penduff, J. M. Molines, and P. Mathiot (2008), Mesoscale eddies in the Labrador Sea and their contributions to conversion and restratification, *J. Phys. Oceanogr.*, *38*(8), 1617–1643.

Cuny, J., P. B. Rhines, and R. Kwok (2005), Davis Strait volume, freshwater and heat fluxes, *Deep Sea Res. I*, *52*(3), 519–542, doi:10.1016/j.dsr.2004.10.006.

Curry, R., M. S. McCartney, and T. M. Joyce (1998), Oceanic transport of subpolar climate signals to mid-depth subtropical waters, *Nature*, *391*, 575–577, doi:10.1038/35356.

Danilov, S., G. Kivman, and J. Schröter (2004), A finite element ocean model: principles and evaluation, *Ocean Modell.*, *6*(2), 125–150, doi:10.1016/S1463-5003(02)00063-X.

Danilov, S., G. Kivman, and J. Schröter (2005), Evaluation of an eddy-permitting finite-element ocean model in the North Atlantic, *Ocean Modell.*, *10*(1-2), 35–49, doi:10.1016/j.ocemod.2004.07.006.

Danilov, S., Q. Wang, M. Losch, D. Sidorenko, and J. Schröter (2008), Modeling ocean circulation on unstructured meshes: comparison of two horizontal discretizations, *Ocean Dynamics*, *58*(5-6), 365–374, doi:10.1007/s10236-008-0138-5.

Dawdy, D. R., and N. C. Matalas (1964), *Statistical and probability analysis of hydrologic data, part III: Analysis of variance, covariance and time series, in Ven Te Chow, ed., Handbook of applied hydrology, a compendium of water-resources technology: New York*, 8.68-8.90 pp., McGraw-Hill Book Company.

Dickson, B., I. Yashayaev, J. Meincke, B. Turrell, S. Dye, and J. Holfort (2002), Rapid freshening of the deep North Atlantic Ocean over the past four decades, *Nature*, *416*, 832–837, doi:10.1038/416832a.

Dickson, R., J. Meincke, S. A. Malmberg, and A. J. Lee (1988), The Great Salinity Anomaly in the Northern North Atlantic 1968-1982, *Prog. Oceanog.*, *20*(2), 103–151, doi:10.1016/0079-6611(88)90049-3.

Dickson, R., J. Lazier, J. Meincke, P. Rhines, and J. Swift (1996), Long-term coordinated changes in the convective activity of the North Atlantic, *Prog. Oceanog.*, *38*(3), 241–295, doi:10.1016/S0079-6611(97)00002-5.

Edwards, M. O. (1989), Global gridded elevation and bathymetry (ETOPO5), Digital raster data on a 5-minute geographic (lat/lon) 2160x4320 (centroid-registered) grid, *NOAA Natl. Geophys. Data Cent., Boulder, Colorado, USA.*

Hurrell, J. W. (1995), Decadal trends in the North Atlantic Oscillation: Regional temperatures and precipitation, *Science*, *269*(5224), 676–679, doi:10.1126/science.269.5224.676.

Josey, S. A. (2003), Changes in the heat and freshwater forcing of the eastern Mediterranean and their influence on deep water formation, *J. Geophys. Res.*, *108*(C7), 3237, doi:10.1029/2003JC001778.

Katsman, C. A., M. A. Spall, and R. S. Pickard (2004), Boundary Current Eddies and their role in the restratification of the Labrador Sea, *J. Phys. Oceanogr.*, *34*(9), 1967–1983, doi:10.1175/1520-0485(2004)034<1967:BCEATR>2.0.CO;2.

Kieke, D., M. Rhein, L. Stramma, W. M. Smethie, D. A. Lebel, and W. Zenk (2006), Changes in the CFC inventories and formation rates of Upper Labrador Sea Water, 1997-2001, *J. Phys. Oceanogr.*, *36*(1), 64–86, doi:10.1175/JPO2814.1.

Kieke, D., M. Rhein, L. Stramma, W. M. Smethie, J. M. Bullister, and D. A. Lebel (2007), Changes in the pool of Labrador Sea Water in the subpolar North Atlantic, *Geophys. Res. Lett.*, *34*(L06605), doi:10.1029/2006GL028959.

Lab Sea Group (1998), The Labrador Sea Deep Convection Experiment, *Bull. Am. Meteorol. Soc.*, *79*(10), 20332058.

Large, W. G., and S. G. Yeager (2009), The global climatology of an interannually varying air-sea flux data set, *Clim. Dyn.*, *33*(2-3), 341–364, doi:10.1007/s00382-008-0441-3.

Lazier, J., R. Hendry, A. Clarke, I. Yashayaev, and P. Rhines (2002), Convection and restratification in the Labrador Sea, 1990-2000, *Deep-Sea Research I*, *49*(10), 1819–1835, doi:10.1016/S0967-0637(02)00064-X.

Marshall, J., and F. Schott (1999), Open-ocean convection: observations, theory, and models, *Review of Geophysics*, *37*(1), 1–64, doi:10.1029/98RG02739.

Münchow, A., and H. Melling (2008), Ocean current observations from Nares Strait to the west of Greenland: Interannual to tidal variability and forcing, *J. Mar. Res.*, *66*(6), 801–833.

Myers, P. G., N. Kulan, and M. H. Ribergaard (2007), Irminger Water variability in the West Greenland Curreng, *Geophys. Res. Lett*, *34*(L17601), doi:10.1029/2007GL030419.

Peterson, I., J. Hamilton, S. Prinsenberg, and R. Pettipas (2012), Wind forcing of volume transport through Lancaster Sound, *Geophys. Res. Lett.*, *117*(C11018), doi: 10.1029/2012JC008140.

Pickart, R. S., D. J. Torres, and R. A. Clarke (2002), Hydrography of the Labrador Sea during active convection, *J. Phys. Oceanogr.*, *32*(2), 428–456, doi:10.1175/1520-0485(2002)032<0428:HOTLSD>2.0.CO;2.

Pickart, R. S., F. Straneo, and G. W. K. Moore (2003), Is Labrador Sea Water formed in the Irminger basin ?, *Deep-Sea Research Part 1*, *50*(1), 23–52, doi:10.1016/S0967-0637(02)00134-6.

Rayner, N. A., D. E. Parker, E. B. Horton, C. K. Folland, L. V. Alexander, D. P. Rowell, E. C. Kent, and A. Kaplan (2003), Global analyses of sea surface temperature, sea ice, and night marine air temperature since the late nineteenth century, *J. Geophys. Res.*, *108*(D14), 4407, doi:10.1029/2002JD002670.

Rhein, M., J. Fischer, W. M. Smethie, D. Smythe-Wright, R. F. Weiss, C. Mertens, D. H. Min, U. Fleischmann, and A. Putzka (2002), Labrador Sea Water: pathways, CFC-inventory and formation rates, *J. Phys. Oceanogr.*, *32*(2), 648–665, doi:10.1175/1520-0485(2002)032<0648:LSWPCI>2.0.CO;2.

Rhein, M., D. Kieke, S. Hüttl-Kabus, A. Roessler, C. Mertens, R. Meissner, B. Klein, C. W. Böning, and I. Yashayaev (2011), Deep water formation, the subpolar gyre, and the meridional overturning circulation in the subpolar North Atlantic, *Deep-Sea Research II*, *58*(17-18), 1819–1832, doi:10.1016/j.dsr2.2010.10.061.

Scholz, P., G. Lohmann, Q. Wang, and S. Danilov (2013), Evaluation of a Finite-Element Sea-Ice ocean model (FESOM) setup to study the interannual to decadal variability in the deep-water formation rates, *Ocean Dynamics*, *63*(4), 347–370, doi:10.1007/s10236-012-0590-0.

Steinfeldt, R., M. Rhein, J. L. Bullister, and T. Tanhua (2009), Inventory changes in anthropogenic carbon from 1997-2003 in the Atlantic Ocean between 20°S and 65°N, *Global Biogeochem. Cycles*, *23*, GB3010, doi:10.1029/2008GB003311.

Stephens, C., J. I. Antonov, T. P. Boyer, M. E. Conkright, R. A. Locarnini, T. D. OBrien, and H. E. Garcia (2002), *World Ocean Atlas 2001, Volume 1: Temperature. S. Levitus, Ed.*, NOAA Atlas NESDIS 49, U.S. Government Printing Office, Wash., D.C., 167 pp.

Stramma, L., D. Kieke, M. Rhein, F. Schott, I. Yashayaev, and K. P. Koltermann (2004), Deep water changes at the western boundary of the subpolar North Atlantic during 1996 to 2001, *Deep-Sea Research I*, *51*(8), 1033–1056, doi:10.1016/j.dsr.2004.04.001.

Timmermann, R., S. Danilov, J. Schröter, C. Böning, D. Sidorenko, and K. Rollenhagen (2009), Ocean circulation and sea ice distribution in a finite element global sea ice-ocean model, *Ocean Modelling*, *27*(3-4), 114–129, doi:10.1016/j.ocemod.2008.10.009.

Vage, K., R. S. Pickard, V. Thierry, G. Reverdin, C. M. Lee, B. Petrie, T. A. Agnew, A. Wong, and M. H. Ribergaard (2009), Surprising return of deep convection to the subpolar North Atlantic Ocean in winter 2007-2008, *Nature Geoscience*, *2*(1), 67–72, doi:10.1038/ngeo382.

von Storch, H., and F. W. Zwiers (2003), *Statistical Analysis in Climate Research*, Cambridge University Press.

Wang, Q., S. Danilov, and J. Schröter (2008), Finite Element Ocean Circulation Model based on triangular prismatic elements, with application in studying the effect of topography representation, *J. Geophys. Res.*, *113*(C05015), doi:10.1029/2007JC004482.

Wekerle, C., Q. Wang, S. Danilov, T. Jung, J. Schröter, and P. G. Myers (2013), The climate relevance of the Canadian Arctic Archipelago: A multi-resolution modeling study, *Geophys. Res. Lett.*, *under revision*.

WOCE Data Product Committee (2002), WOCE Global Data, Version 3.0, WOCE International Project Office, WOCE Report No. 180/02, Southampton, UK.

Wu, P., R. Wood, and P. Stott (2004), Does the recent freshening trend in the North Atlantic indicate a weakening thermohaline circulation?, *Geophys. Res. Lett.*, *31*(L02301), doi:10.1029/2003GL018584.

Yashayaev, I. (2007), Hydrographic changes in the Labrador Sea, 1960-2005, *Prog. Oceanog.*, *73*(3-4), 242–276, doi:10.1016/j.pocean.2007.04.015.

Yashayaev, I., and A. Clark (2005), Recent warming of the Labrador Sea, *ASOF News Lett.*, *4*, 17–18.

Yashayaev, I., and J. W. Loder (2009), Enhanced production of Labrador Sea Water in 2008, *Geophys. Res. Lett.*, *36*(L01606), doi:10.1029/2008GL036162.

Yashayaev, I., M. Bersch, and H. M. van Aken (2007), Spreading of the Labrador Sea Water to the Irminger and Iceland basins, *Geophys. Res. Lett.*, *34*(L10602), doi:10.1029/2006GL028999.

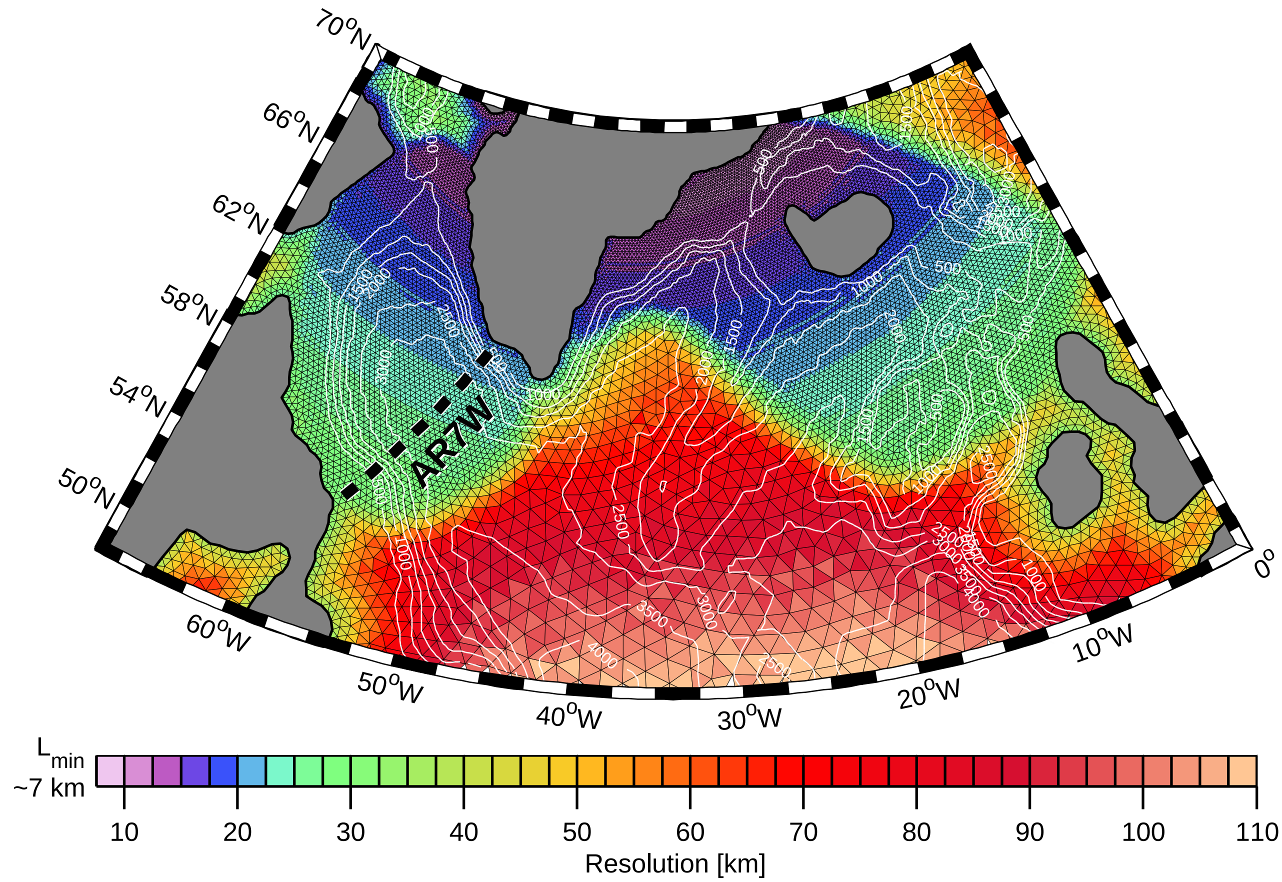

Figure 1. Regional resolution and bottom topography of the global model setup in the Northwest Atlantic Ocean. The dashed line marks the position of the AR7W cruise line [*Lazier et al.*, 2002].

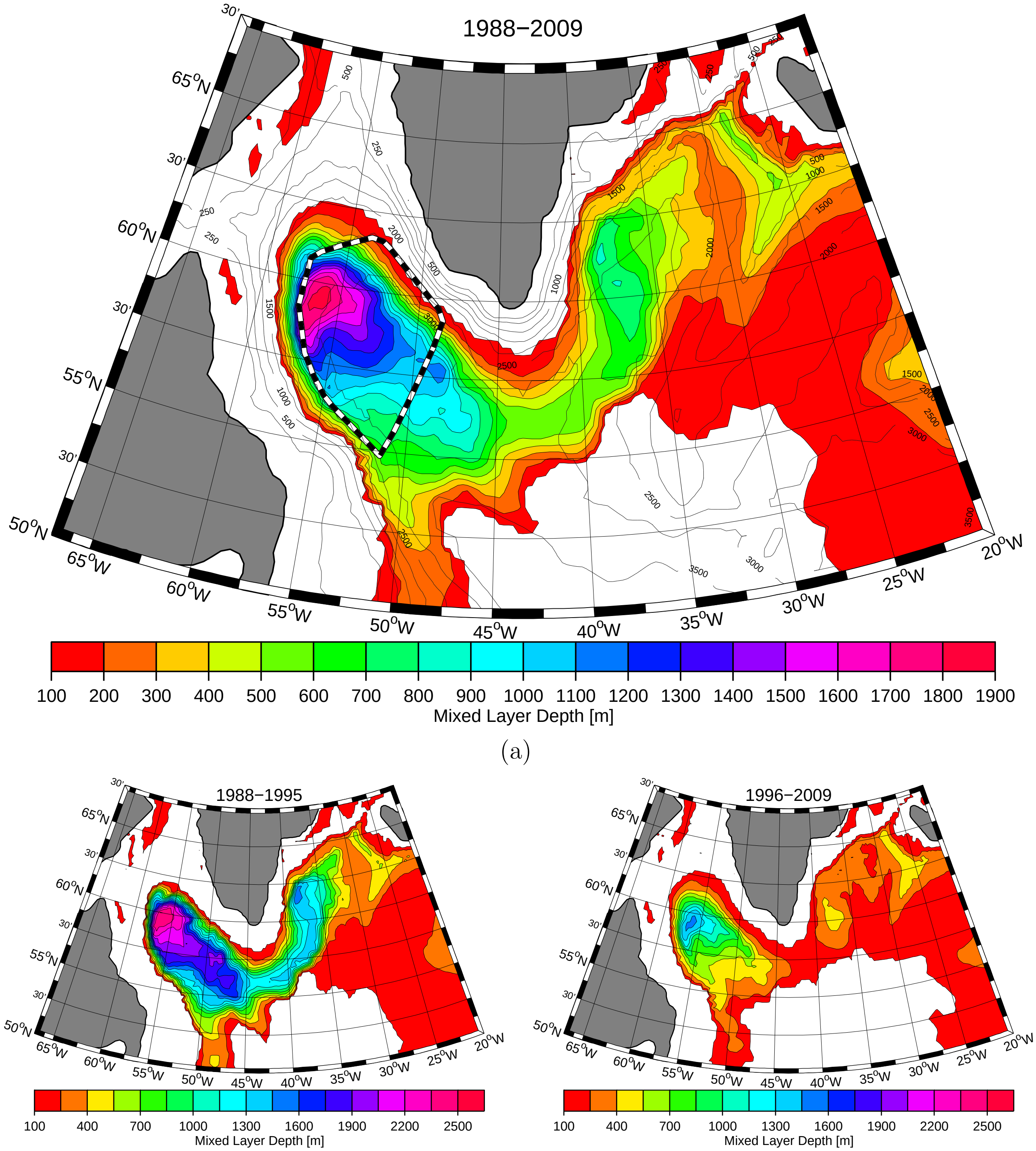

(a)

(b) (c)

Figure 2. (a): Mixed layer depth (≥ 100 m) for the month of March, shown for the North Atlantic and averaged over the period 1988-2009. Superimposed is the bottom topography (black contour line) of the model and the area (dashed line) considered for the time evolution indices shown in Fig. 3 and Fig. 4.

(b), (c): March mixed layer depth, averaged over the years 1988-1995 (b) and 1996-2009 (c). Please note the different scales in (a) vs. (b) and (c).

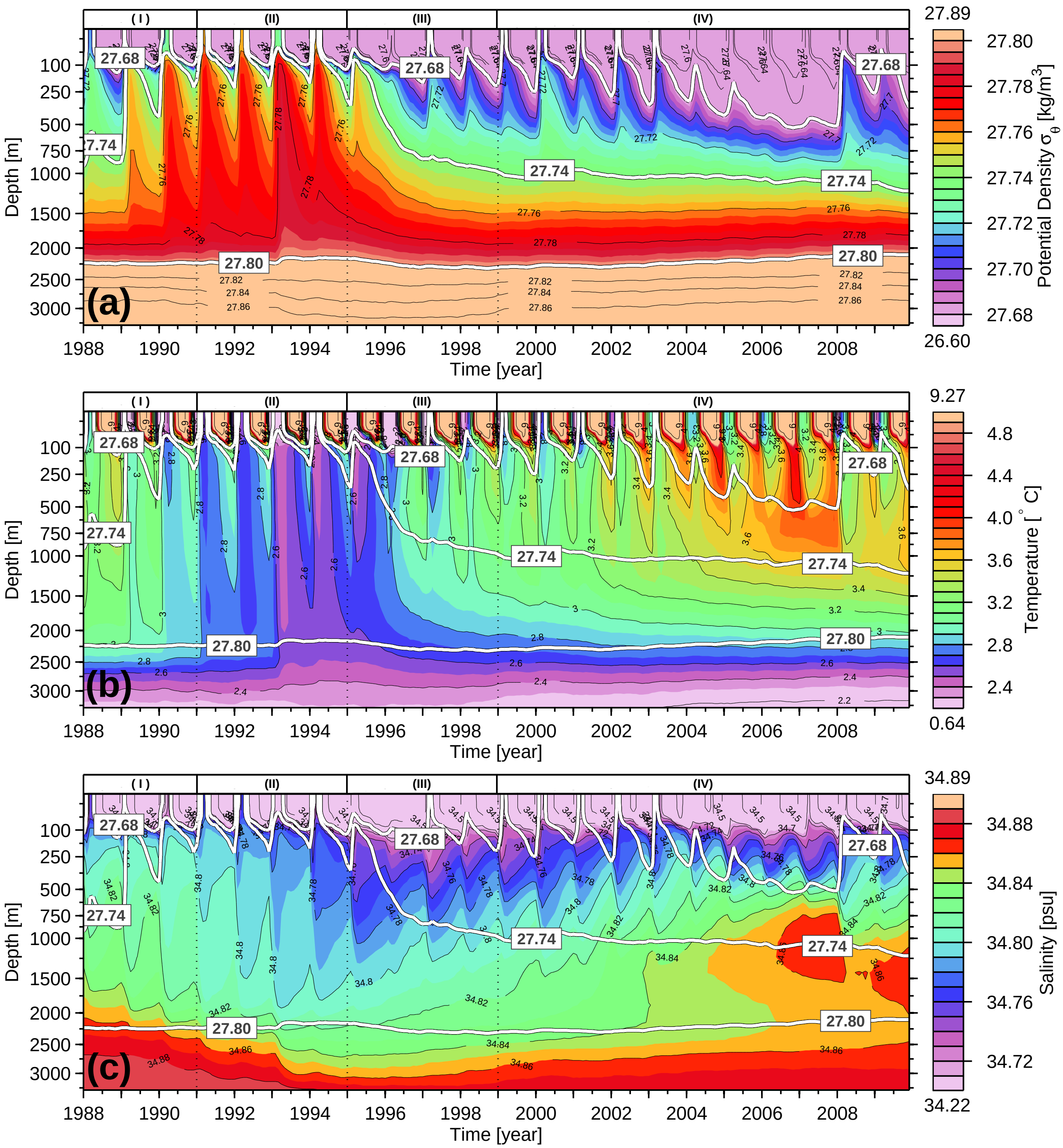

Figure 3. Time evolution of the monthly mean potential density (a), temperature (b) and salinity (c) over depth for the central Labrador Sea (dashed contour indicated in Fig. 2) for the years 1988-2009. Thick white lines indicate the isopycnals $\sigma_\theta = 27.68\ \mathrm{kg\,m^{-3}}$, $\sigma_\theta = 27.74\ \mathrm{kg\,m^{-3}}$ and $\sigma_\theta = 27.80\ \mathrm{kg\,m^{-3}}$ to separate between light (uLSW) and dense (dLSW) Labrador Sea Water.

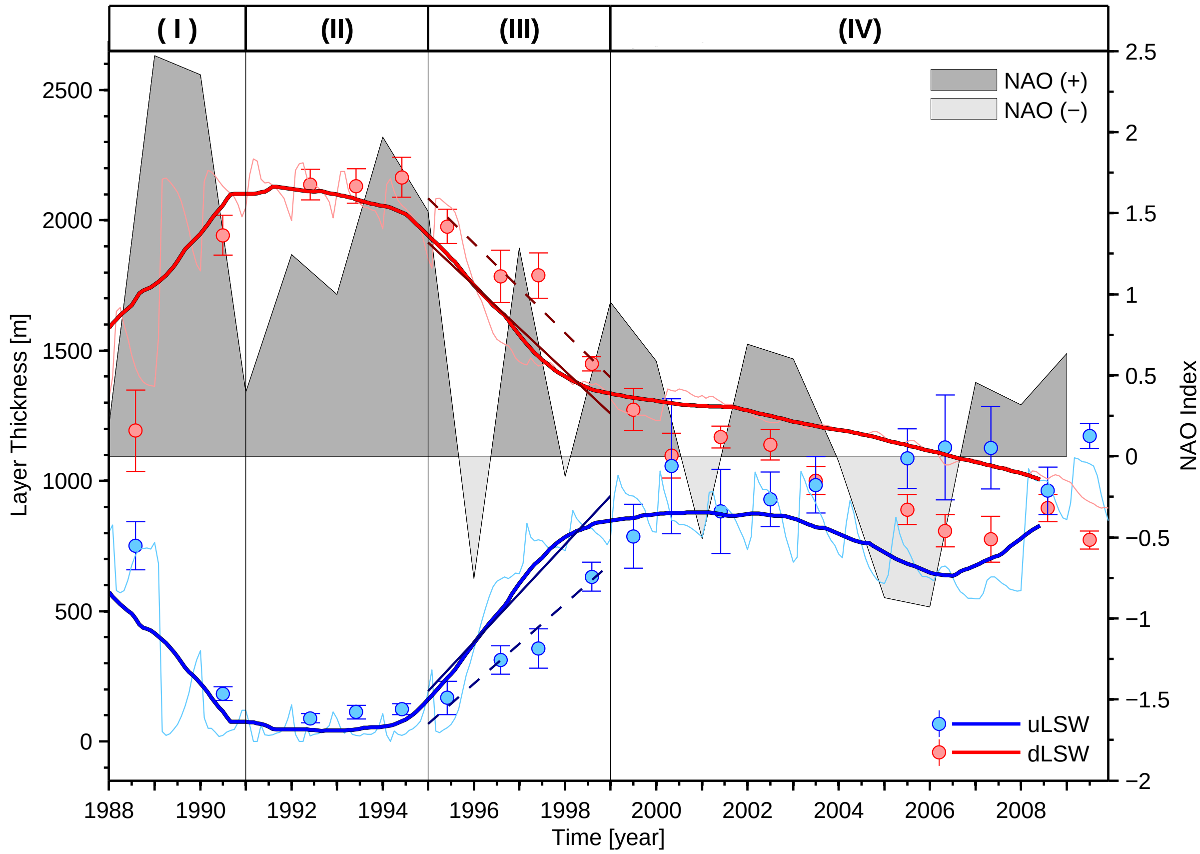

Figure 4. Temporal evolution of the layer thickness of upper and deep Labrador Sea Water (LSW) for the years 1988-2009. Blue: upper LSW (uLSW), bounded by the isopycnals $\sigma_\theta = 27.68 - 27.74\,\mathrm{kg\,m^{-3}}$; Red: deep LSW (dLSW), bounded by the isopycnals $\sigma_\theta = 27.74 - 27.80\,\mathrm{kg\,m^{-3}}$. The monthly values and the 3-years-running-mean filtered dLSW and uLSW data of the model run are shown by thin and thick lines, respectively. The dLSW and uLSW time series derived from observations are shown as filled circles including the uncertainties [*Rhein et al.*, 2011]. Solid (model) and dashed (observed) dark blue and dark red lines indicate the slope of the decreasing dLSW and increasing uLSW layer thickness for the period 1995-1998, respectively. The positive and negative phase of the January, February and March averaged normalized NAO index derived from the COREv2 data set [*Large and Yeager*, 2009] are indicated by dark- and light grey areas, respectively. Phases of increasing (I), maximal (II), decreasing (III) and minimal (IV) dLSW layer thickness are separated by vertical lines.

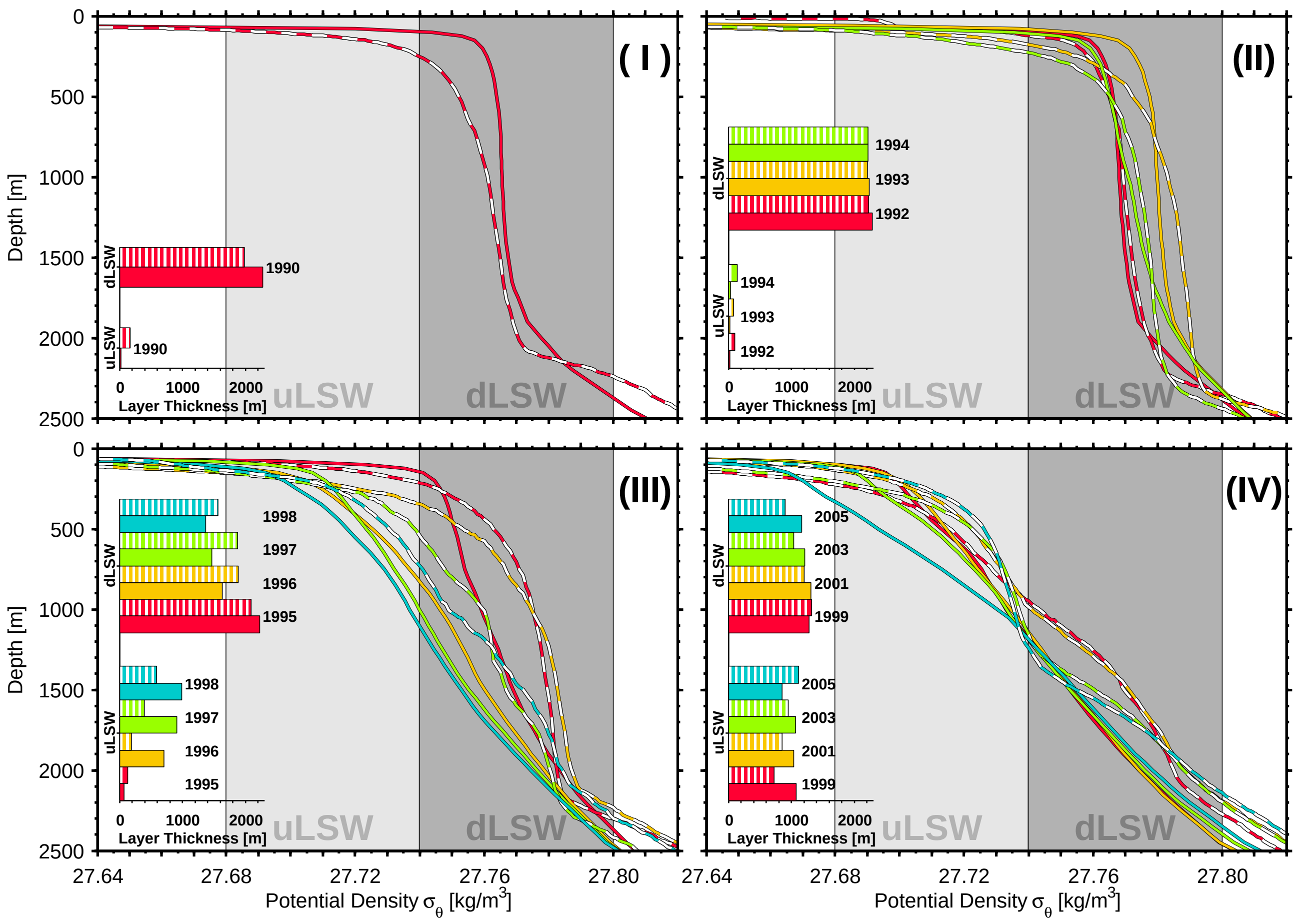

Figure 5. Vertical depth profiles of observed (dashed lines) potential density averaged over the AR7W cross section (http://cchdo.ucsd.edu) and modeled (JJA, solid lines) potential density averaged over the Labrador Sea index area (see Fig. 2a) for various years in the phase of increasing (I), maximal (II), decreasing (III) and minimal (IV) dLSW layer thickness (see Fig. 4). The density range of uLSW and dLSW is indicated by light- and dark grey areas, respectively. Horizontal bars present the observed (hashed) and modeled (solid) uLSW and dLSW layer thickness estimated from the density profile data.

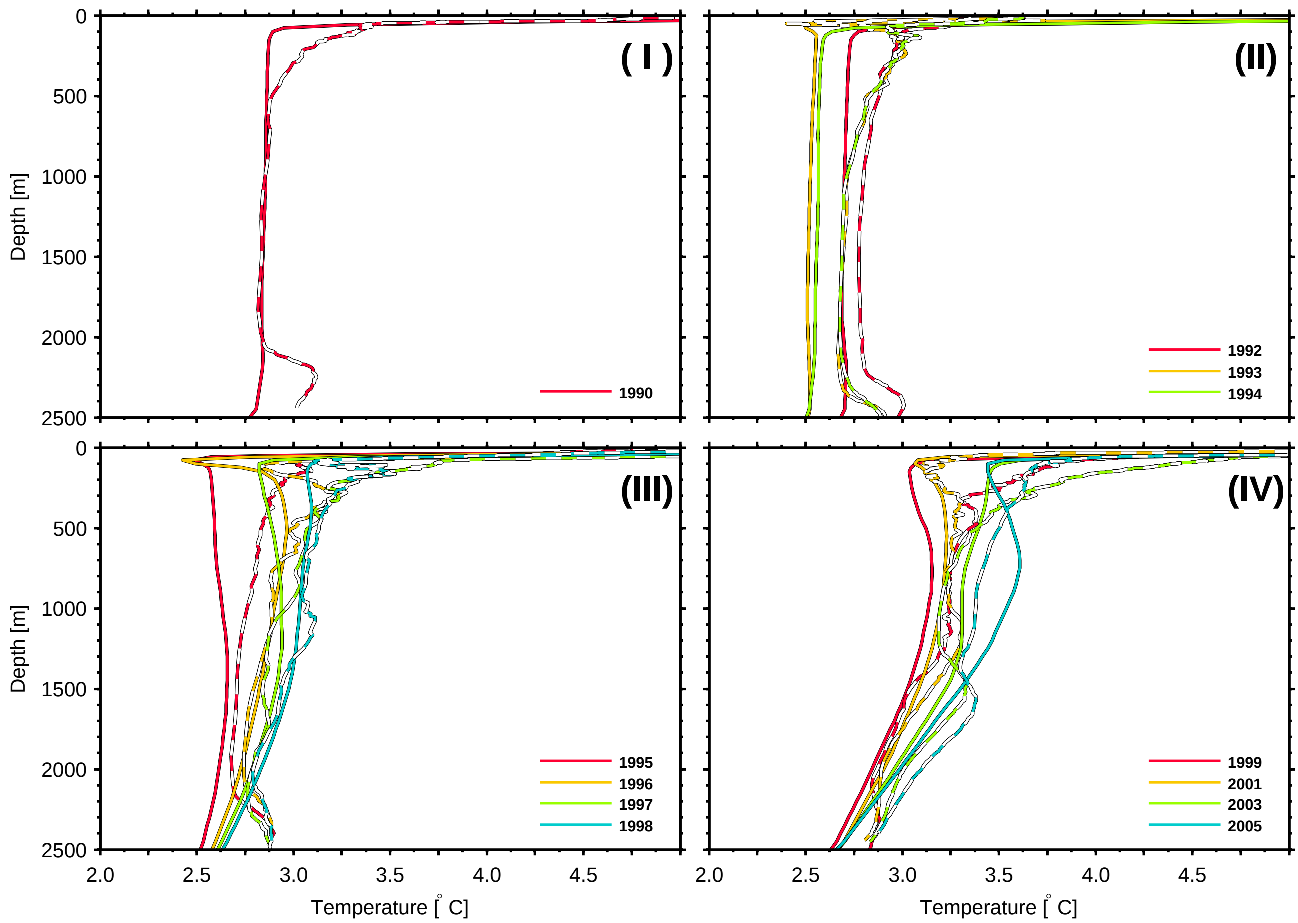

Figure 6. Vertical depth profiles of observed (dashed lines) temperature averaged over the AR7W cross section (http://cchdo.ucsd.edu) and modeled summer (JJA, solid lines) temperature averaged over the Labrador Sea index area (see Fig. 2a) for various years in the phase of increasing (I), maximal (II), decreasing (III) and minimal (IV) dLSW layer thickness (see Fig. 4).

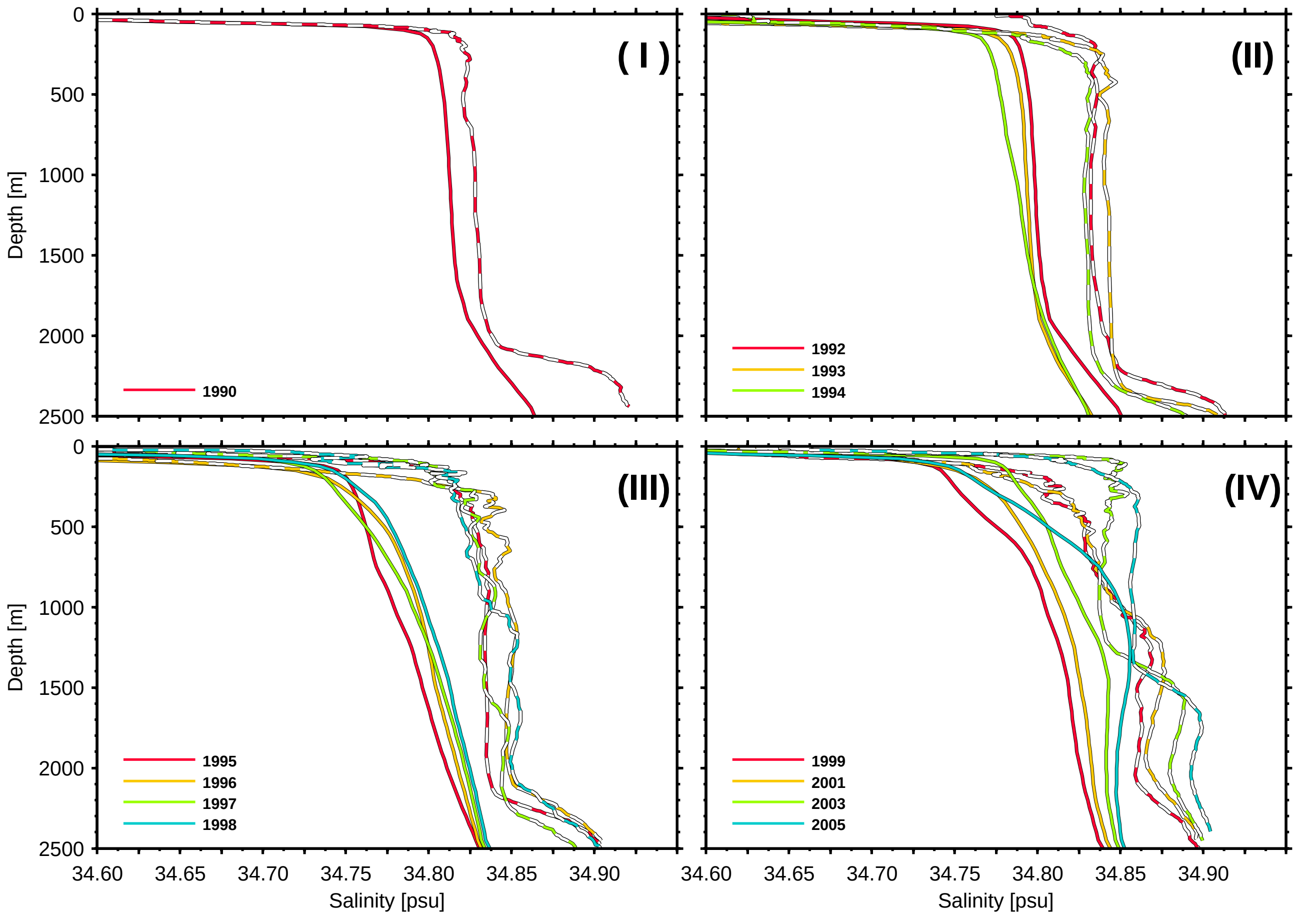

Figure 7. Vertical depth profiles of observed (dashed lines) salinity averaged over the AR7W cross section (http://cchdo.ucsd.edu) and modeled summer (JJA, solid lines) salinity averaged over the Labrador Sea index area (see Fig. 2a) for various years in the phase of increasing (I), maximal (II), decreasing (III) and minimal (IV) dLSW layer thickness (see Fig. 4).

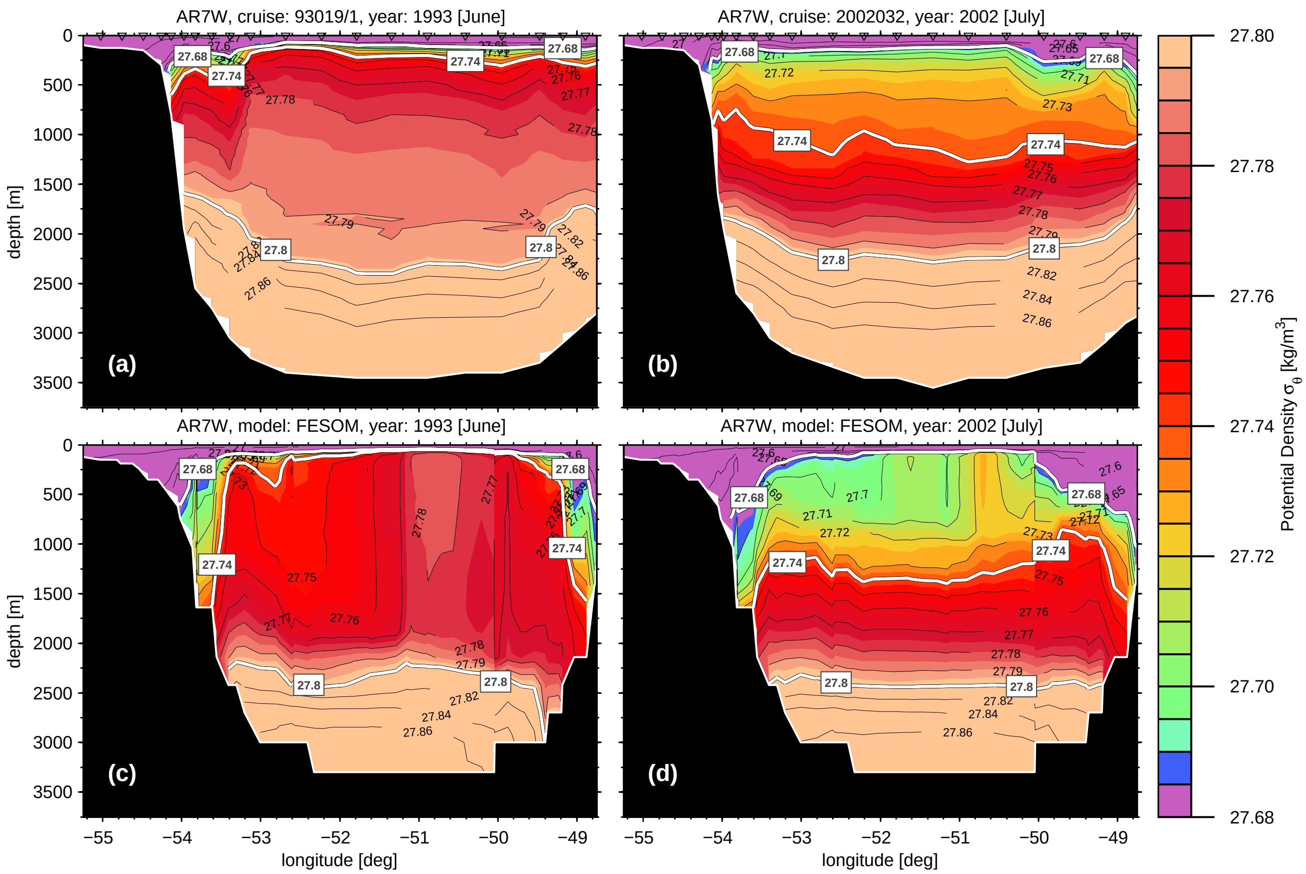

Figure 8. Potential density of the observed [*WOCE Data Product Committee*, 2002] (a)-(b) and modeled (c)-(d) AR7W cross sections in June and July for years with a thicker (1993, left column) and thinner (2002, right column) dLSW layer thickness. Thick white lines indicate the $\sigma_\theta = 27.68\,\mathrm{kg\,m^{-3}}$, $\sigma_\theta = 27.74\,\mathrm{kg\,m^{-3}}$ and $\sigma_\theta = 27.80\,\mathrm{kg\,m^{-3}}$ isopycnals to separate between uLSW and dLSW.

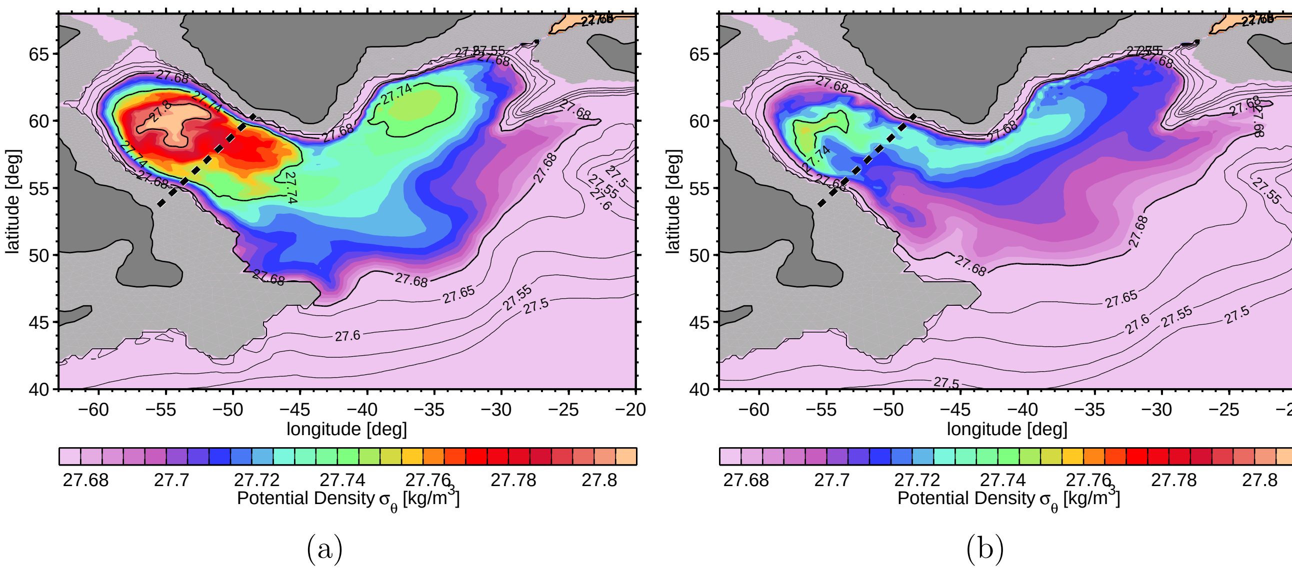

Figure 9. Horizontal mean potential density of the model data in the northwest Atlantic Ocean averaged over a depth from 500 m - 1000 m. In (a): June 1993 and (b): July 2002 for events with thicker and thinner dLSW layer thickness, respectively. Thick lines indicate the $\sigma_\theta = 27.68\ \mathrm{kg\,m^{-3}}$, $\sigma_\theta = 27.74\ \mathrm{kg\,m^{-3}}$ and $\sigma_\theta = 27.80\ \mathrm{kg\,m^{-3}}$ isopycnals. The dashed line marks the location of the AR7W cruise line.

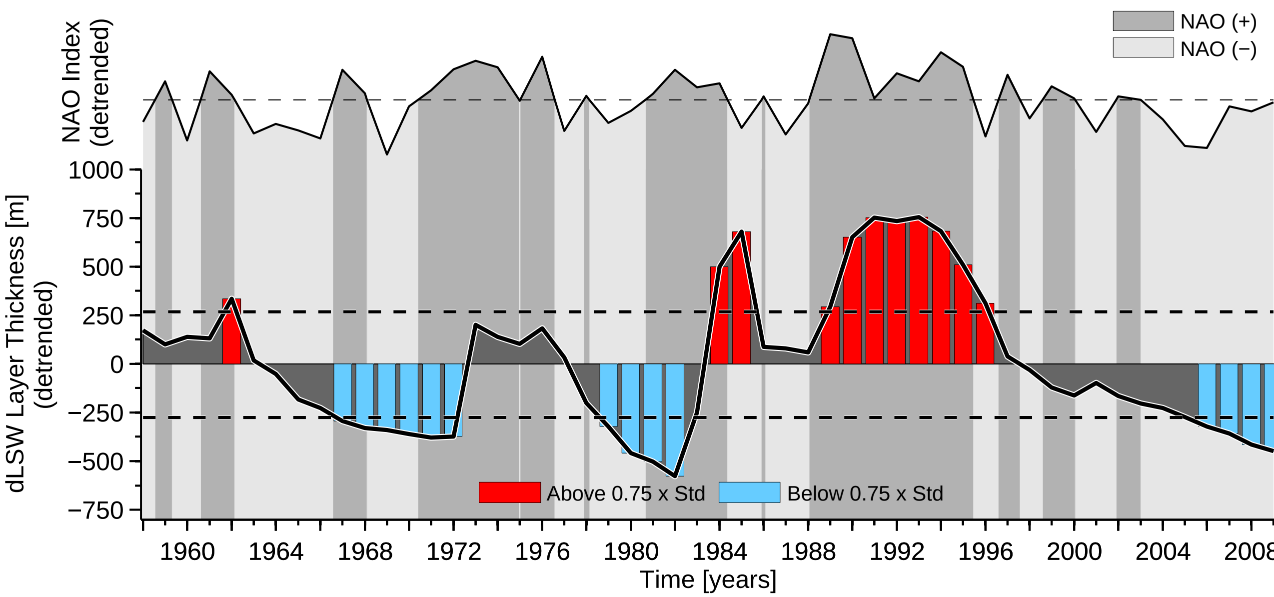

Figure 10. Detrended January, February and March averaged dLSW index (solid black line) for the entire simulation period from 1958 to 2009 and the 75% of standard deviation limits (dashed lines). Years when the dLSW layer thickness was above and below 75% of standard deviation are marked by red and blue bars, respectively. These time slices are used in the composite map analysis (CMA) (Figs. 11, 12 and 13b). Dark and light grey areas in the background indicate the positive and negative phases of the detrended normalized NAO index averaged over January, February and March and derived from the COREv2 data set [*Large and Yeager*, 2009], respectively. Std: standard deviation.

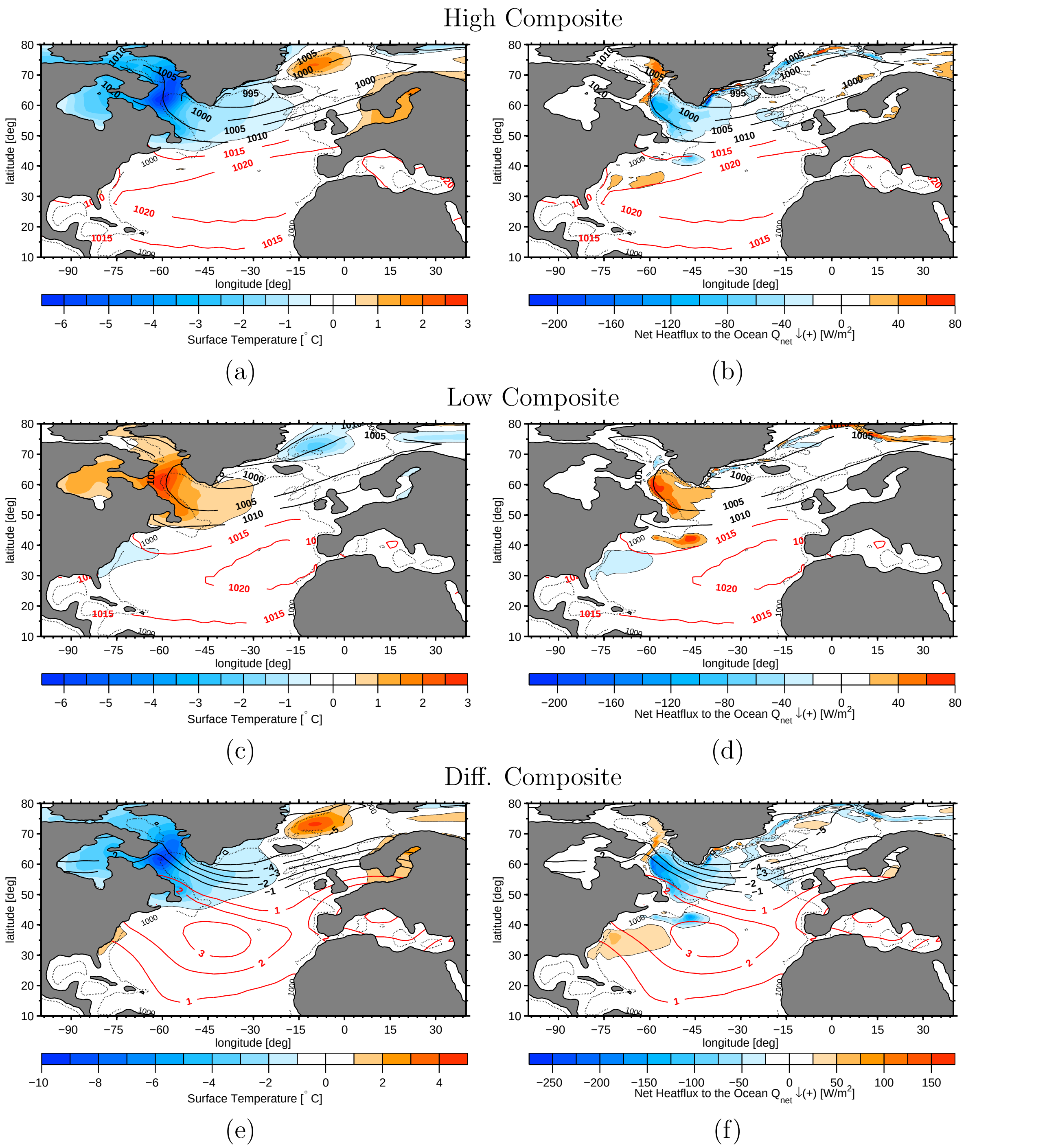

Figure 11. Composite maps of the winter (DJF) seasonal atmospheric surface temperature (left column) and net heat flux to the ocean (right column, downward heat flux positive) with the January, February and March averaged dLSW index (see Fig. 10). (a)-(b): high composite maps, (c)-(d): low composite maps and (e)-(f): difference between high and low composite maps. Contour lines show the composite maps of SLP (units SLP: hPa). Black and red contour lines mark the low and high pressure systems, respectively. The 1000 m bathymetry is indicated by a dotted contour line.

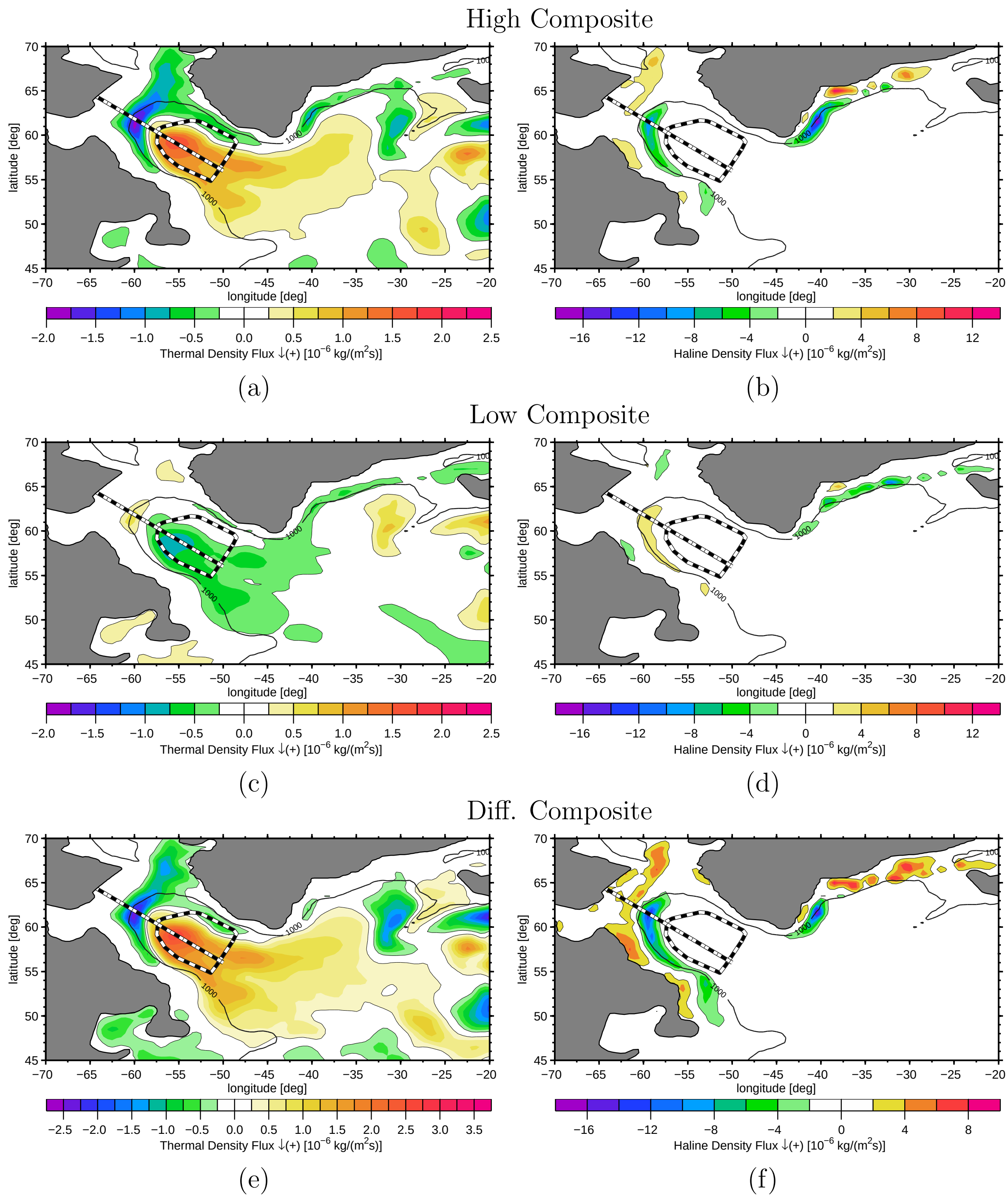

Figure 12. Composite maps of the winter (DJF) seasonal thermal (left column) and haline (right column) surface density flux (downward density flux = surface density gain: positive values) with the January, February and March averaged dLSW index (see Fig. 10). (a)-(b): high composite maps, (c)-(d): low composite maps, and (e)-(f): difference between high and low composite maps (units are $10^{-6}\,\mathrm{kg/(m^2s)}$). The dashed and dashed-dotted lines mark the area of the LSW index definition and the cross-section used in Fig. 13b, respectively. The 1000 m bathymetry is indicated by a solid contour line. Note the different scaling for the left and right

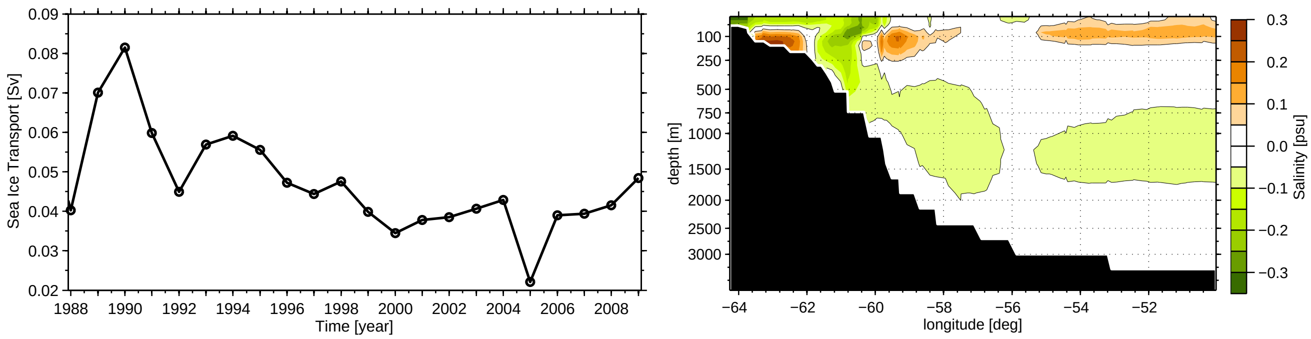

(a) (b)

Figure 13. (a): Time evolution of winter (DJF) seasonal sea ice transport through Davis Strait for the period from 1988-2009. (b): difference composite map of the winter (DJF) salinity of a northwest to southeast vertical cross section through the Labrador Sea (Fig. 10) with the January, February and March averaged dLSW index.

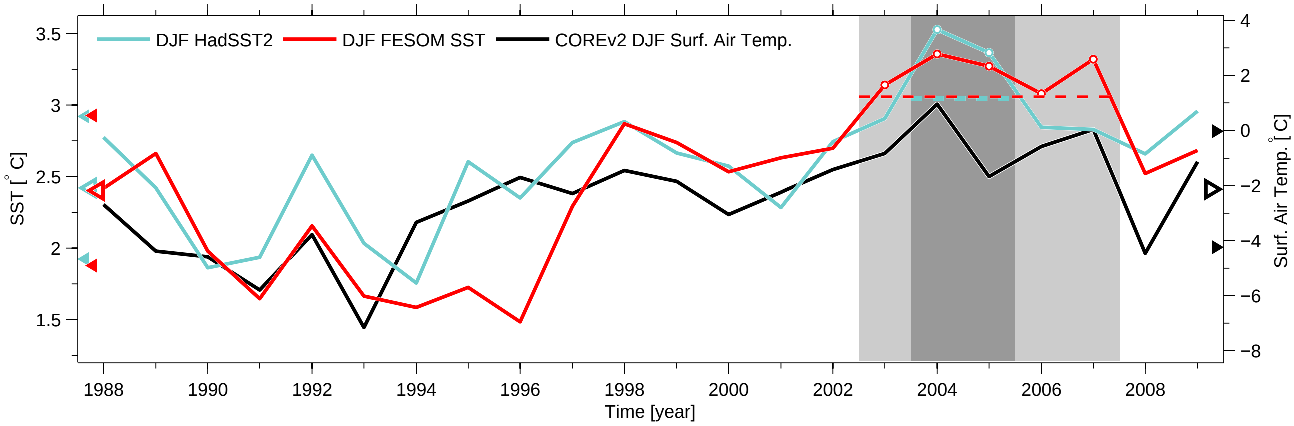

Figure 14. Mean winter (DJF) observational derived Hadley Centre v2 (blue line, *Rayner et al.* [2003], http://www.metoffice.gov.uk/hadobs/hadsst2/) and modeled FESOM (red line) sea surface temperature (SST) averaged over the Labrador Sea index area (see Fig. 2a). Mean values and standard deviations for the period 1958-2009 are indicated by empty and filled triangles, respectively. The above 125% of standard deviation limit is indicated by dashed lines. Years when the SST in the Labrador Sea was above this limit are highlighted by circles. The different time spans when the FESOM and Hadley Center SST was above 125% of standard deviation are highlighted by light and dark grey areas, respectively. The black line represents the time evolution of the COREv2 surface air temperature forcing field averaged over the Labrador Sea index area.

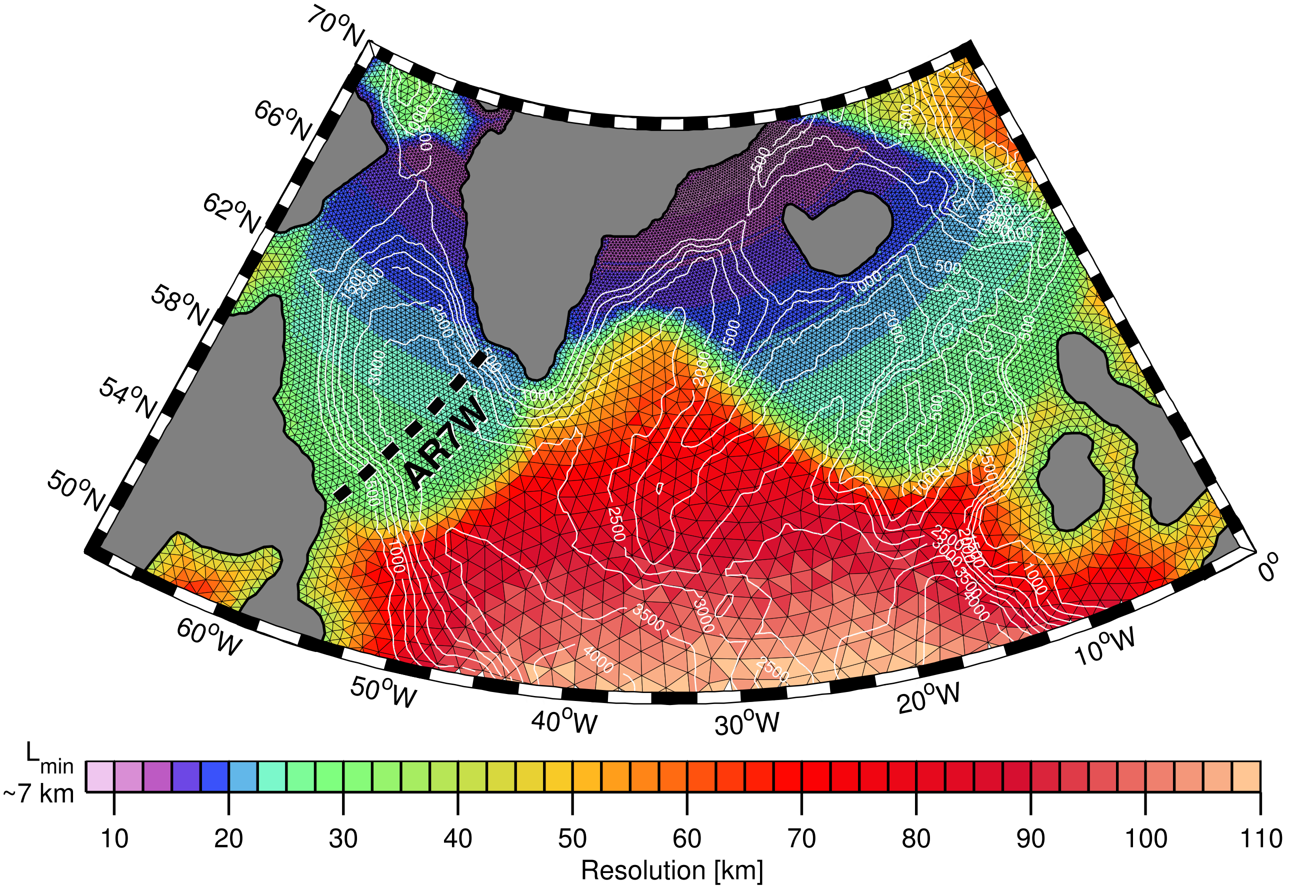

70°N
66°N
62°N
58°N
54°N
50°N
60°W
50°W
40°W
30°W
20°W
10°W
0°
AR7W
L min ~7 km
10
20
30
40
50
60
70
80
90
100
110
Resolution [km]

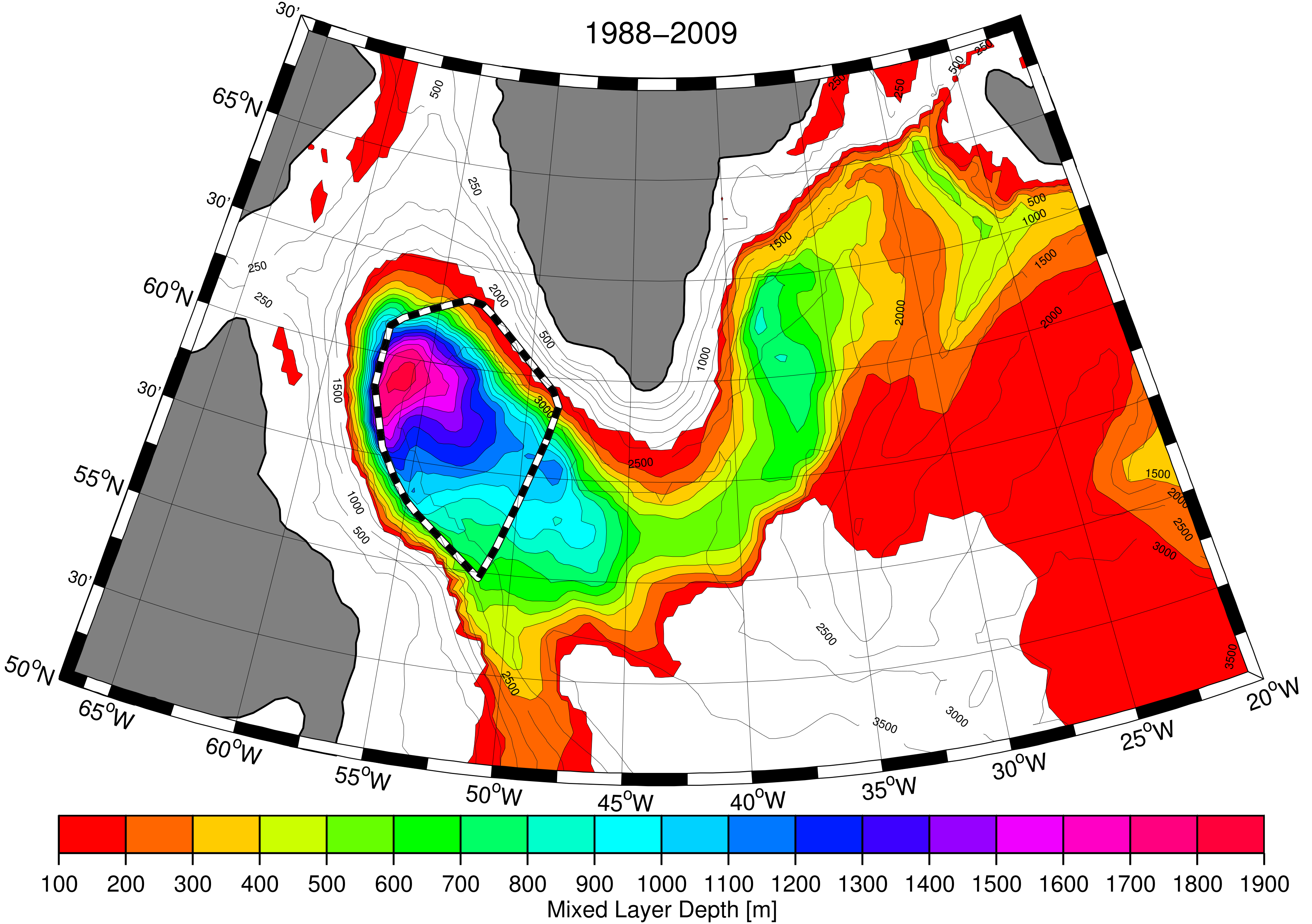
1988–2009
65°N
60°N
55°N
50°N
30'
65°W
60°W
55°W
50°W
45°W
40°W
35°W
30°W
25°W
20°W
250
500
1000
1500
2000
2500
3000
3500
100
200
300
400
500
600
700
800
900
1000
1100
1200
1300
1400
1500
1600
1700
1800
1900
Mixed Layer Depth [m]

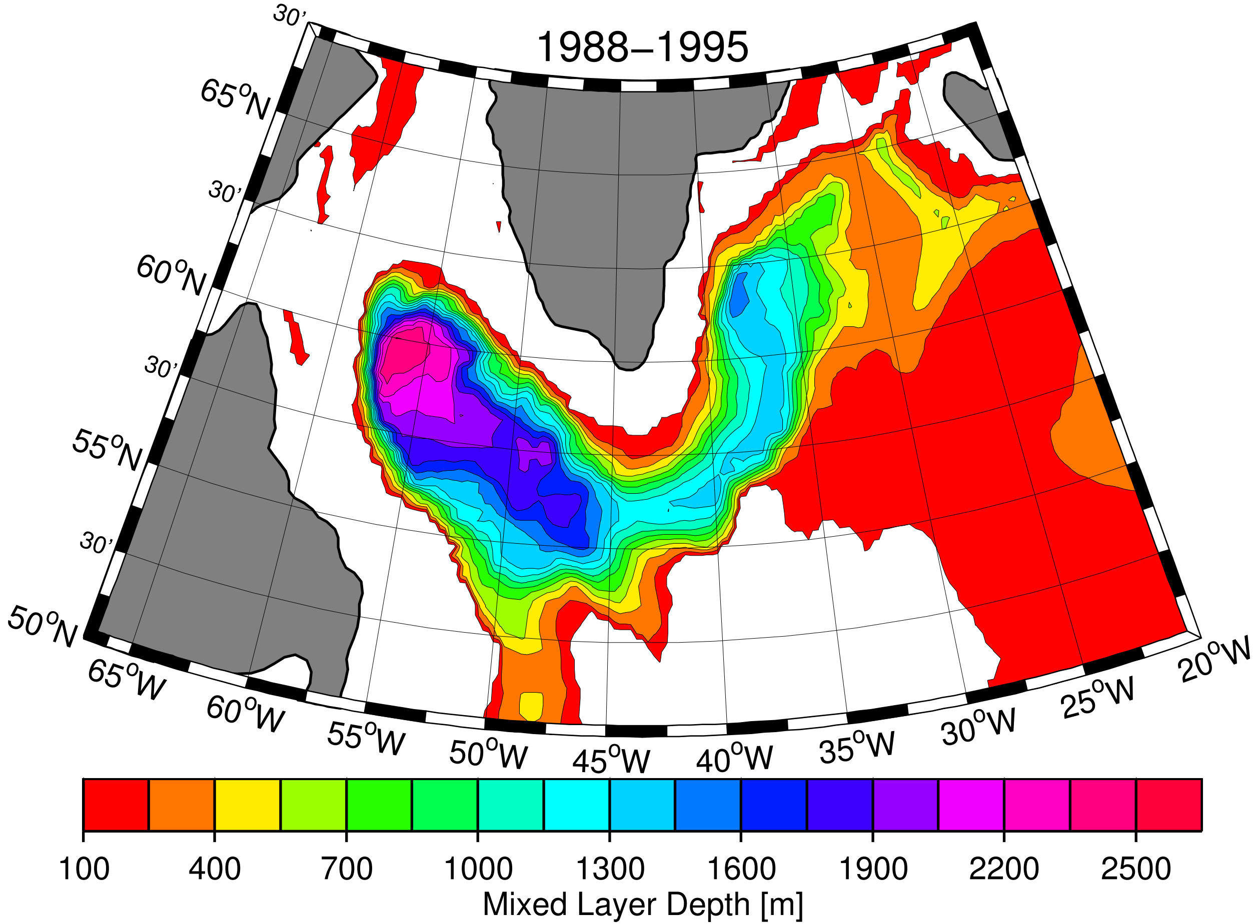

1988–1995
65°N
60°N
55°N
50°N
30'
65°W
60°W
55°W
50°W
45°W
40°W
35°W
30°W
25°W
20°W
100
400
700
1000
1300
1600
1900
2200
2500
Mixed Layer Depth [m]

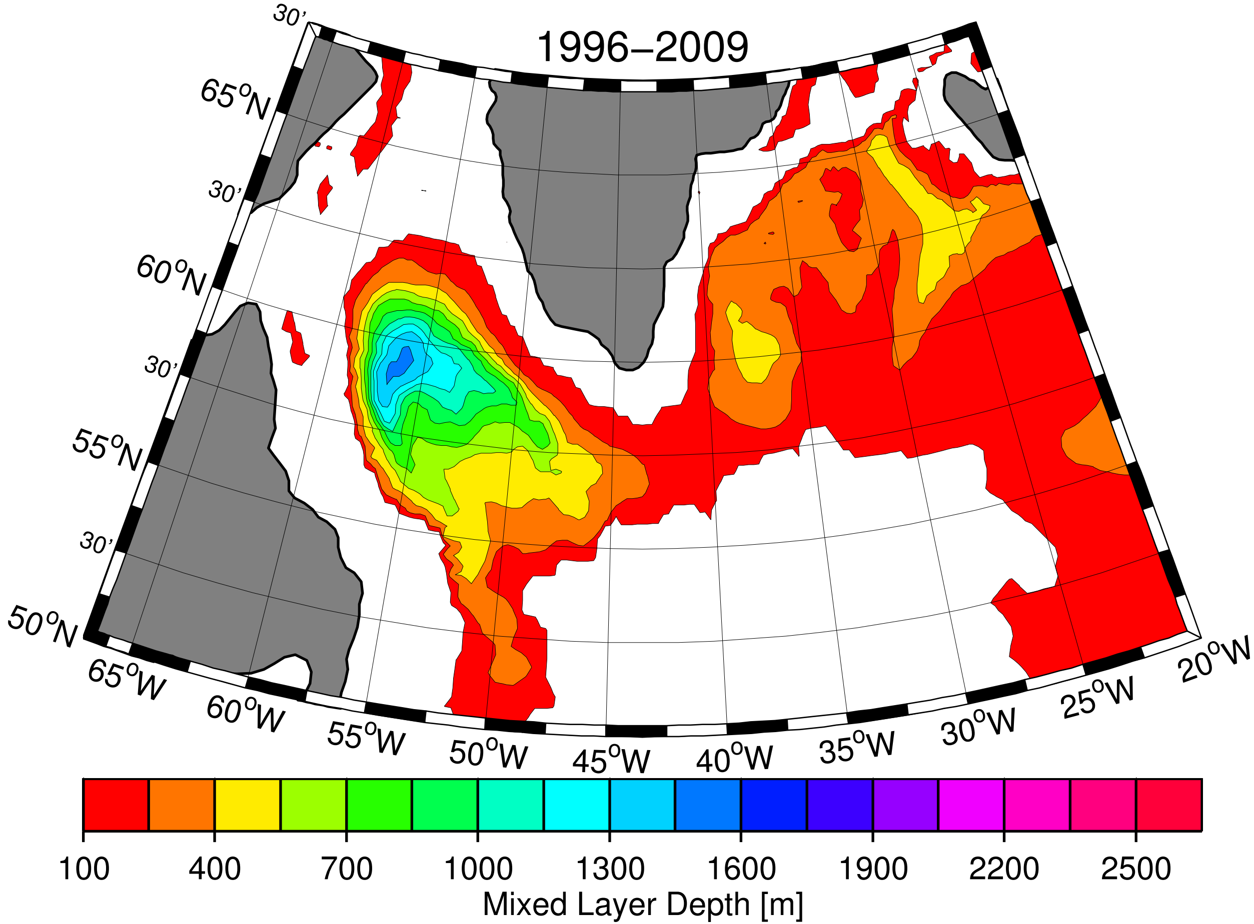
1996–2009
65°N
60°N
55°N
50°N
30'
30'
30'
30'
65°W
60°W
55°W
50°W
45°W
40°W
35°W
30°W
25°W
20°W
100
400
700
1000
1300
1600
1900
2200
2500
Mixed Layer Depth [m]

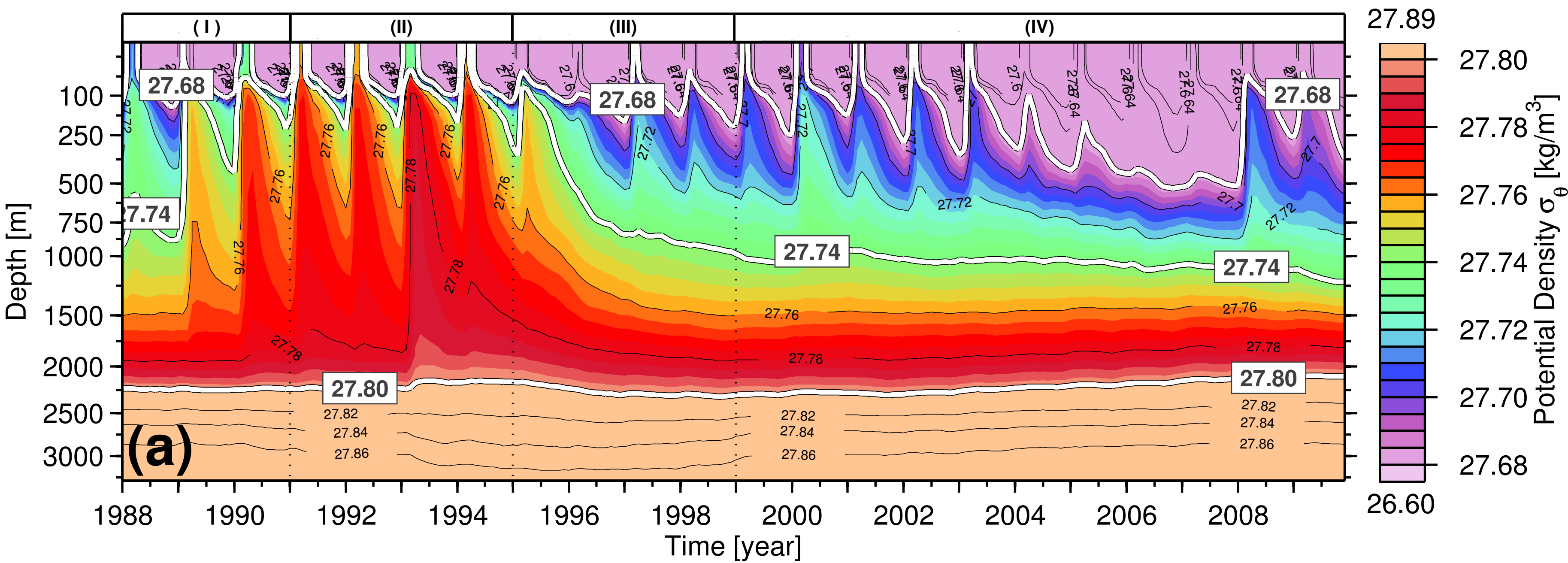

(I)
(II)
(III)
(IV)
27.68
27.74
27.80
27.76
27.78
27.72
27.7
27.82
27.84
27.86
(a)
Depth [m]
100
250
500
750
1000
1500
2000
2500
3000
Time [year]
1988
1990
1992
1994
1996
1998
2000
2002
2004
2006
2008
27.89
26.60
Potential Density σ_θ [kg/m^3]

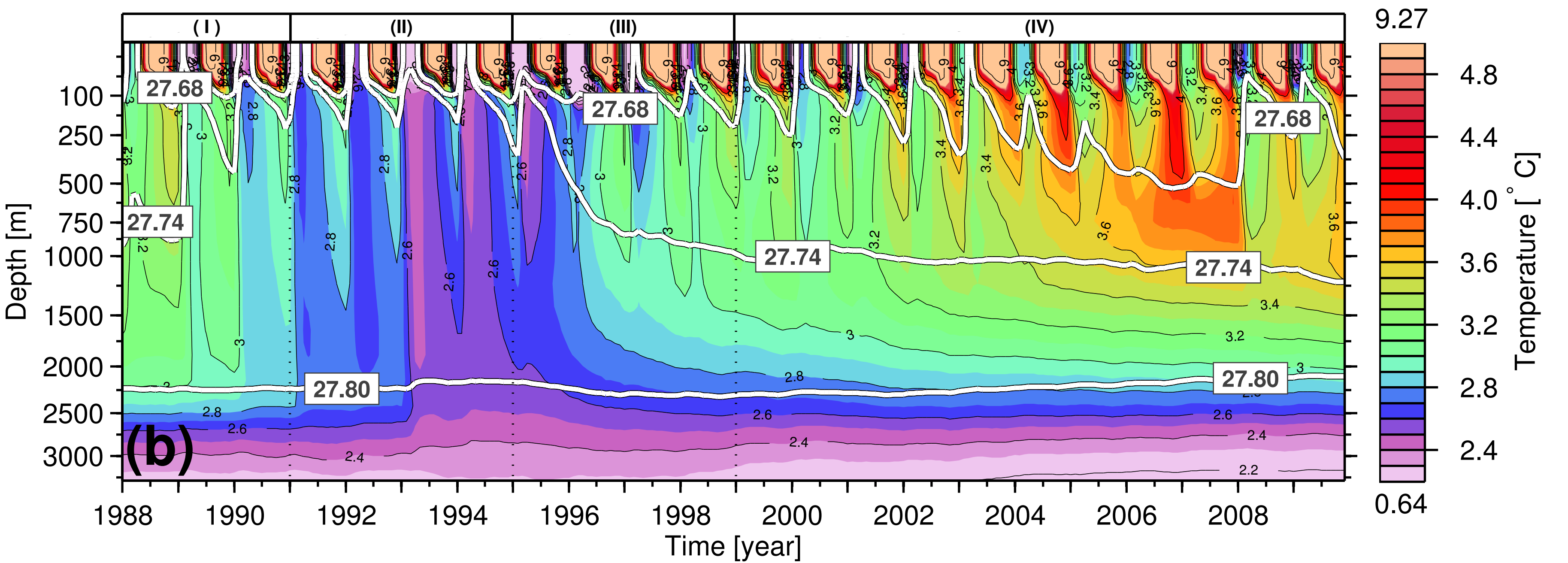

(I)
(II)
(III)
(IV)
27.68
27.74
27.80
(b)
Depth [m]
Time [year]
Temperature [°C]
9.27
0.64

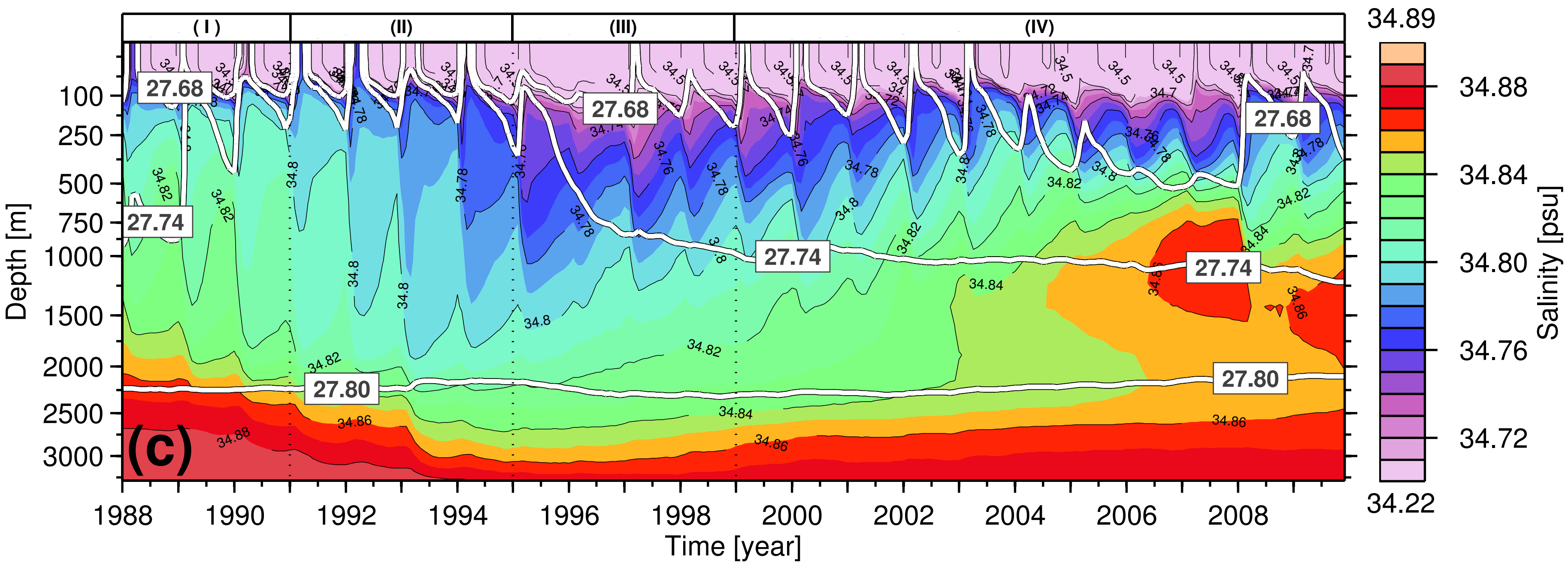

(I)
(II)
(III)
(IV)
27.68
27.74
27.80
(c)
Depth [m]
Time [year]
Salinity [psu]
34.89
34.88
34.84
34.80
34.76
34.72
34.22

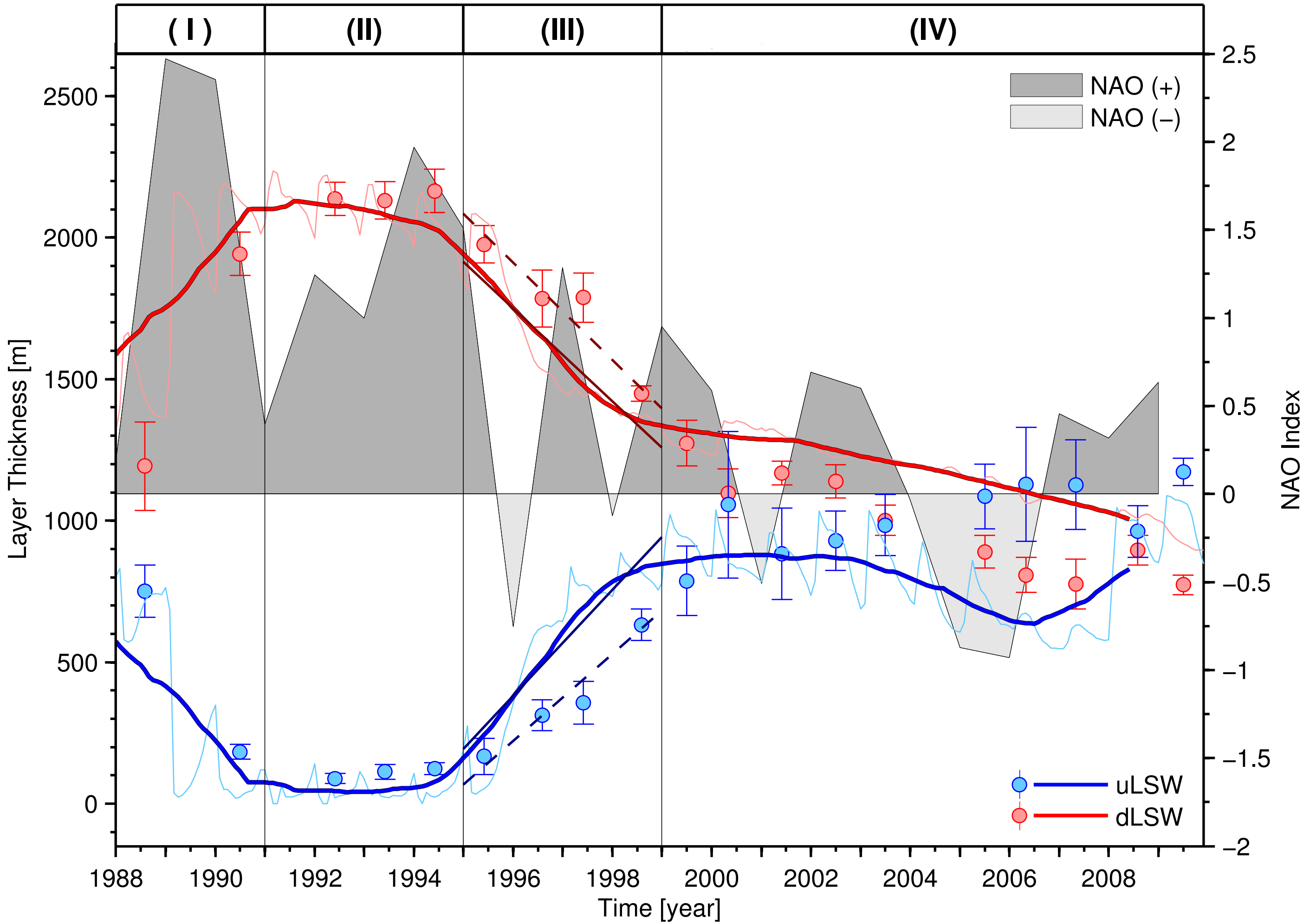

(I)
(II)
(III)
(IV)
NAO (+)
NAO (–)
uLSW
dLSW
Layer Thickness [m]
NAO Index
Time [year]
2500
2000
1500
1000
500
0
2.5
2
1.5
1
0.5
0
–0.5
–1
–1.5
–2
1988
1990
1992
1994
1996
1998
2000
2002
2004
2006
2008

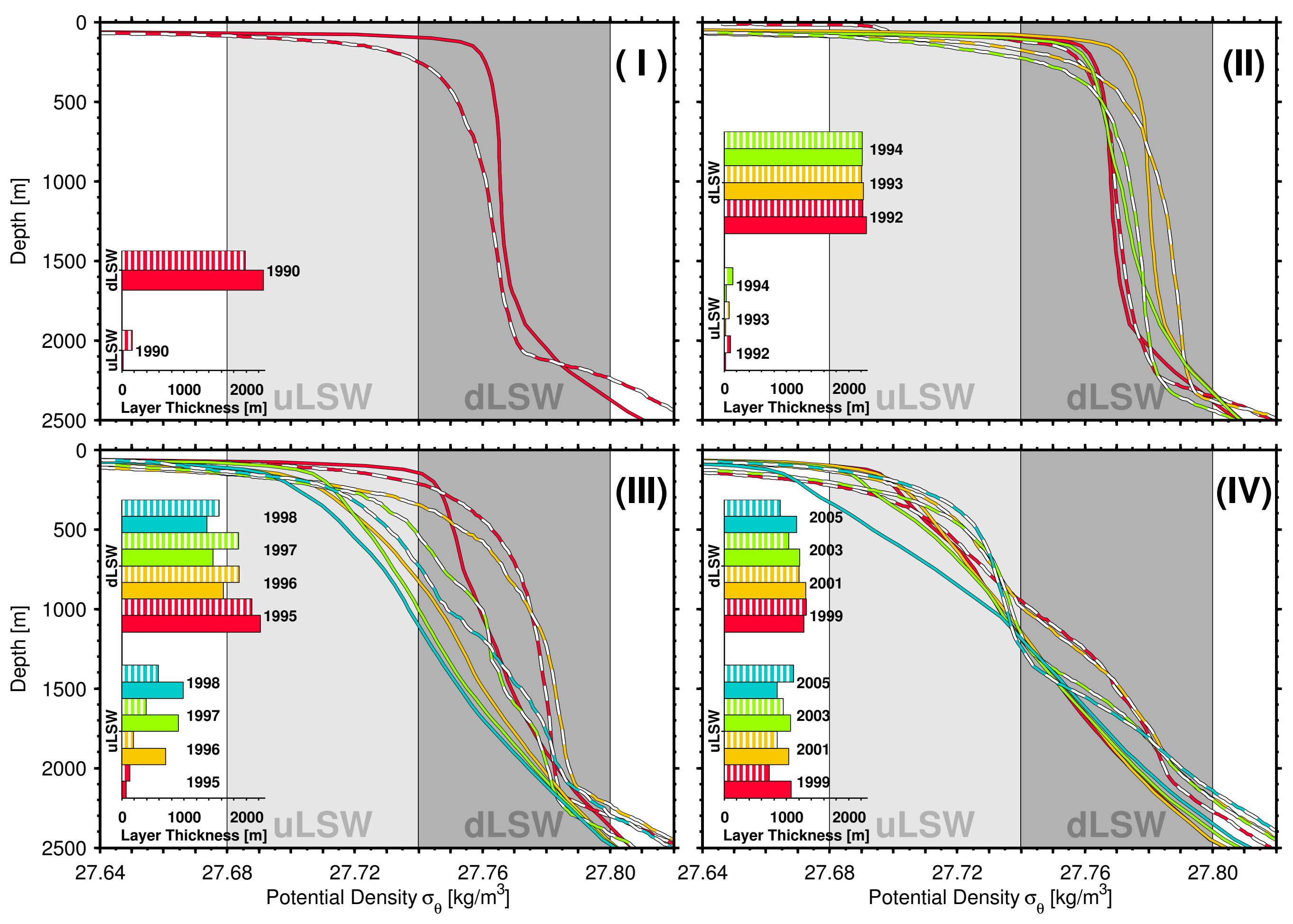

(I)
(II)
(III)
(IV)
Depth [m]
0
500
1000
1500
2000
2500
dLSW
uLSW
1990
1994
1993
1992
1998
1997
1996
1995
2005
2003
2001
1999
0
1000
2000
Layer Thickness [m]
uLSW
dLSW
27.64
27.68
27.72
27.76
27.80
Potential Density σ_θ [kg/m^3]

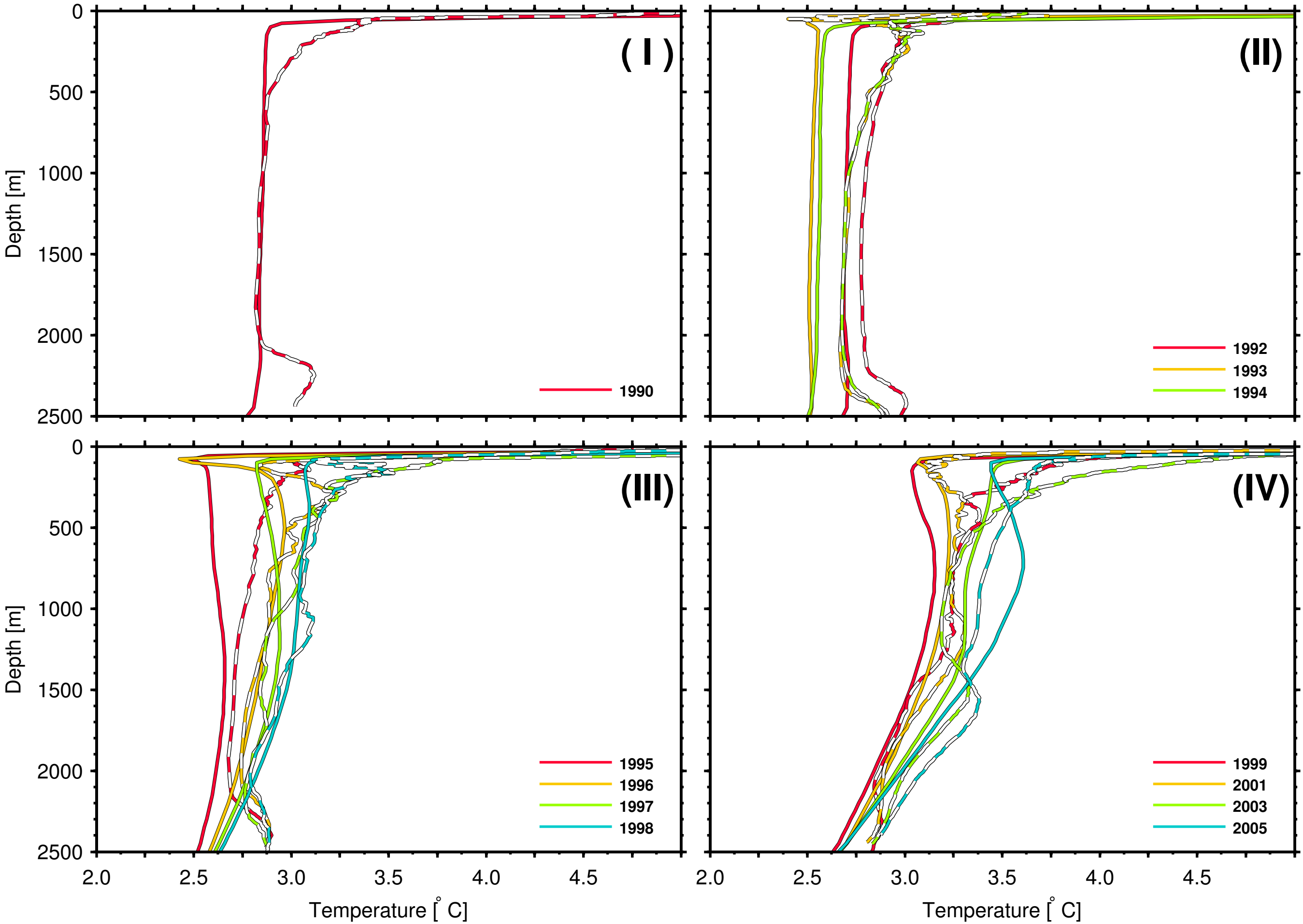

(I)
(II)
(III)
(IV)
1990
1992
1993
1994
1995
1996
1997
1998
1999
2001
2003
2005
Depth [m]
Temperature [° C]
0
500
1000
1500
2000
2500
2.0
2.5
3.0
3.5
4.0
4.5

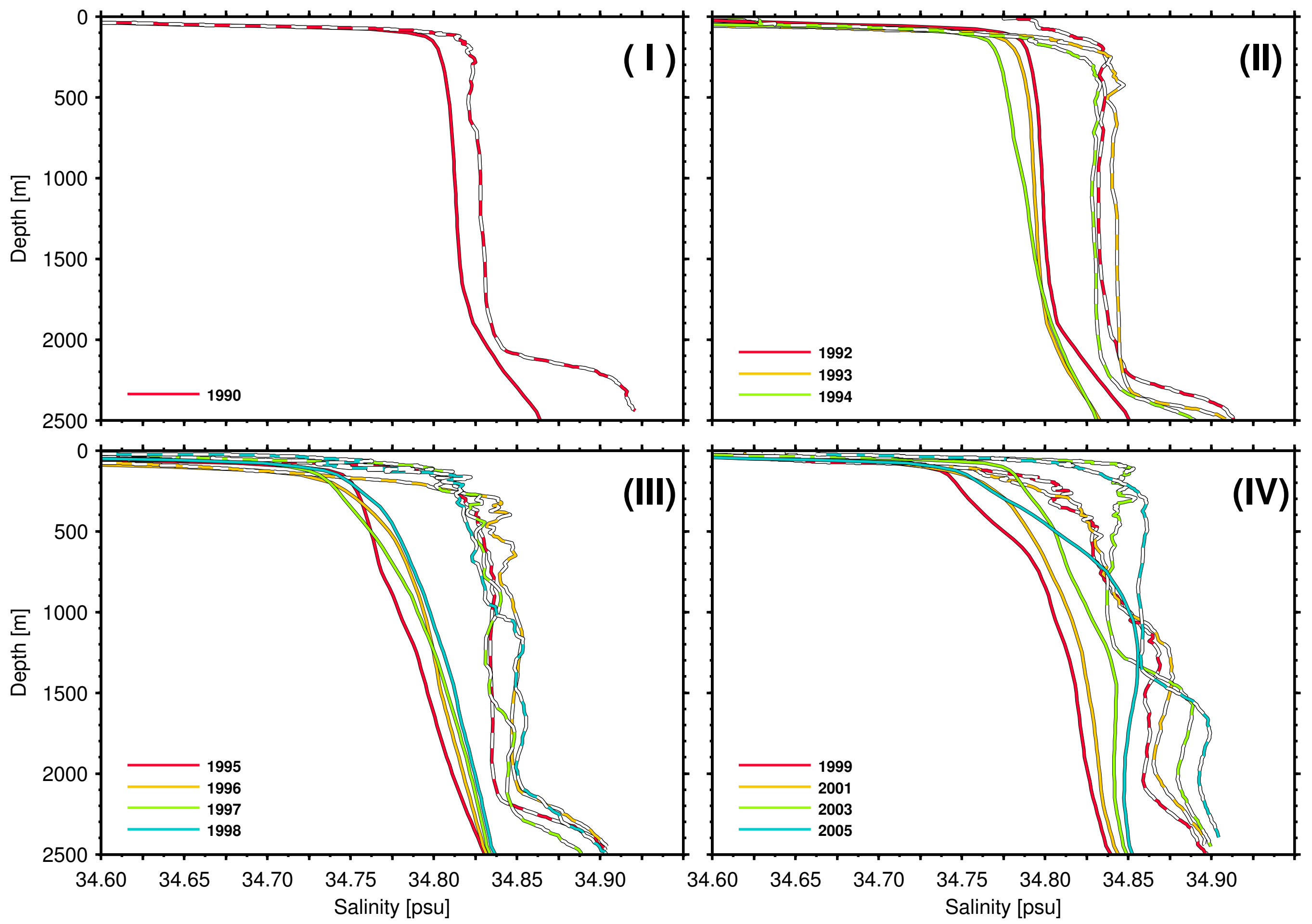

(I)
(II)
(III)
(IV)
1990
1992
1993
1994
1995
1996
1997
1998
1999
2001
2003
2005
Depth [m]
Salinity [psu]
0
500
1000
1500
2000
2500
34.60
34.65
34.70
34.75
34.80
34.85
34.90

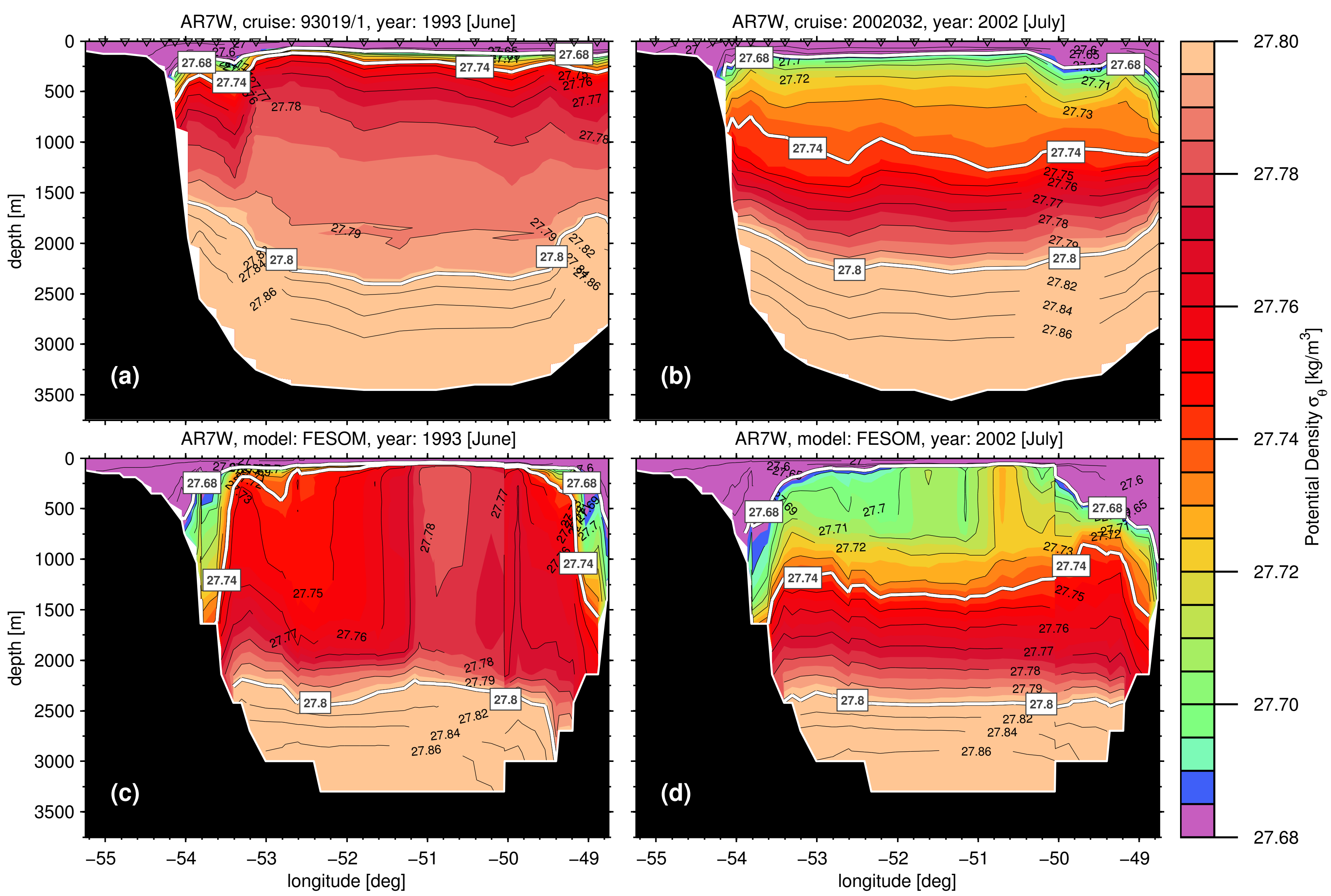

AR7W, cruise: 93019/1, year: 1993 [June]
AR7W, cruise: 2002032, year: 2002 [July]
AR7W, model: FESOM, year: 1993 [June]
AR7W, model: FESOM, year: 2002 [July]
(a)
(b)
(c)
(d)
depth [m]
longitude [deg]
Potential Density σθ [kg/m3]
27.68
27.74
27.8

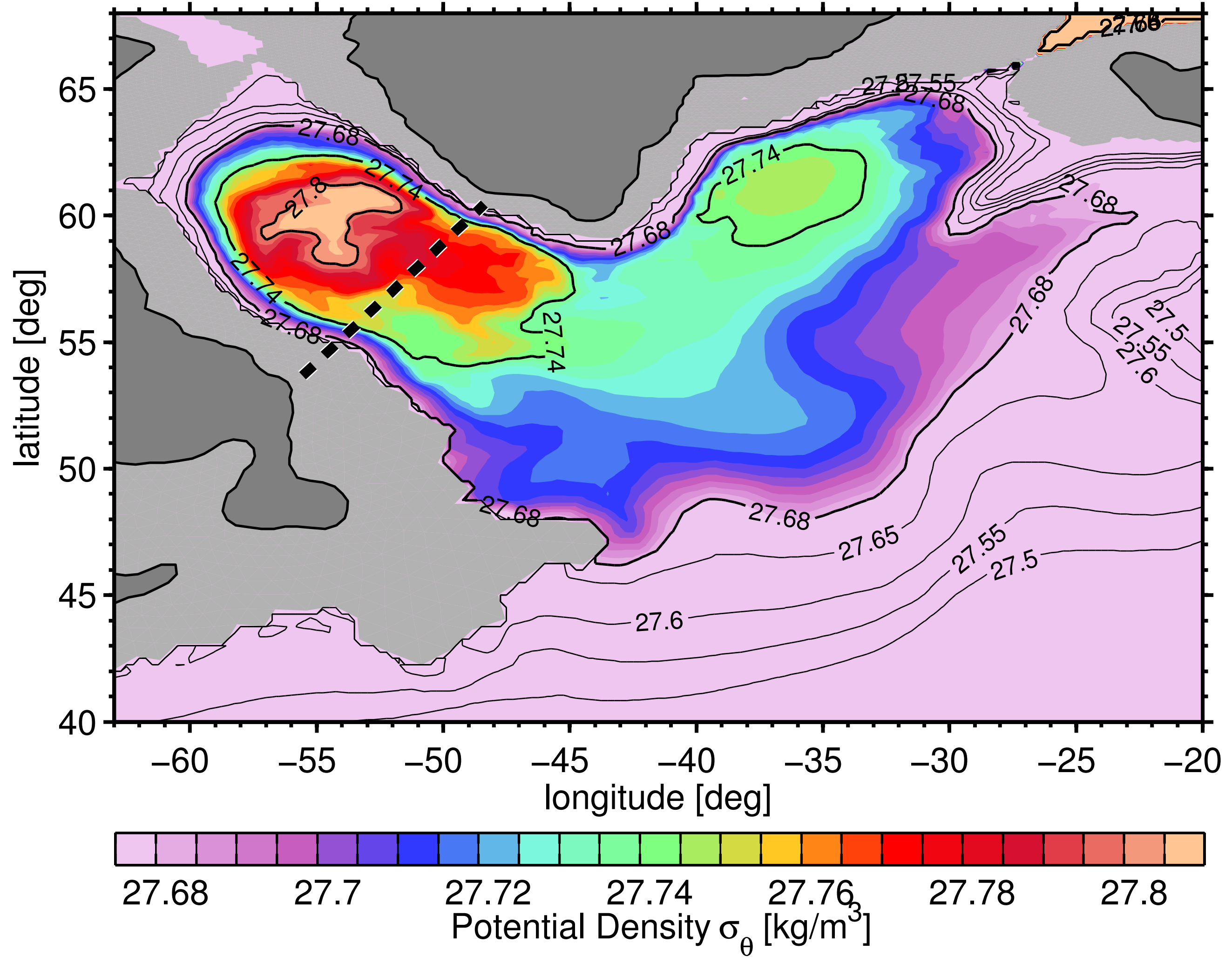
latitude [deg]
longitude [deg]
Potential Density σ_θ [kg/m^3]
27.68
27.7
27.72
27.74
27.76
27.78
27.8
27.74
27.65
27.6
27.55
27.5

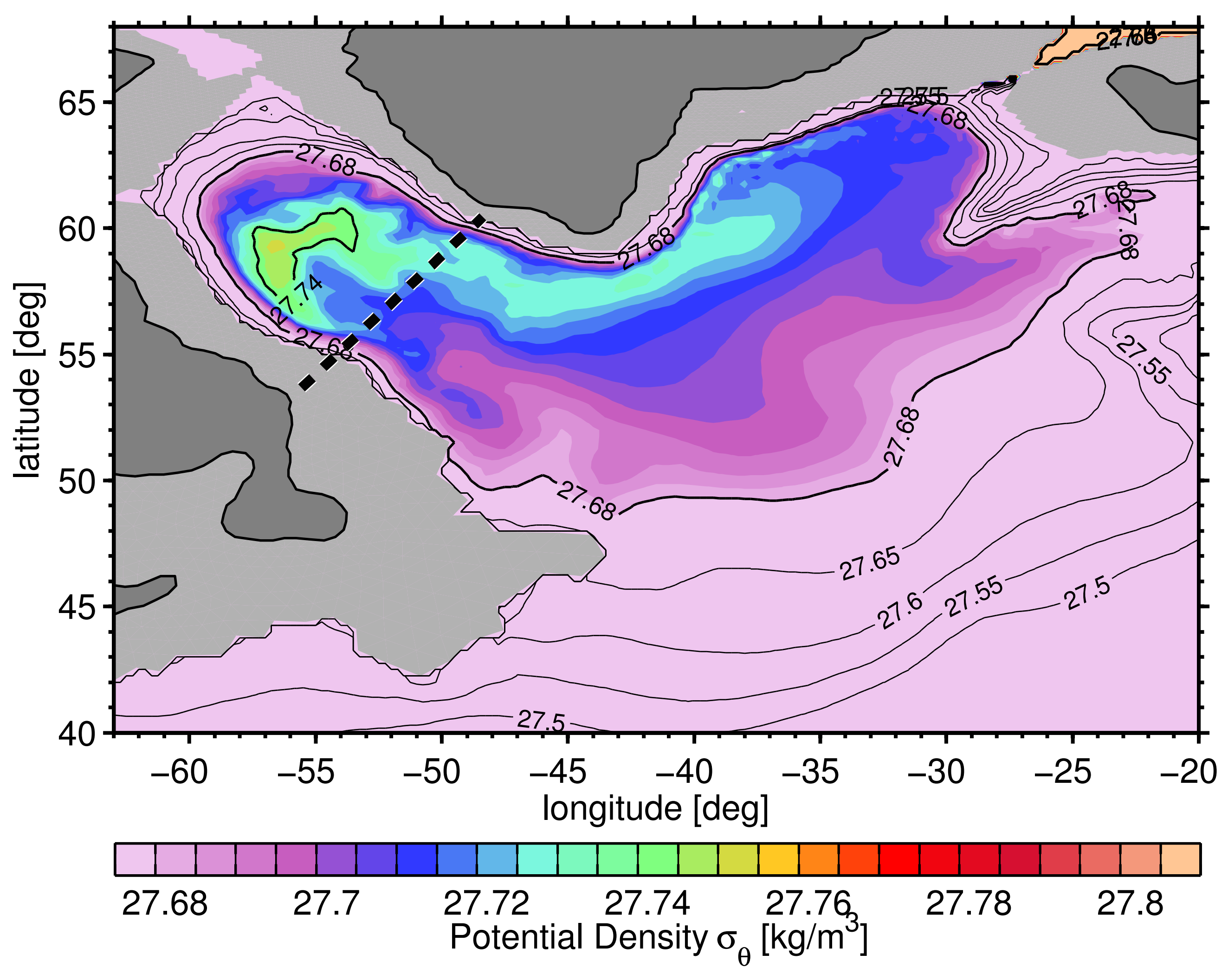

latitude [deg]
longitude [deg]
Potential Density σ_θ [kg/m^3]
27.68
27.7
27.72
27.74
27.76
27.78
27.8
27.65
27.6
27.55
27.5

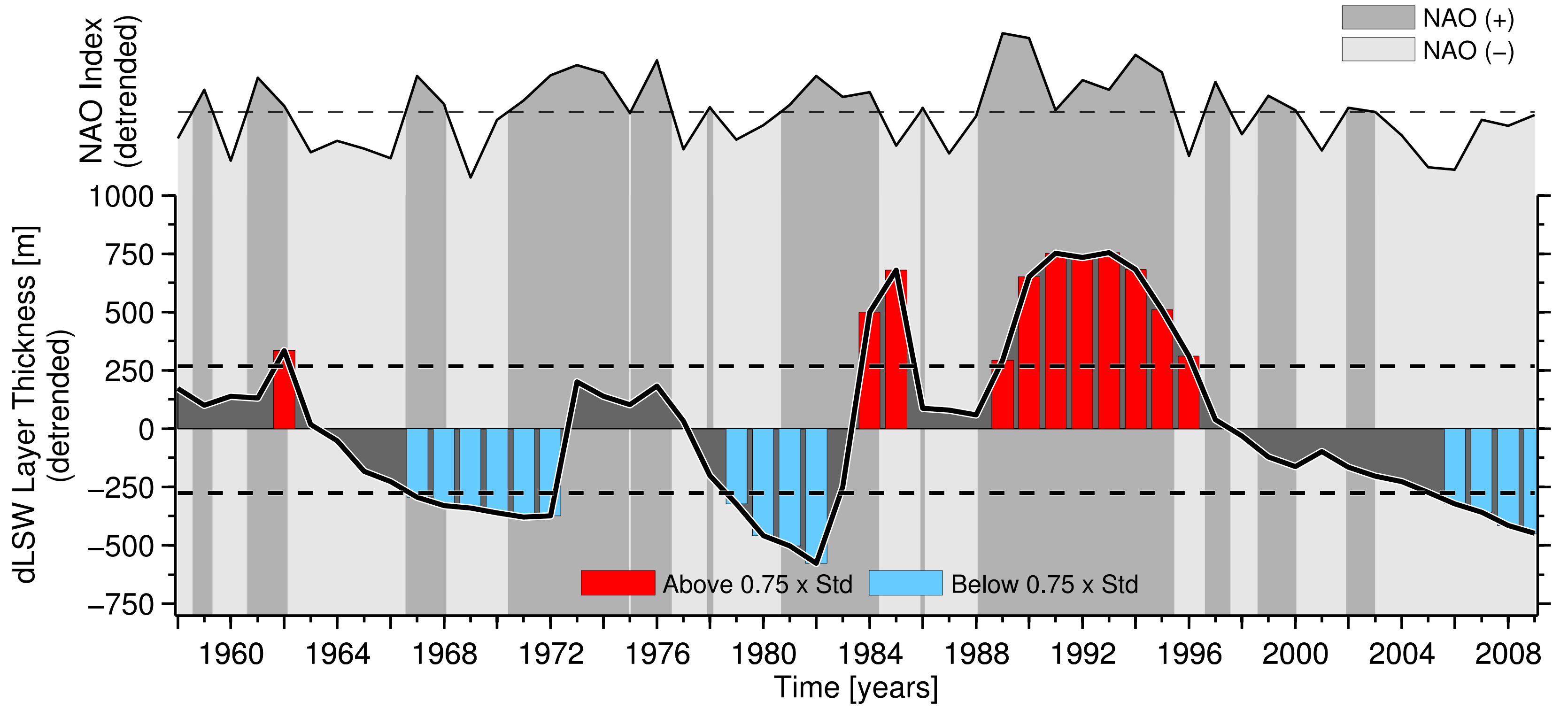
NAO (+)
NAO (–)
NAO Index (detrended)
dLSW Layer Thickness [m] (detrended)
1000
750
500
250
0
−250
−500
−750
Above 0.75 x Std
Below 0.75 x Std
1960
1964
1968
1972
1976
1980
1984
1988
1992
1996
2000
2004
2008
Time [years]

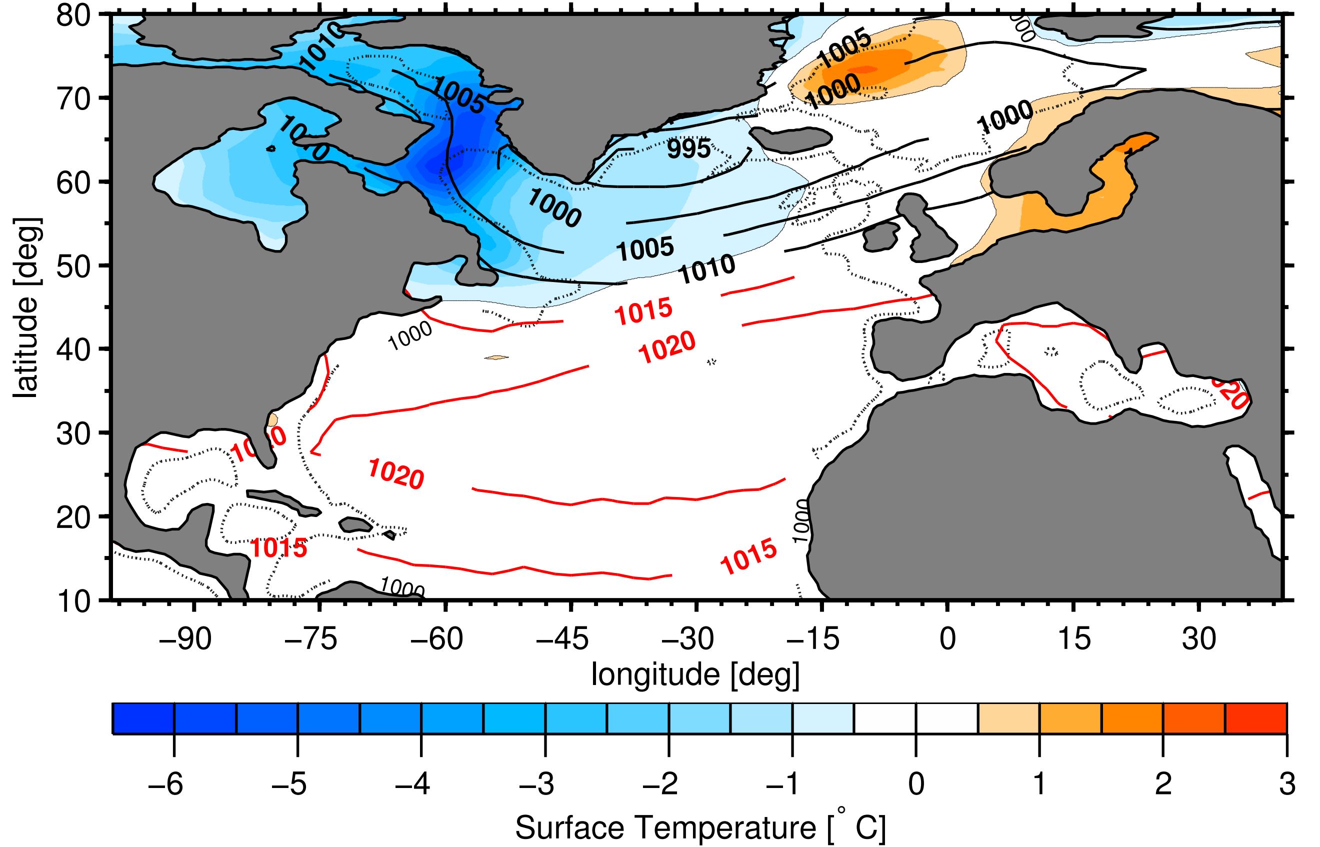

latitude [deg]
longitude [deg]
80
70
60
50
40
30
20
10
−90
−75
−60
−45
−30
−15
0
15
30
1010
1005
1000
995
1005
1010
1015
1020
1015
1020
1015
1005
1000
1000
1000
1000
1000
−6
−5
−4
−3
−2
−1
0
1
2
3
Surface Temperature [° C]

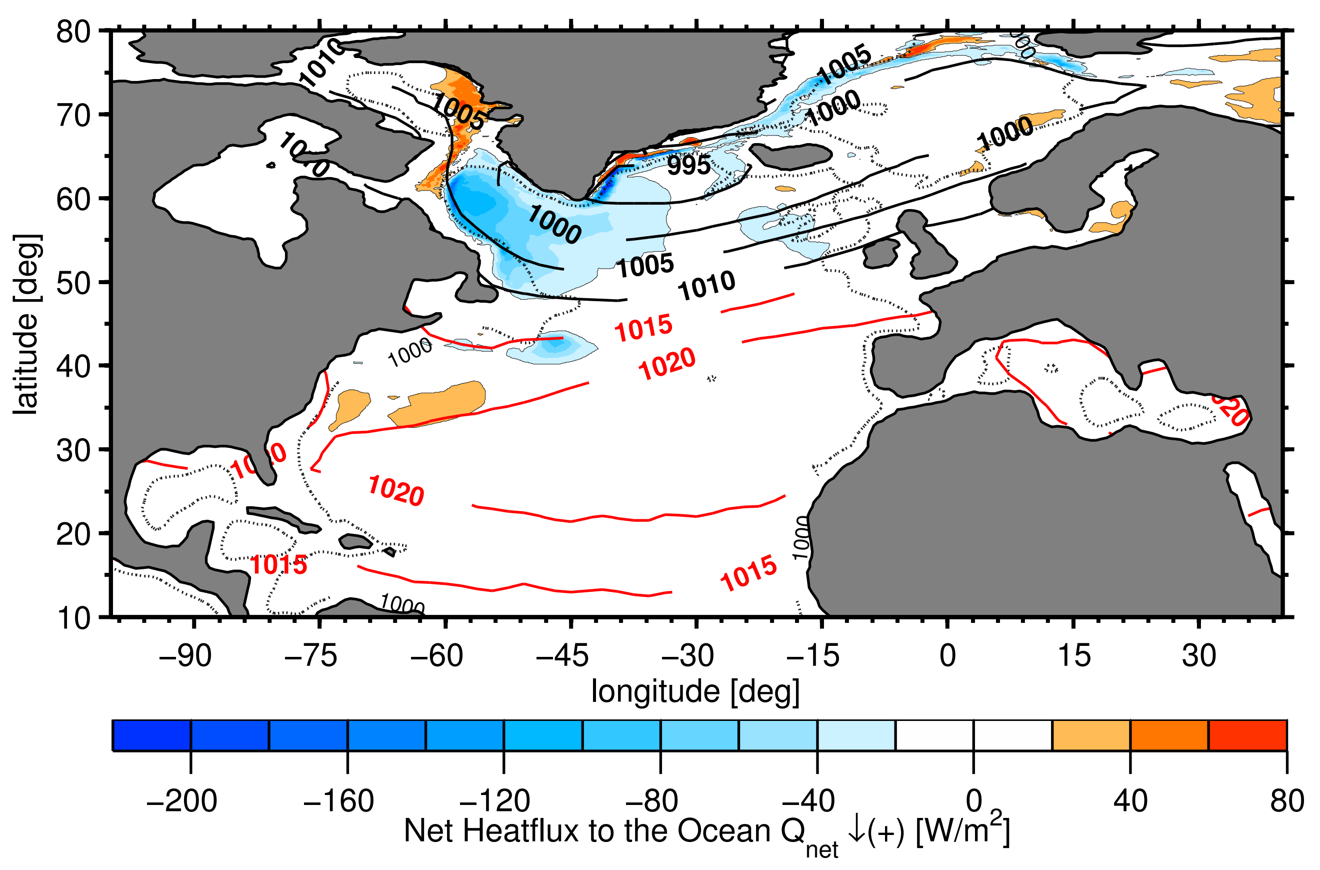

latitude [deg]
longitude [deg]
Net Heatflux to the Ocean $Q_{net}\downarrow(+)$ [W/m^2]
80
70
60
50
40
30
20
10
−90
−75
−60
−45
−30
−15
0
15
30
−200
−160
−120
−80
−40
0
40
80
1010
1005
1000
995
1015
1020

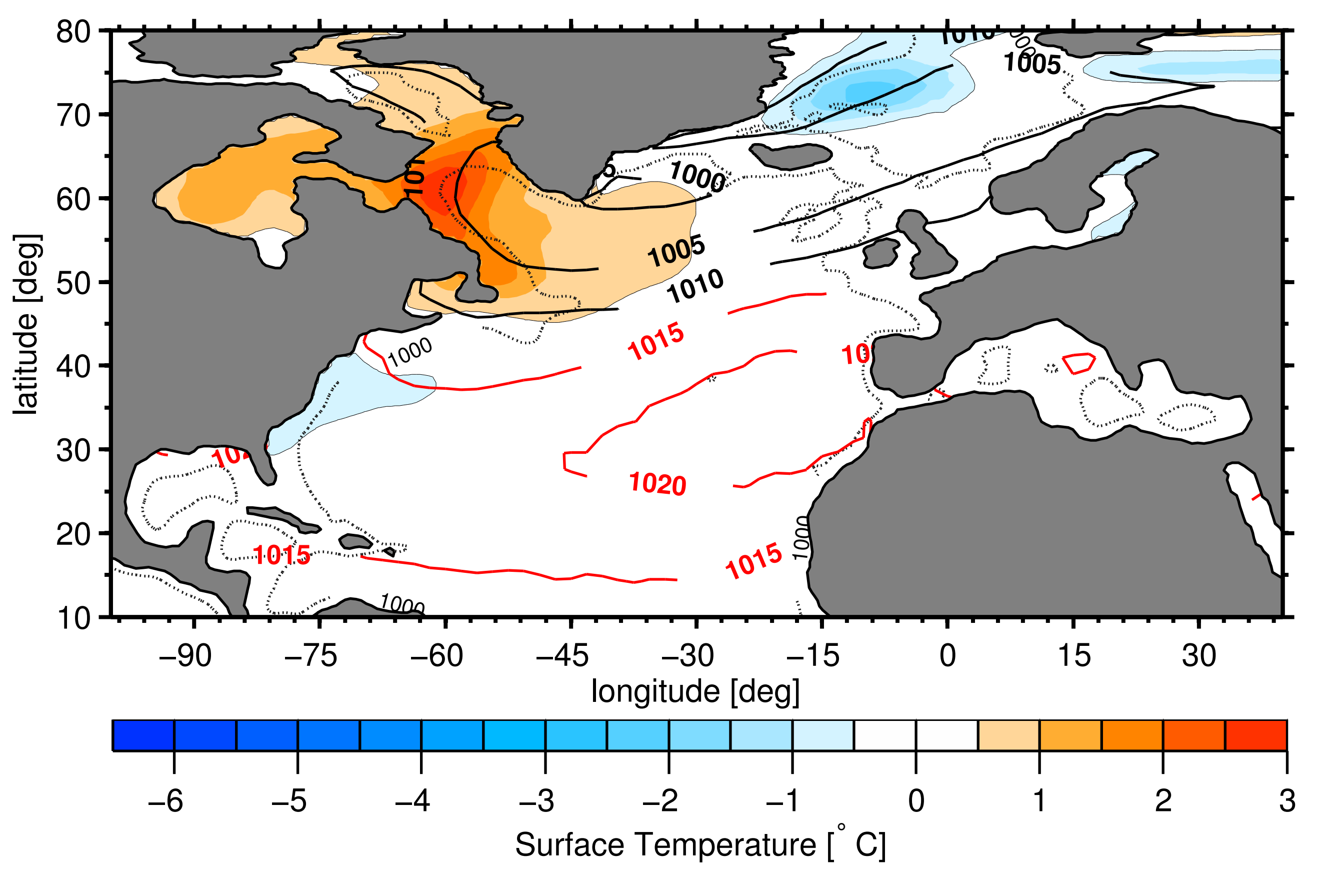

latitude [deg]
longitude [deg]
Surface Temperature [°C]
80
70
60
50
40
30
20
10
−90
−75
−60
−45
−30
−15
0
15
30
−6
−5
−4
−3
−2
−1
0
1
2
3
1000
1005
1010
1015
1020

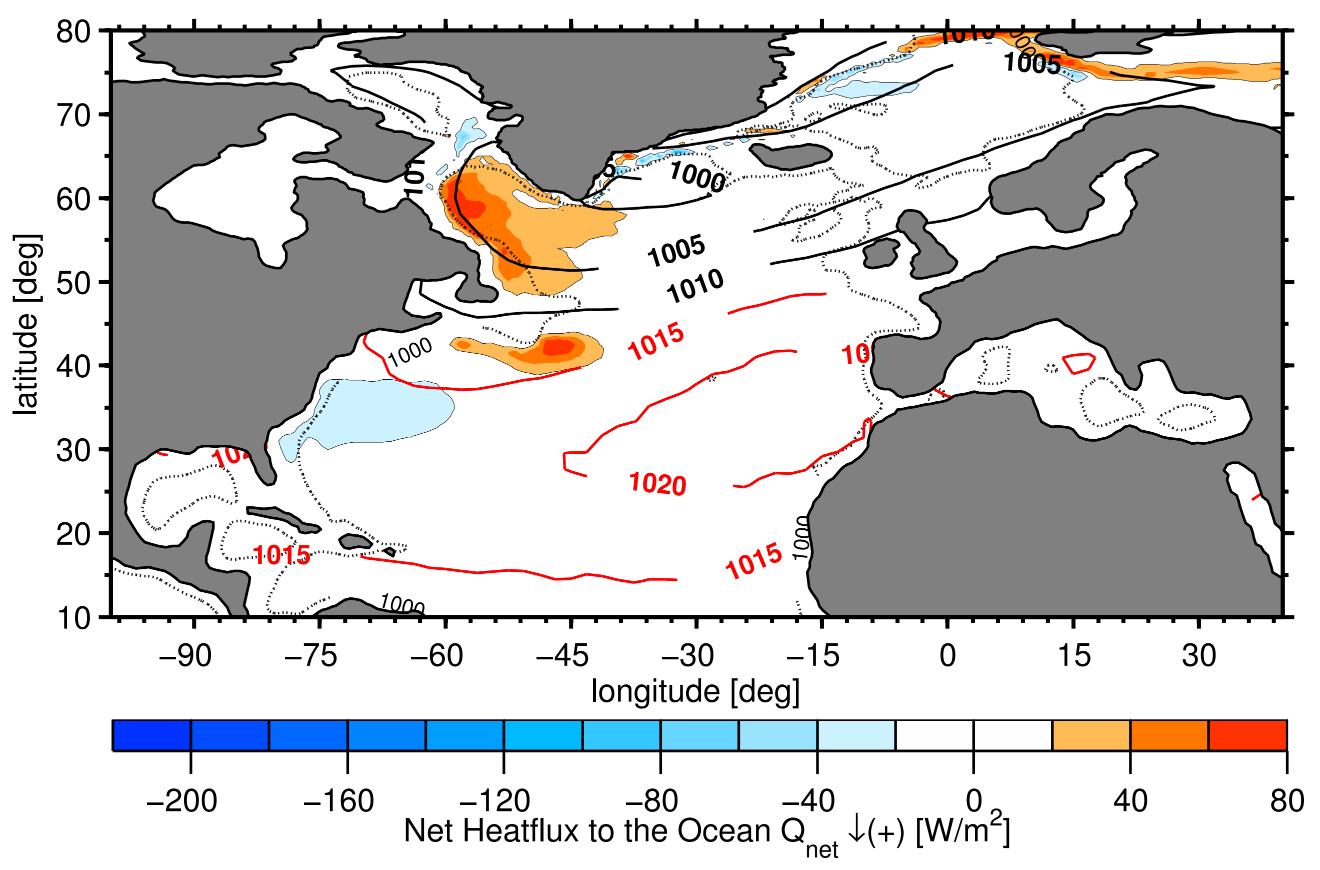

latitude [deg]
longitude [deg]
80
70
60
50
40
30
20
10
−90
−75
−60
−45
−30
−15
0
15
30
1000
1005
1010
1015
1020
−200
−160
−120
−80
−40
0
40
80
Net Heatflux to the Ocean $Q_{net}\downarrow(+)$ [W/m^2]

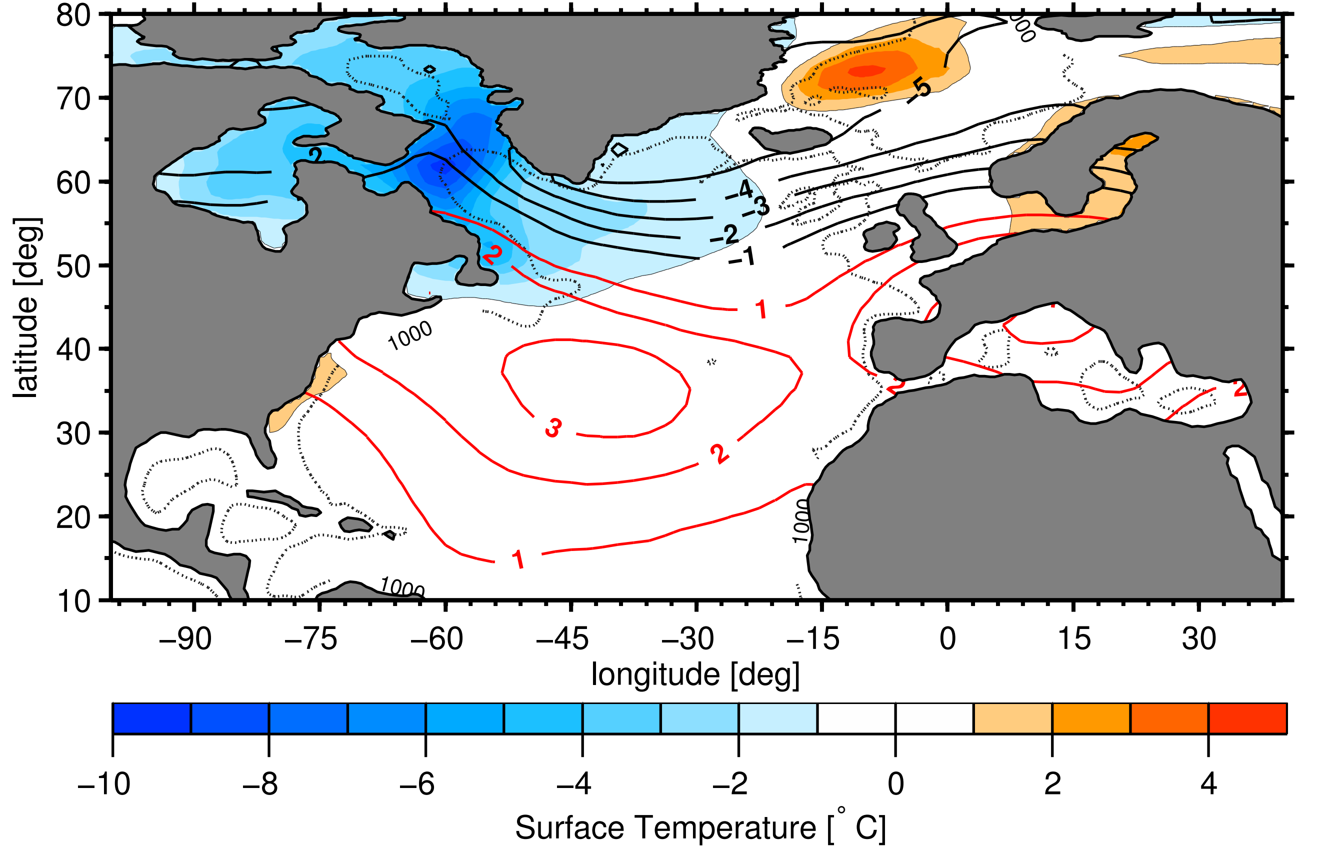

latitude [deg]
longitude [deg]
80
70
60
50
40
30
20
10
–90
–75
–60
–45
–30
–15
0
15
30
1000
–5
–4
–3
–2
–1
1
2
3
–10
–8
–6
–4
–2
0
2
4
Surface Temperature [° C]

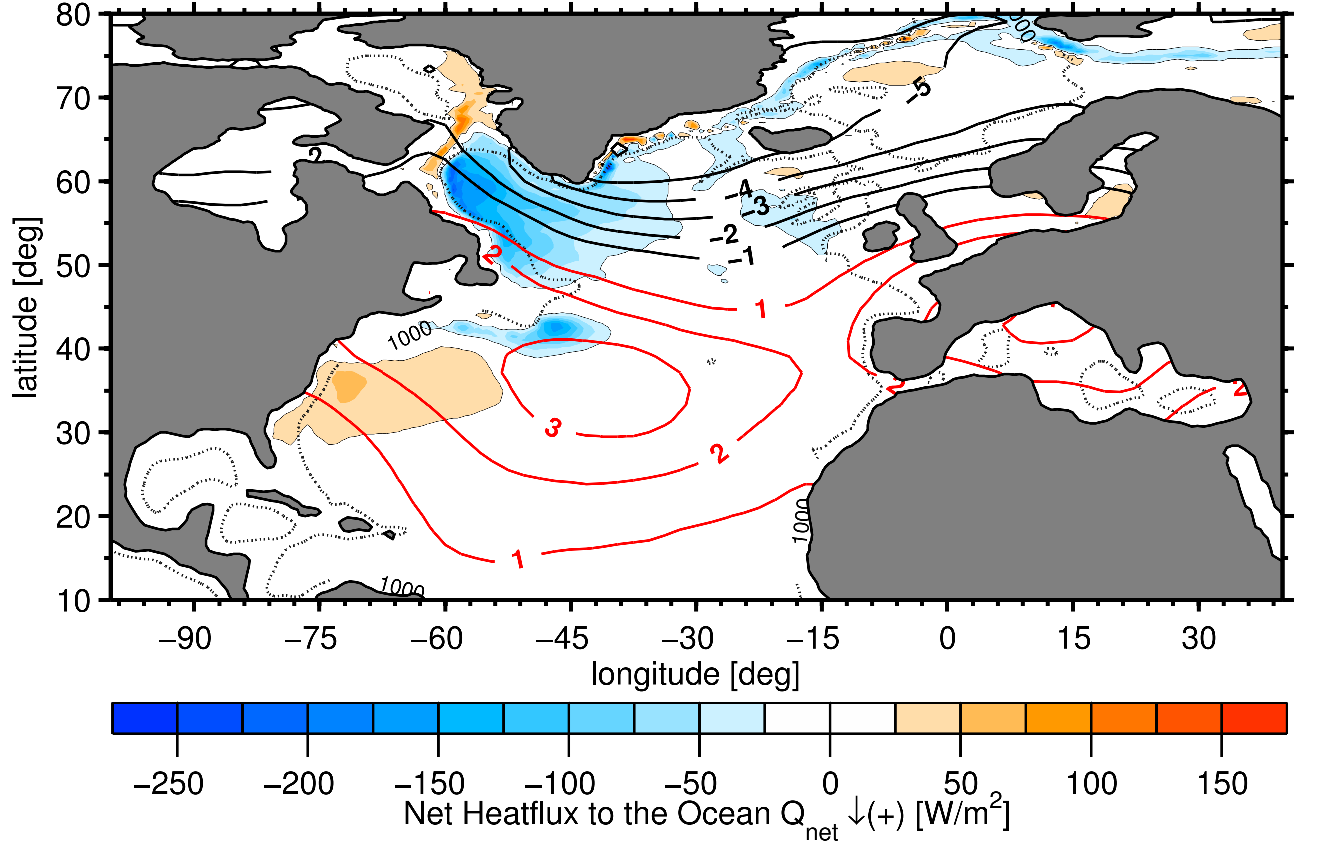

80
70
60
50
40
30
20
10
latitude [deg]
−90
−75
−60
−45
−30
−15
0
15
30
longitude [deg]
1000
−5
−4
−3
−2
−1
1
2
3
−250
−200
−150
−100
−50
0
50
100
150
Net Heatflux to the Ocean $Q_{net}\downarrow(+)$ [W/m^2]

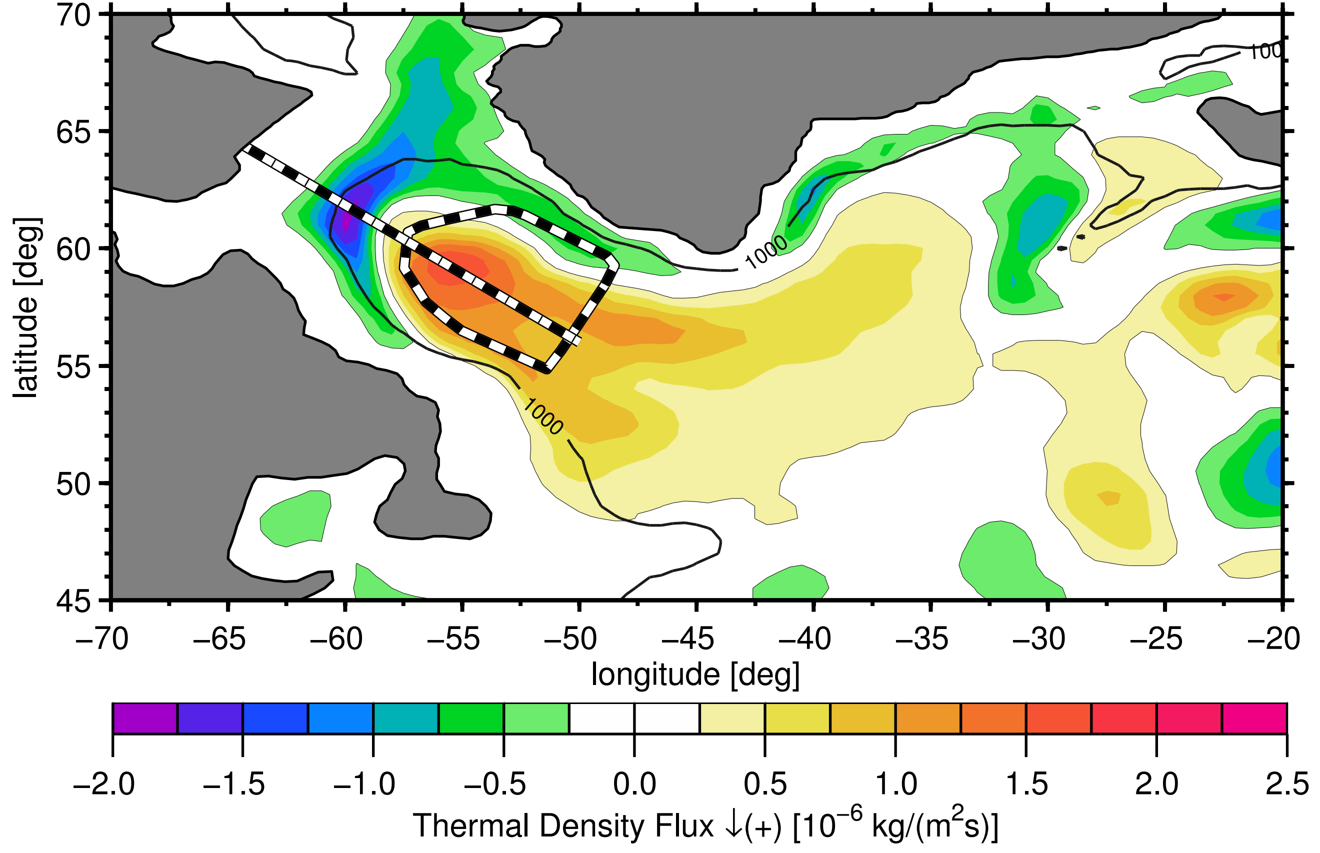

70
65
60
55
50
45
latitude [deg]
−70
−65
−60
−55
−50
−45
−40
−35
−30
−25
−20
longitude [deg]
1000
1000
1000
100
−2.0
−1.5
−1.0
−0.5
0.0
0.5
1.0
1.5
2.0
2.5
Thermal Density Flux ↓(+) [10^{-6} kg/(m^{2}s)]

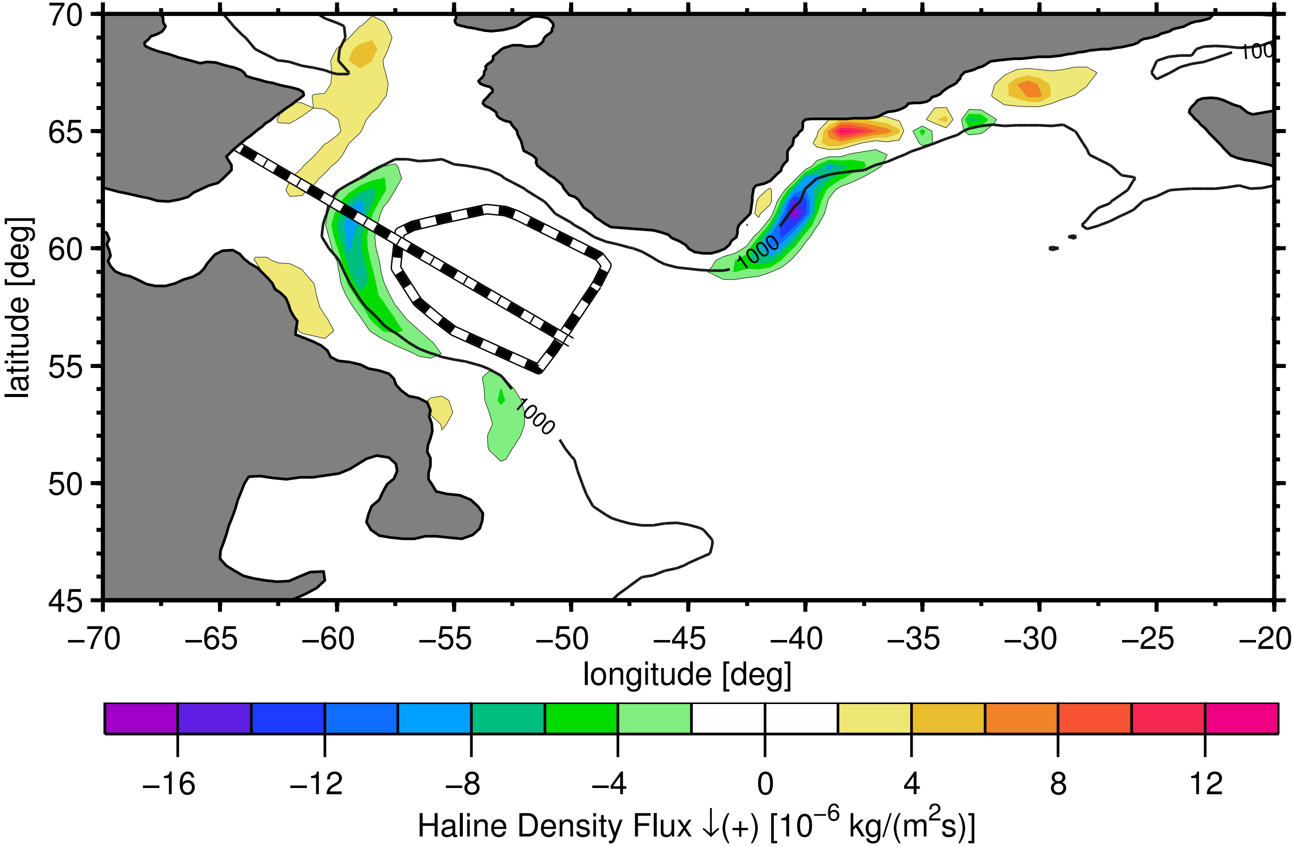

70
65
60
55
50
45
latitude [deg]
−70
−65
−60
−55
−50
−45
−40
−35
−30
−25
−20
longitude [deg]
1000
1000
1000
100
−16
−12
−8
−4
0
4
8
12
Haline Density Flux ↓(+) [10^−6 kg/(m^2s)]

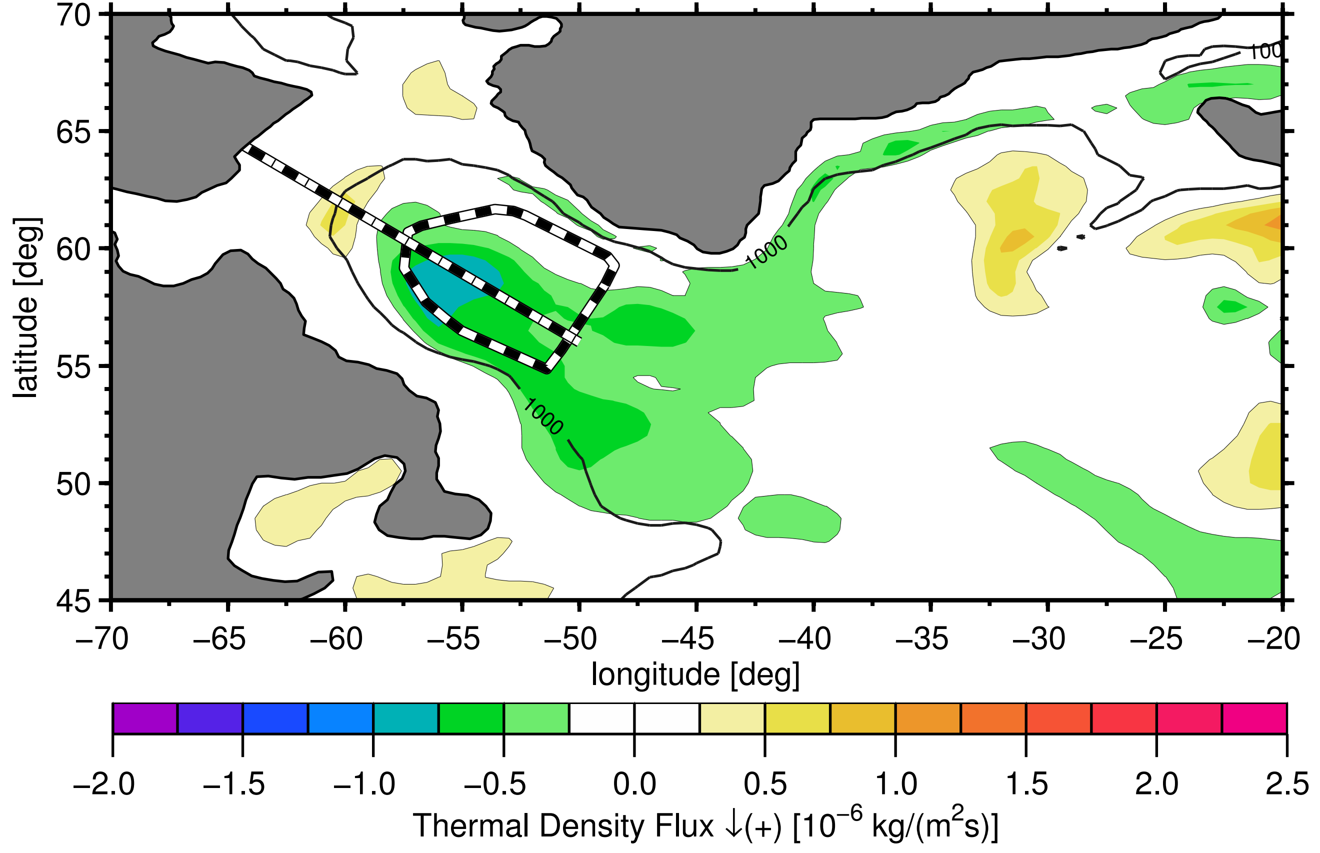

70
65
60
55
50
45
latitude [deg]
−70
−65
−60
−55
−50
−45
−40
−35
−30
−25
−20
longitude [deg]
1000
1000
1000
100
−2.0
−1.5
−1.0
−0.5
0.0
0.5
1.0
1.5
2.0
2.5
Thermal Density Flux ↓(+) [10−6 kg/(m2s)]

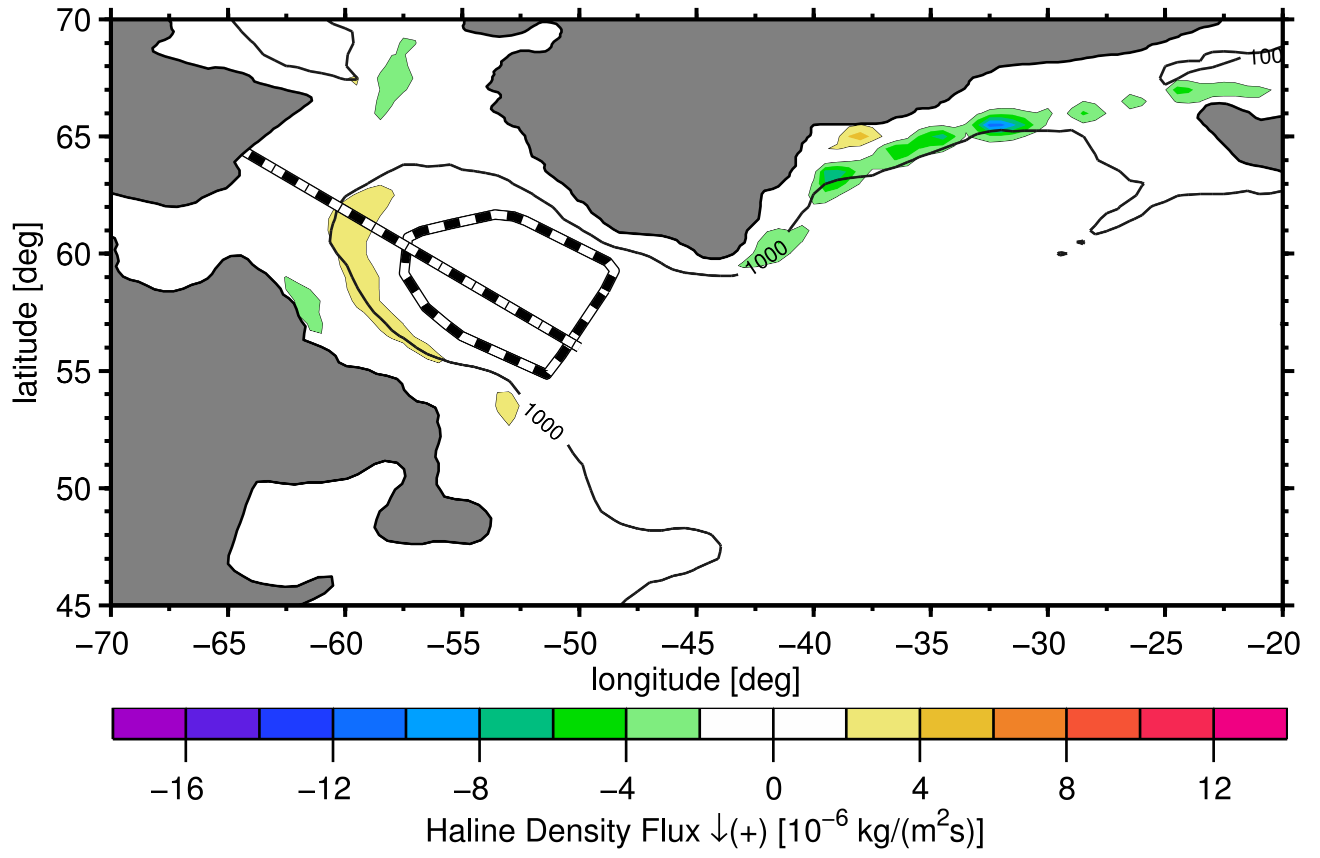

70
65
60
55
50
45
latitude [deg]
−70
−65
−60
−55
−50
−45
−40
−35
−30
−25
−20
longitude [deg]
1000
1000
100
−16
−12
−8
−4
0
4
8
12
Haline Density Flux ↓(+) [10^−6 kg/(m^2s)]

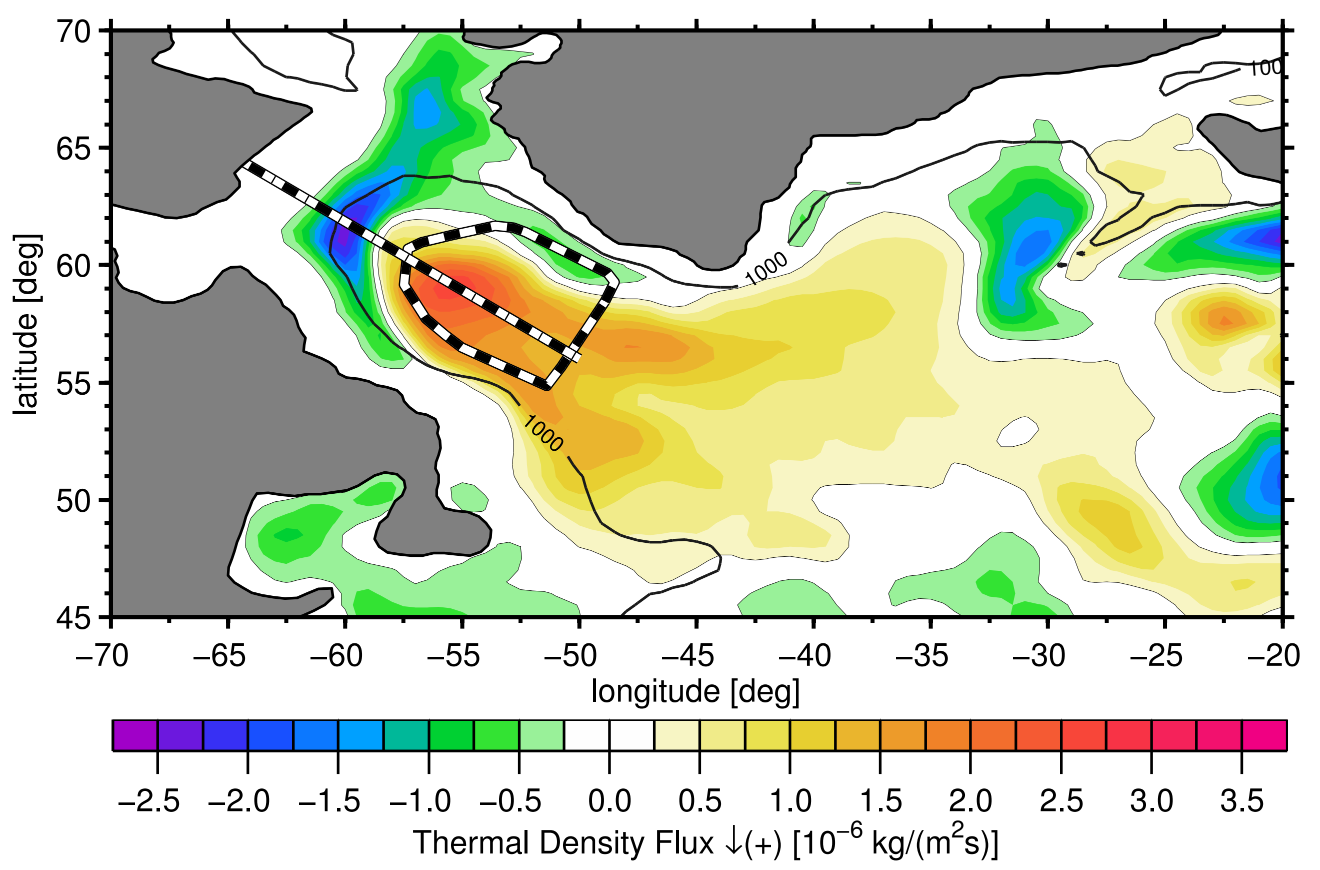
70
65
60
55
50
45
latitude [deg]
−70
−65
−60
−55
−50
−45
−40
−35
−30
−25
−20
longitude [deg]
1000
1000
100
−2.5
−2.0
−1.5
−1.0
−0.5
0.0
0.5
1.0
1.5
2.0
2.5
3.0
3.5
Thermal Density Flux ↓(+) [10^{-6} kg/(m^{2}s)]

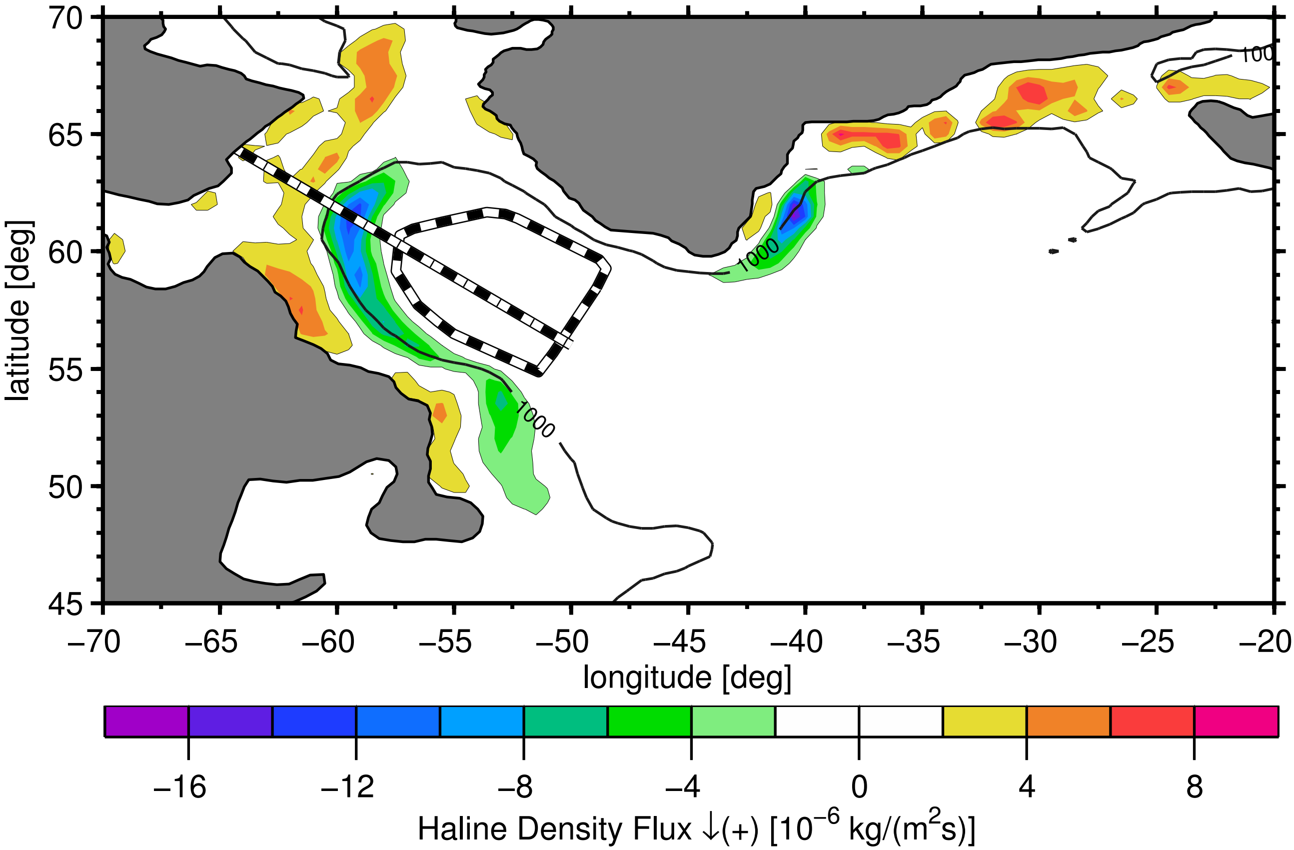

70
65
60
55
50
45
latitude [deg]
–70
–65
–60
–55
–50
–45
–40
–35
–30
–25
–20
longitude [deg]
1000
1000
1000
100
–16
–12
–8
–4
0
4
8
Haline Density Flux ↓(+) [10^{-6} kg/(m^{2}s)]

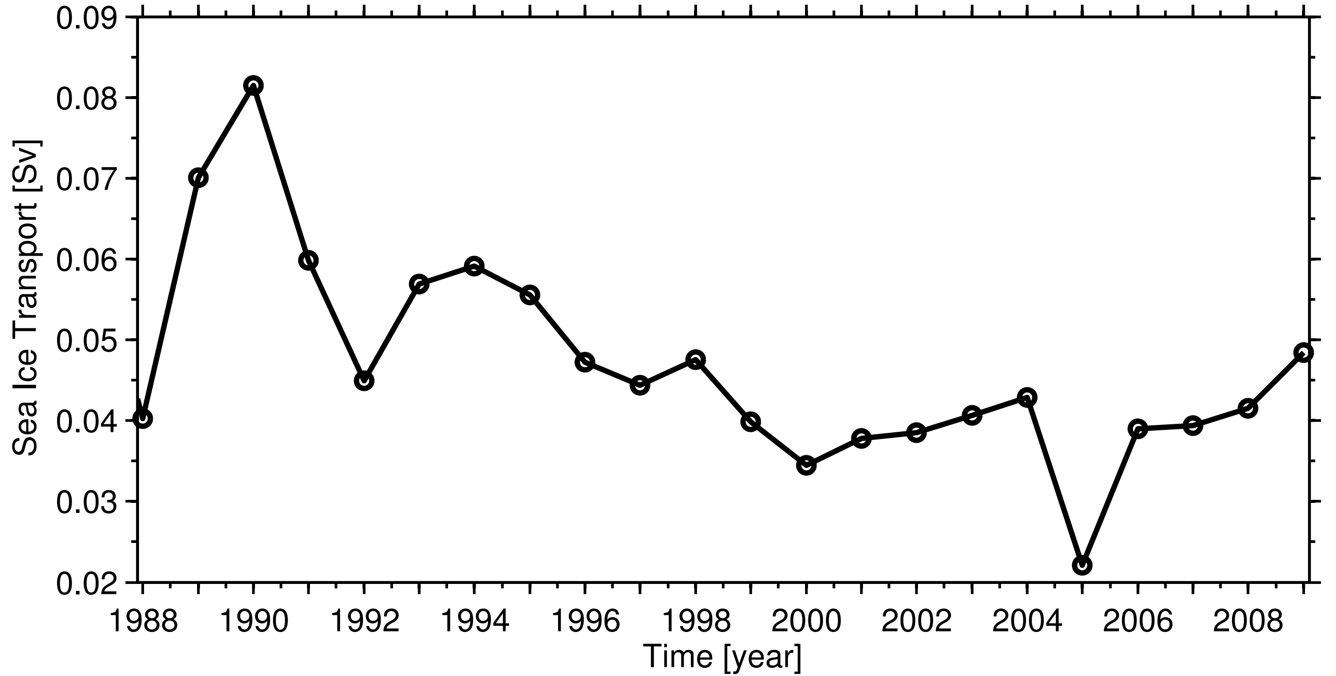
0.09
0.08
0.07
0.06
0.05
0.04
0.03
0.02
Sea Ice Transport [Sv]
1988
1990
1992
1994
1996
1998
2000
2002
2004
2006
2008
Time [year]

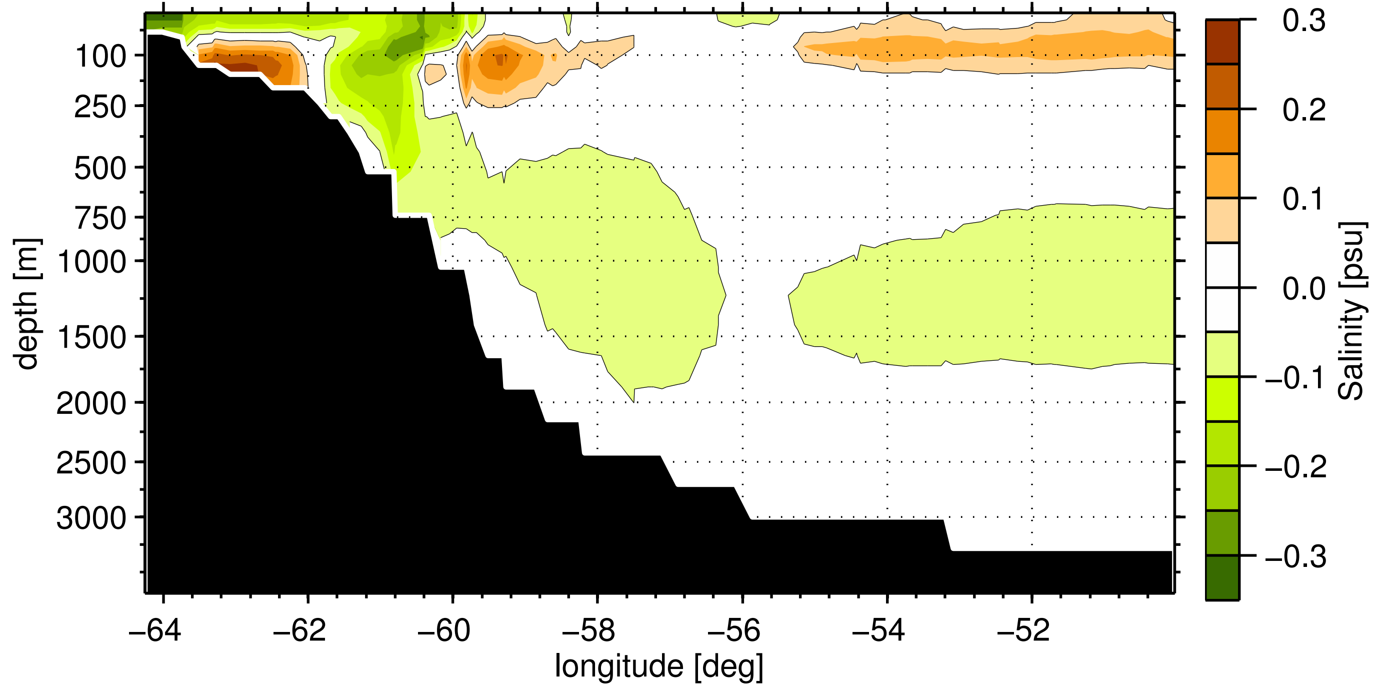

100
250
500
750
1000
1500
2000
2500
3000
depth [m]
−64
−62
−60
−58
−56
−54
−52
longitude [deg]
0.3
0.2
0.1
0.0
−0.1
−0.2
−0.3
Salinity [psu]

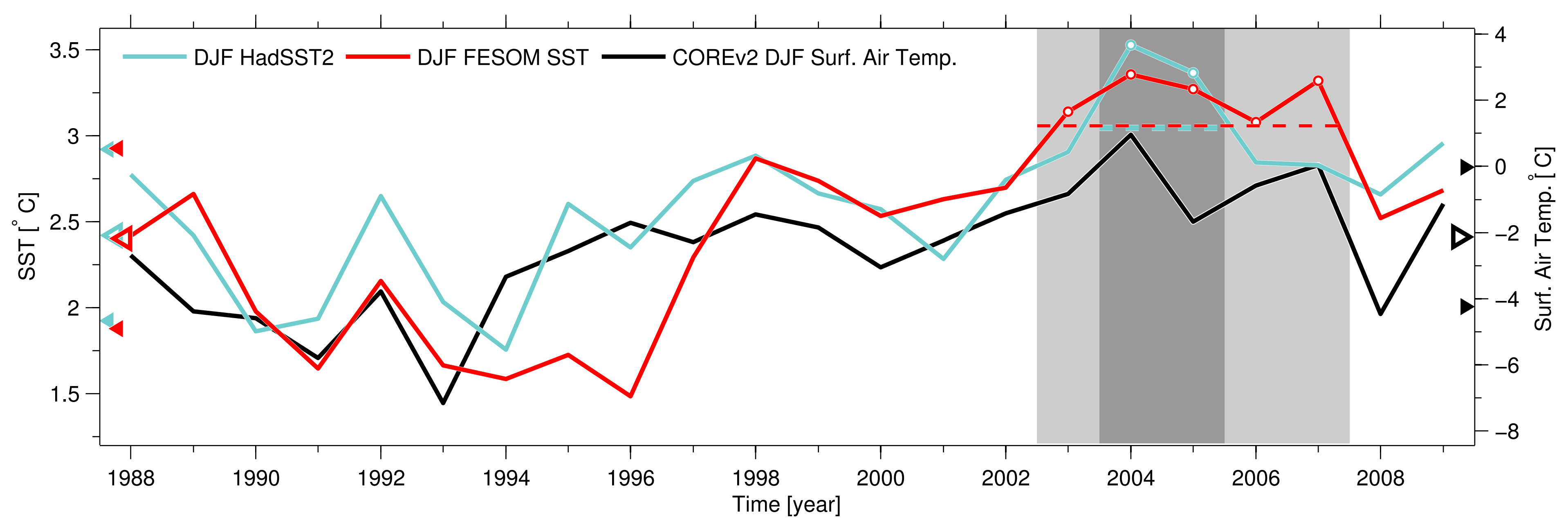
DJF HadSST2
DJF FESOM SST
COREv2 DJF Surf. Air Temp.
SST [°C]
Surf. Air Temp. [°C]
Time [year]
3.5
3
2.5
2
1.5
4
2
0
−2
−4
−6
−8
1988
1990
1992
1994
1996
1998
2000
2002
2004
2006
2008